AD-A145 781 WEAR AND CORROSION OF COMPONENTS UNDER STRESS AND SUBJECTED TO MOTION(U) IIT RESEARCH INST CHICAGO IL K Y KIM ET AL. 05 MAR 84 IITRI-M06060-16 NADC-79137-60 1/2

UNCLASSIFIED N62269-79-C-0702 F/G 20/11 NL

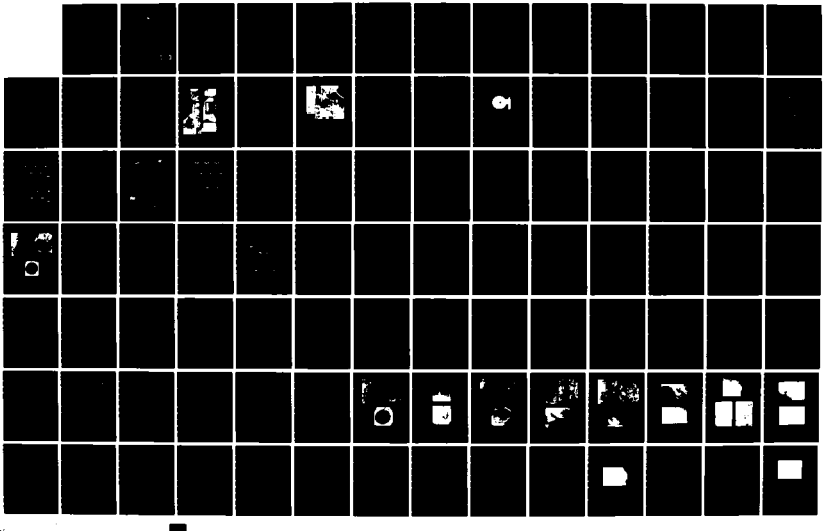

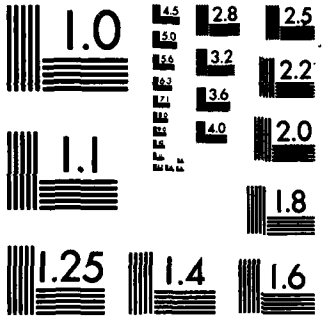

(11)

REPORT NO. NADC-79137-60

AD-A145 781

WEAR AND CORROSION OF COMPONENTS UNDER STRESS AND SUBJECTED TO MOTION

K. Y. Kim and S. Bhattacharyya
I.I.T. RESEARCH INSTITUTE
10 West 35th Street
Chicago, Illinois 60616

5 MARCH 1984

FINAL REPORT
TASK AREA WRO2201-001

APPROVED FOR PUBLIC RELEASE; DISTRIBUTION UNLIMITED

DTIC FILE COPY

Prepared for
NAVAL AIR DEVELOPMENT CENTER
Aircraft and Crew Systems Technology Directorate
Warminster, Pennsylvania 18974

UNCLASSIFIED

SECURITY CLASSIFICATION OF THIS PAGE (When Data Entered)

REPORT DOCUMENTATION PAGE	READ INSTRUCTIONS BEFORE COMPLETING FORM
1. REPORT NUMBER: NADC-79137-60	2. GOVT ACCESSION NO: AD-A145781
3. RECIPIENT'S CATALOG NUMBER:	
4. TITLE (and Subtitle): Wear and Corrosion of Components Under Stress and Subjected to Motion	5. TYPE OF REPORT & PERIOD COVERED: Final - 14 Sept. 1981-14 Sept. 1983
	6. PERFORMING ORG. REPORT NUMBER: IITRI-M06060-16
7. AUTHOR(s): K. Y. Kim and S. Bhattacharyya	8. CONTRACT OR GRANT NUMBER(s): N62269-79-C-0702
9. PERFORMING ORGANIZATION NAME AND ADDRESS: IIT Research Institute, 10 West 35 Street, Chicago, IL 60616	10. PROGRAM ELEMENT, PROJECT, TASK AREA & WORK UNIT NUMBERS: TASK AREA WR02201-001, Work Unit No. DG212
11. CONTROLLING OFFICE NAME AND ADDRESS: Naval Air Development Center, Aircraft & Crew Systems Technology Directorate, Warminster, PA 18974	12. REPORT DATE: ~~20 January 1984~~ 5 MARCH 1984
	13. NUMBER OF PAGES: 135
14. MONITORING AGENCY NAME & ADDRESS (if different from Controlling Office)	15. SECURITY CLASS. (of this report): UNCLASSIFIED
	15a. DECLASSIFICATION/DOWNGRADING SCHEDULE

16. DISTRIBUTION STATEMENT (of this Report)

Approved for public release; distribution unlimited.

17. DISTRIBUTION STATEMENT (of the abstract entered in Block 20, if different from Report)

18. SUPPLEMENTARY NOTES

19. KEY WORDS (Continue on reverse side if necessary and identify by block number)

Rubbing surfaces, wear, oscillatory motion, corrosion, electrochemical polarization, open-circuit potential, corrosion current density, friction coefficient, active, passive, M50, 52100, NaCl, $Na_2Cr_2O_7$, $NaNO_2$, Na_2MoO_4.

20. ABSTRACT (Continue on reverse side if necessary and identify by block number)

The initial two-year study with full rotational motion (NADC-79137-60) was further extended with investigations under oscillatory motion to advance understanding of simultaneously occurring corrosion-wear phenomena in Navy aircraft components, and to use this knowledge to improve reliability in component performance. An additional corrosion-wear parameter, namely, coefficient of friction, was evaluated along with open-circuit potential, corrosion current density, and wear loss, which were statistically analyzed in terms of load,

DD FORM 1 JAN 73 1473 EDITION OF 1 NOV 65 IS OBSOLETE

UNCLASSIFIED

SECURITY CLASSIFICATION OF THIS PAGE (When Data Entered)

20. ABSTRACT (cont.)

frequency, corrosion inhibitor, and lubricant, as well as run-in time. Corrosion-wear surface morphologies were examined with SEM and EDX, and surface roughness measurements were analyzed.

The effect of wear on the corrosion process was very marked for alloys which were able to form a passive film. Disruption of the passive film was the principal factor leading to an increase in corrosion rate and wear loss, while surface deformation by increasing load and motion within the range evaluated appeared to be secondary. An increase in load at a constant frequency did not affect the polarization reaction processes as much as an increase in frequency at a constant load.

It was clearly demonstrated that wear phenomena dominate the anodic polarization process, but not the cathodic polarization process. This understanding of the corrosion-wear mechanism indicated that the stability and repairability of the passive film with a careful selection of corrosion inhibitors will be of paramount importance in these tribological systems.

In the unlubricated system, friction coefficient was observed to be a complex function of tribochemical parameters so that the effect of load, motion, and electrolyte composition on friction coefficient depended on the relative effectiveness of each of the competing parameters. However, it was noted that friction coefficient of tool steels (52100 and M50) in NaCl solutions tended to increase with the addition of corrosion inhibitors, most significantly by sodium dichromate. The addition of a small quantity of water-soluble oil, however, had an overwhelming influence in greatly decreasing the friction coefficient.

All corrosion inhibitors used in this program effectively passivated 52100 and M50 steels under the no-wear condition. Under wear conditions, in 100% sliding motion (with no rolling component present), corrosion inhibitors decreased corrosion activities, but the inhibitors were not always equally beneficial to wear processes. The extent depended significantly on the type of interface motions (100% sliding vs. rolling sliding). Actual Naval aircraft components will always suffer a combination of sliding-rolling motion (with rolling motion predominating). Inhibitors added to a lubricant under such surface motion conditions are recommended for evaluation using the "Dynamic Corrosion-Wear Cell" developed in the program and modified to take into consideration the higher resistance of the lubricant.

FOREWORD

This final report, "Wear and Corrosion of Components Under Stress and Subjected to Motion," summarizes the study for the period 14 September 1981 to 14 September 1983, and is designated internally as Report No. IITRI-M06060-16.

In this study, the dynamic corrosion-wear equipment developed and reported earlier (Interim Report NADC-79137-60) was modified from full rotational to oscillatory motion and a torque cell was incorporated to measure friction coefficient in addition to other wear and electrochemical parameters. M50 and 52100 bearing steels were used in different electrolytes containing NaCl, with inhibitors such as dichromates, molybdates, and nitrites. To simulate bearing lubrication, 10% water-soluble oil was added to the electrolyte. Of the 51 tests conducted, 19 were statistically designed, and the data were analyzed both phenomenologically and statistically. Metallurgical analysis and surface roughness measurements of corrosion-wear surfaces were made and correlated with electrochemical, wear, and friction observations.

The study revealed that the steel surfaces suffered significant wear, corrosion, and pitting in the absence of any inhibitor or lubricant. With different inhibitors, lubricant, overpotential, and run-in time, complex and often beneficial effects were observed. Mechanisms for an understanding of these complex phenomena were suggested. Recommendations were made to modify pure sliding motion to rolling-sliding, to realistically simulate the bearing conditions of naval aircraft.

We acknowledge with gratitude the support of Dr. V. Agarwala, and his critical evaluation and suggestions at different stages of the program. At IITRI, the contributions from H. Nichols, J. Mok, M. Dimenn, and Dr. S. Agarwal are gratefully acknowledged.

The report was edited by Violet Johnson and typed by Marilynn Rhein and Mary Dineen.

K. Y. Kim
Research Metallurgist

S. Bhattacharyya
Senior Engineer

Maurice A. H. Howes, Director
Materials Technology Division

TABLE OF CONTENTS

TABLE OF CONTENTS (cont.)

LIST OF TABLES

LIST OF FIGURES

LIST OF FIGURES (cont.)

LIST OF FIGURES (cont.)

LIST OF FIGURES (cont.)

LIST OF FIGURES (cont.)

1. INTRODUCTION

Corrosion-wear phenomena which may lead to service failure of load-bearing components in Navy aircraft were studied by the electrode polarization technique in a dynamic corrosion-wear system. Using pin and disk electrodes under sliding contact, various electrochemical and tribological factors were examined to understand the basic aspects of the corrosion-wear process as well as its control through inhibitor/lubricant application. After an initial two-year study with full rotational motion, further investigations with oscillatory motion were performed in the next two years, and these results are given in this report.

The corrosion-wear parameters--including the open-circuit potential, corrosion current density, friction coefficient, and wear loss--were examined in terms of load, frequency, corrosion inhibitor, and lubricant, as well as run-in time. Corrosion-wear surface morphologies were analyzed with SEM and surface roughness measurements. A set of statistically designed corrosion-wear tests based on a Plackett-Burman test matrix was performed to demonstrate the significance and effectiveness of the several selected tribochemical parameters on the corrosion-wear process.

2. PROGRAM OBJECTIVE AND TEST PARAMETERS

2.1 PROGRAM OBJECTIVE

The objective of the second phase of the corrosion-wear study was to advance understanding of simultaneously occurring corrosion-wear phenomena in Navy aircraft components and to use this knowledge to improve reliability in component performance. This objective involved the following studies:

1) Role of naval environment in corrosion-wear systems and naval aircraft bearing materials.

2) Mechanisms of corrosion under interfacial motion and stress.

3) Modification of damaging effects of corrosion and wear with inhibitors in Navy aircraft bearing materials and structures.

4) Corrosion-wear surface characterization and development of relationship between observed phenomena and surface structural changes.

2.2 TEST PARAMETERS

To accomplish the above objectives, the selected test parameters and their ranges for corrosion-wear study under oscillatory motion were as follows:

1)	Material	- 52100 and M50 steels
2)	Electrolyte	- Varying concentrations of NaCl in distilled water (0 to 100 ppm)
3)	Inhibitors	- $Na_2Cr_2O_7$, Na_2MoO_4, Na_2CrO_4, and $NaNO_2$
4)	Oscillatory motion frequency	- 1 to 10 cpm (17 to 170 mHz)
5)	Oscillatory motion amplitude	- 20° to 60° ($\pi/9$ to $\pi/3$ rad)
6)	Environment	- Aerated
7)	Load	- 8 to 56 lbf (35.6 to 249 N)
8)	Lubricant	- Lubricants compatible with electrochemical measurement (e.g., water-soluble lubricant).

3. CORROSION-WEAR TEST EQUIPMENT

It was demonstrated in the Phase I study[1] with full rotational motion, that the IITRI-designed "Dynamic Corrosion-Wear Cell" apparatus is a versatile tool capable of conducting a meaningful and reproducible study of simultaneous occurrence of corrosion and wear in any electrolytic system. To simulate the service condition experienced by load-bearing components of Navy aircraft bearings, the existing corrosion-wear apparatus was modified in Phase II to provide an oscillatory motion. The loading mechanism was changed from spring loading to deadweight loading, and a torque measurement unit was incorporated into this modification to measure friction coefficient. Details of each modification are explained in Appendix A as well as in the following sections. Since the use of the electrode polarization technique for a corrosion-wear system was successfully demonstrated by the existing corrosion-wear cell apparatus, the main procedure for electrochemical measurement was maintained as reported earlier.[1]

3.1 OSCILLATORY MOTION

Figure 1 shows a view of the corrosion-wear electrochemical cell apparatus with oscillatory motion device: the electrochemical cell (A), loading mechanism (B and C), torque cell (D), and oscillatory motion device (E, F, G, H, and I). The oscillatory motion is obtained by conversion of rotary motion through a crank (G), a set of connecting rods (F), and lever arm (E).

The amplitude of oscillatory motion is selected by simply adjusting the lengths of both connecting rod and lever arm, and values up to 90° ($\pi/2$ rad) are readily obtainable. The frequency of motion is controlled by a variable speed controller (I in Fig. 1). The load-bearing components of Navy aircraft are also subjected to low-frequency cyclic motions, and the equipment

---

[1]K. Y. Kim and S. Bhattacharyya, "Wear and Corrosion of Components Under Stress and Subjected to Motion," Interim Report, NADC-79137-60, Naval Air Development Center, Warminster, PA, February 1982.

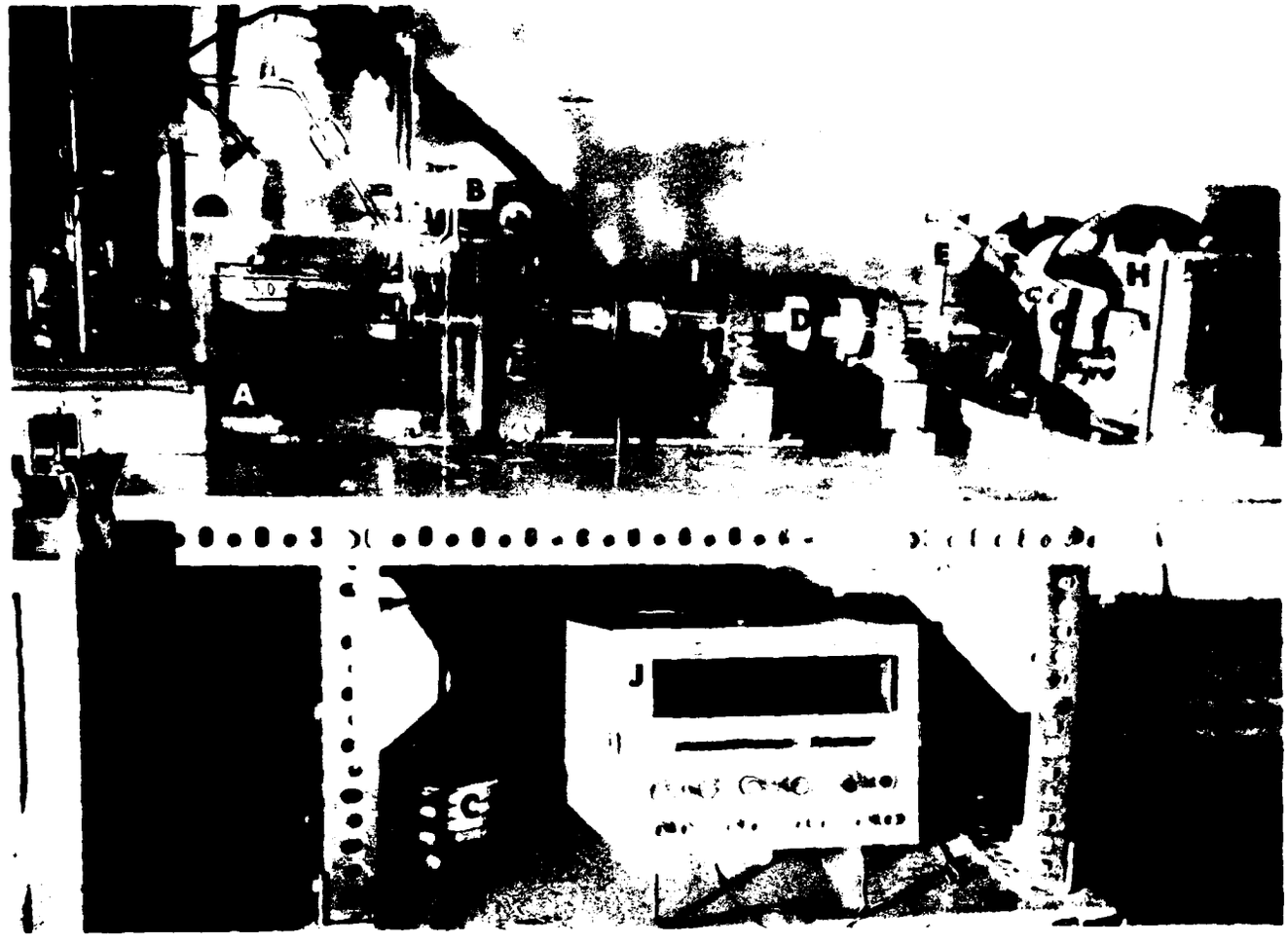

Neg. No. 54152

A - Electrochemical Cell with Electrodes
B - Load Arm
C - Suspended Weights
D - Torque Cell
E - Lever Arm
F - Connecting Rod
G - Crank
H - Speed Reducer Attached to Motor
I - Speed Controller
J - Digital Strain Indicator

Figure 1. View of the corrosion-wear electrochemical cell apparatus with oscillatory motion device.

frequency range of 0.9 to 44 rpm (15 to 730 mHz) is well suited for this study.

3.2 LOADING MECHANISM

The deadweight loading mechanism is shown in Figs. 1 and 2. Load is applied through the pin electrode mounted on a cantilever arm (G in Fig. 2), which is aligned with the center of the disk electrode. One end of this cantilever arm has a suspended pan (C in Fig. 1) on which the standard weights are placed.

3.3 TORQUE MEASUREMENT

A torque cell (D in Fig. 1) measures the frictional coefficient experienced by the pin and disk electrodes under various environmental corrosion-wear conditions. The torque cell is placed between the main shaft of the test unit and the lever arm of the oscillatory motion linkage, as shown in Fig. 1.

Calibration tests were conducted to obtain the relationship between applied load (torque) and corresponding strain experienced by the torque cell. The strain experienced by the torque cell was measured with a digital strain indicator. The calibration curves are shown in Fig. 3. The lower range of the applied torque vs. strain relationship is shown in the inset. Each point represents at least four independent measurements. Readings at all levels were highly reproducible. The best fit of all data points is represented by a straight line in both sets.

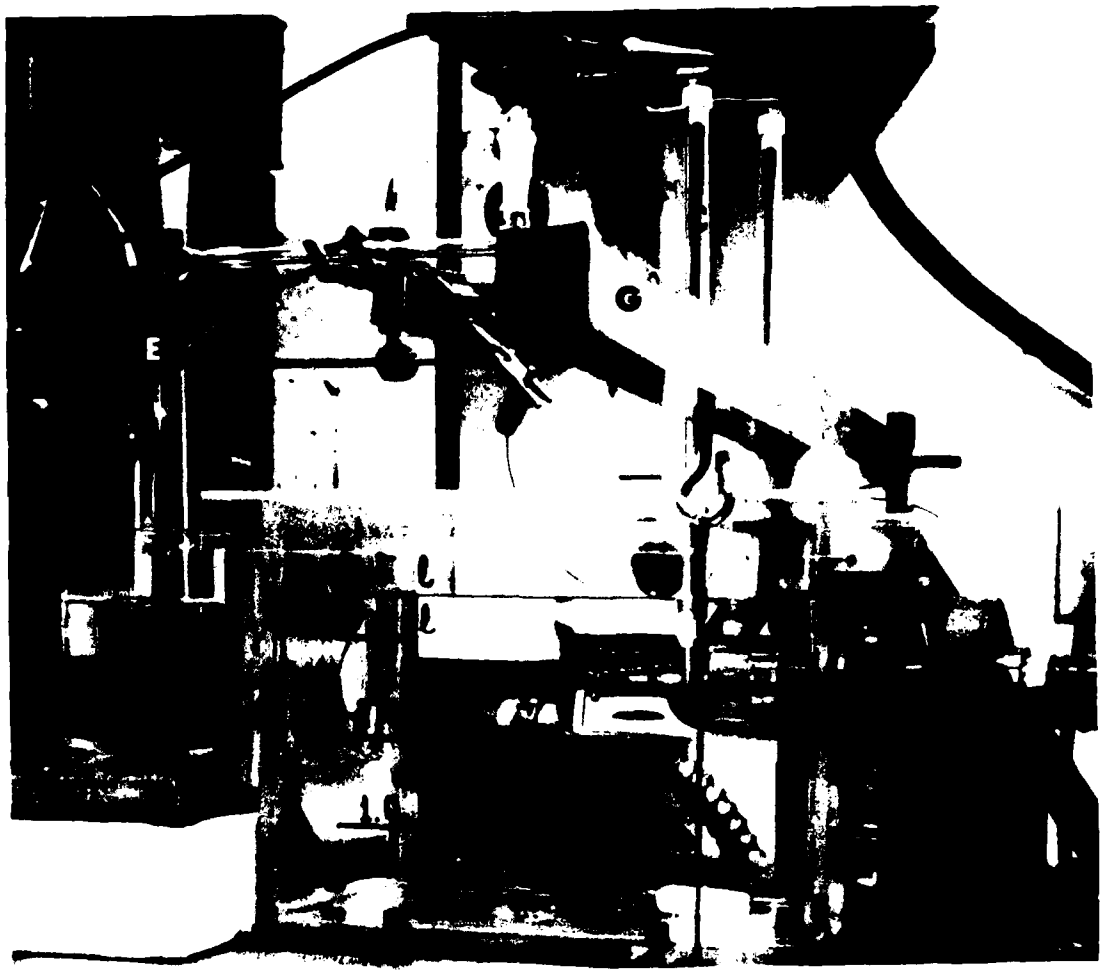

Neg. No. 54155

A - Clear Plastic Cell
B - Specimen (Working Electrode)
C - Counter Electrode
D - Luggin Capillary Bridge
E - SCE
F - Plastic Holder with Current-Collecting Pin
G - Lever Arm

Figure 2. Close-up view of the corrosion-wear electrochemical cell.

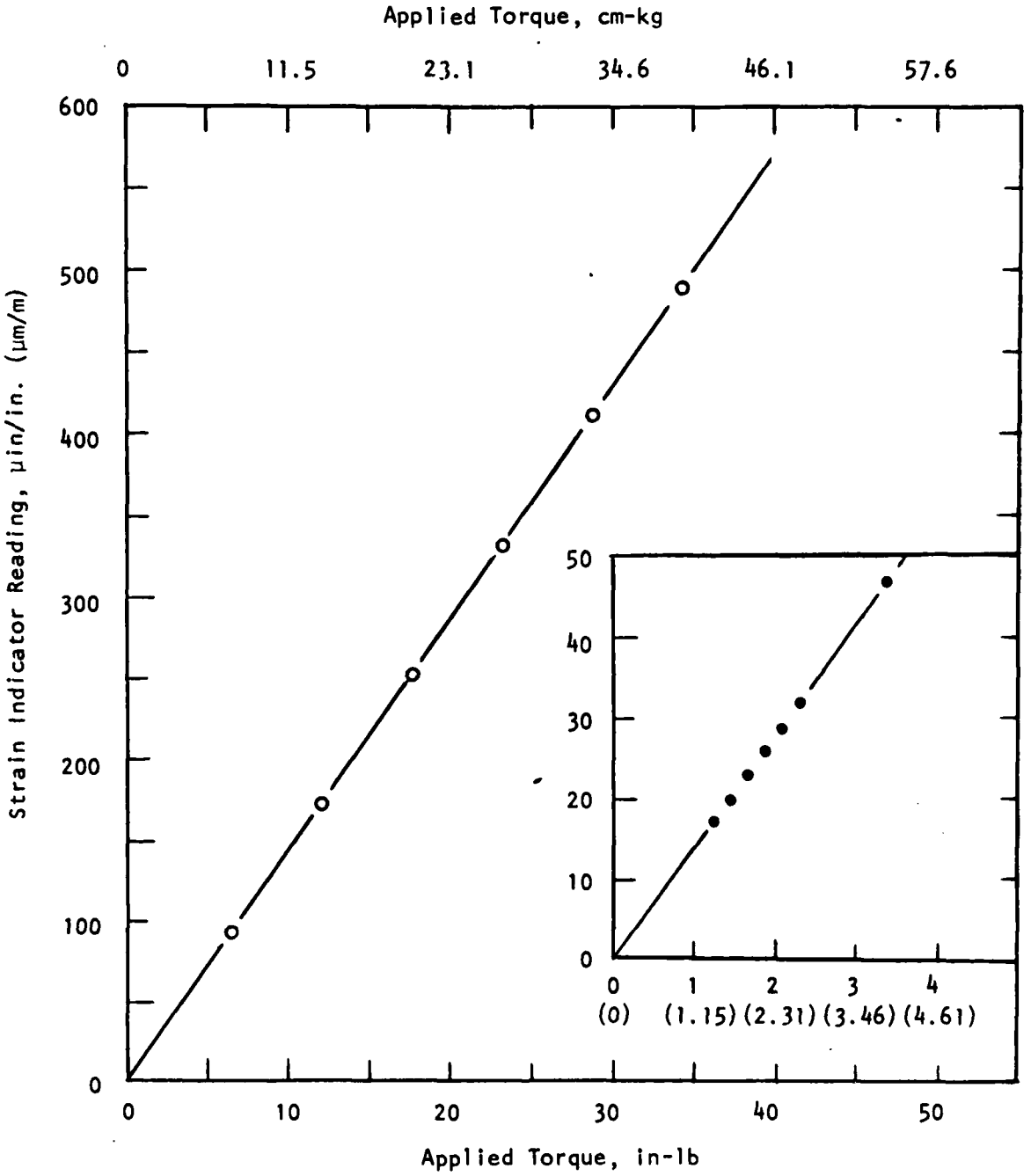

Figure 3. Calibration curve of full bridge SR-4 torque cell.

4. SAMPLE PREPARATION AND TEST PROCEDURE

4.1 SAMPLE PREPARATION

The steels 52100 and M50 were selected for study because they are commonly used in bearing systems. Their nominal compositions are given in Table 1.

TABLE 1. NOMINAL COMPOSITIONS OF TEST MATERIALS

Steel	Composition, wt%								
	C	Mn	Si	Cr	Ni	V	Mo	Fe	Others
52100	0.98-1.10	0.25-0.45	0.15-0.35	1.30-1.60	-	-	-	Bal.	P & S 0.025 max
M50	0.80	0.25	0.25	4.0	0.1	1.0	4.5	Bal.	P & S 0.015

The disk electrode is 0.40 in. (10 mm) thick and 1.5 in. (38 mm) in diameter. The pin is 1.5 in. (38 mm) long and 0.25 in. (6.3 mm) in diameter with a 1/8 in. (3.1 mm) radius hemispherical end. After final machining to approximately 10 μin. (0.25 μm) rms roughness, the surface hardness readings of both disk and pin electrodes of these steels were HRC 60-63 (except for the pin electrodes used for tests 202 through 211a). In all tests, the disk and pin electrodes were made of the same material to eliminate possible galvanic coupling. The electrode surfaces were polished with 600 grit paper, degreased with acetone, and cleaned with distilled water. All the electrode surfaces except the contact area were coated with epoxy resin (as shown in Fig. 4).

4.2 ELECTROLYTE PREPARATION AND POLARIZATION MEASUREMENTS

The electrolytes were made from distilled water containing various concentrations of reagent grade sodium chloride (NaCl). The corrosion inhibitors used in this study were reagent grade sodium dichromate ($Na_2Cr_2O_7 \cdot 2H_2O$), sodium chromate ($Na_2CrO_4 \cdot 4H_2O$), sodium molybdate ($Na_2MoO_4 \cdot 2H_2O$), and sodium

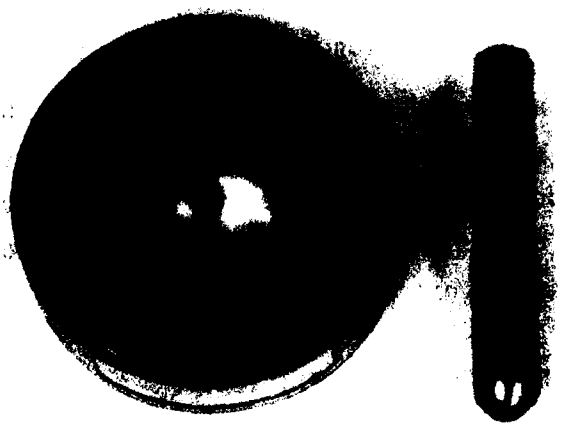

Neg. No. 54421 1.5X

(a) (b)

Figure 4. Oscillating disk and pin electrodes used for corrosion-wear tests.

nitrite ($NaNO_2$). A water-soluble cutting oil (WHITE KUT 210)* was used as a lubricant since it was compatible with electrochemical measurements. The electrolyte was continuously stirred during the test, and all the tests were performed at ambient temperature and pressure.

The polarization procedure used in this program was basically similar to that of ASTM Standard Method G5-78. Detailed descriptions of the polarization test procedure and instrumentation other than those described in Appendix C were published earlier.[1] In Appendix C, three different potential scanning methods, used for polarization measurement in this program, are described.

For aeration, air bubbles (Matheson Air, Zero Gas) were introduced through fritted glass to the electrolyte. When water-soluble oil was used, however, introduction of air bubbles in the cell caused foaming and created difficulties in corrosion-wear monitoring. This problem was effectively solved by adapting an external stirring system.

4.3 EVALUATION OF FRICTION COEFFICIENT

The friction coefficient, f, between two surfaces in relative motion under stress is customarily expressed as the ratio of the observed torque, T_{obs}, to the applied torque, T_{app}, i.e.,

$$f = T_{obs}/T_{app}$$

T_{obs} was determined by measuring frictional torque strain with an SR-4 torque cell and BLH digital strain indicator (Model 1200). This torque cell was pre-calibrated to obtain a relationship between applied torque and corresponding torque strain (Fig. 3). The value of T_{app} was equal to r x P, where r is the radius of the disk electrode 0.75 in. (19 mm) and P, the applied normal load in lbf (N). The observed torque included the torque due to bearing friction which was subtracted to obtain the net torque. A detailed discussion of the determination of friction coefficient is presented in Appendices A and B.

---

*WHITE KUT 210 - Trade name of Metal Fluid Products, 7540 N. Linder Ave., Skokie, Illinois 60076.

Depending on test conditions, friction between loaded surfaces in relative motion changed initially and then stabilized to a steady-state value, provided the test conditions remained unchanged. This is usually called "run-in" in tribology. The period of run-in may vary from a few minutes to many hours. The friction coefficients reported in this study refer to the values obtained after a 2 h run-in under no externally impressed potential, unless otherwise stated.

5. RESULTS AND DISCUSSION

In this program, a total of 51 tests were conducted in different electrolytes under varying load, oscillatory frequencies, and time periods, and with or without a lubricant in the electrolyte. Both phenomenological and statistical analyses were conducted to determine the effects of inhibitors, load, frequency, time, oil, chloride level, running-in time, and material hardness on corrosion current, open-circuit and pitting potentials, wear, and friction. The complete data are given in Appendix D.

In the following sections, the Appendix D results are discussed phenomenologically in terms of

- Friction coefficient
- Electrochemical behavior
- Weight loss
- Scanning electron microscopy
- Surface roughness.

Following the analysis, the statistically designed test matrix data (12 tests with replicates) were analyzed both phenomenologically and statistically. Finally, significant conclusions of the study are summarized along with future recommendations for a more critical study involving rolling-sliding interface motion.

5.1 FRICTION COEFFICIENT

Friction coefficients of 52100 and M50 steels were measured under a wide range of tribo-electrochemical conditions. Table D-1 of Appendix D summarizes the corrosion-wear test conditions and friction coefficients. All the friction coefficient values shown in Table D-1 represent the friction coefficient measured after a 2 h run-in at open-circuit potential, i.e., under no externally applied potential. It is to be noted that the hardnesses of the pin electrodes were HRC 20-25 in tests 202 to 211a, and HRC 60-63 in tests 211b through 250. The hardnesses of the disk electrode were HRC 60-63 in all tests.

5.1.1 Effect of Load, Environment, and Oscillatory Motion on Frictional Torque Strain

Table 2 lists frictional torque strains between 52100 steel disk and pin electrodes measured at different positions along the oscillatory motion path (refer to Appendix A for position identification) under 8 lbf (35.6 N) in air and water. The actual frictional torque strain traces are shown in Figs. 5 and 6 for air and water, respectively. Time had a significant effect on frictional torque strain as shown in Fig. 5 for air. A much smaller effect was noted for water.

TABLE 2. FRICTIONAL TORQUE STRAIN BETWEEN 52100 STEEL DISK AND PIN ELECTRODES (TEST 202)

Time, h	Strain Measured at Given Position, μin/in.			
	+30°	+0°	-30°	-0°
	In Ambient Air			
2	-85	+80	+76	-100
	-81	+80	+75	-101
	-81	+82	+75	-100
	In Distilled Water[a]			
At start	-58	+72	+73	-53
	-58	+72	+74	-52
	-57	+73	+74	-52
1	-64	+73	+73	-50
	-64	+73	+73	-50
	-64	+73	+78	-50
2	-67	+73	+79	-52
	-66	+74	+79	-54
	-66	+73	+80	-52

Test Conditions: Load - 8 lbf (35.6 N)
Amplitude - 60° (π/3 rad)
Frequency - 1 cpm (17 mHz)

[a]After a 2-h test in air.

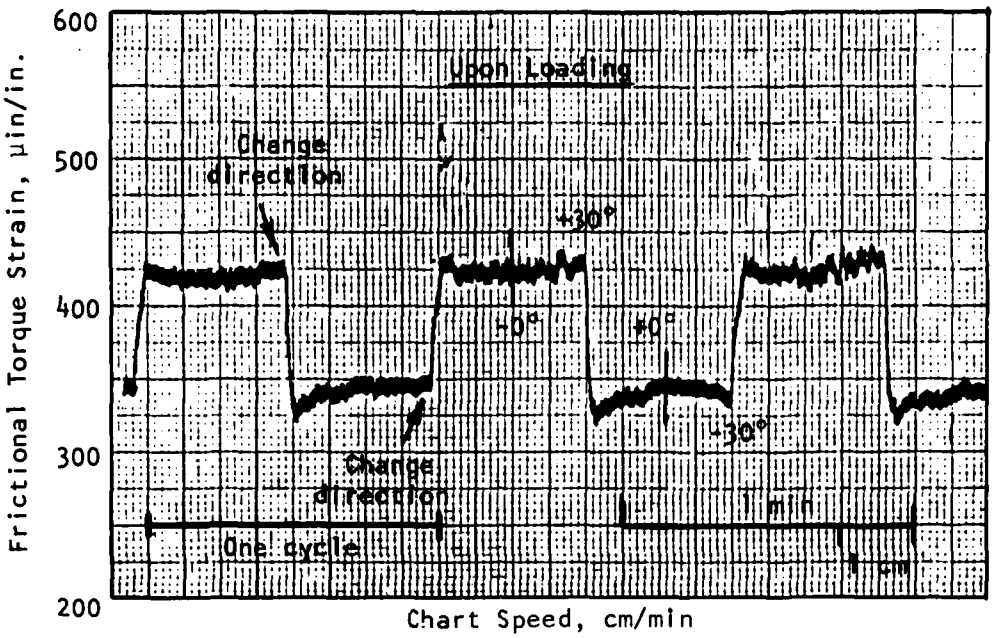

(a)

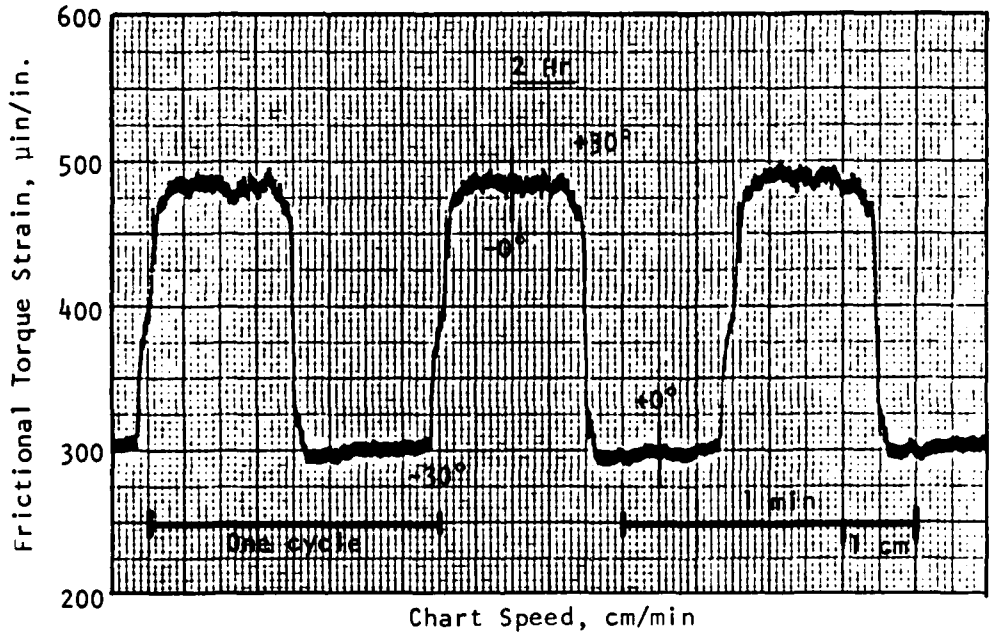

(b)

Figure 5. Traces of frictional torque strain observed in various time periods for 52100 steel under 8 lbf (35.6 N) in ambient air (test 202). Amplitude: 60° (π/3 rad); frequency: 1 cpm (17 mHz).

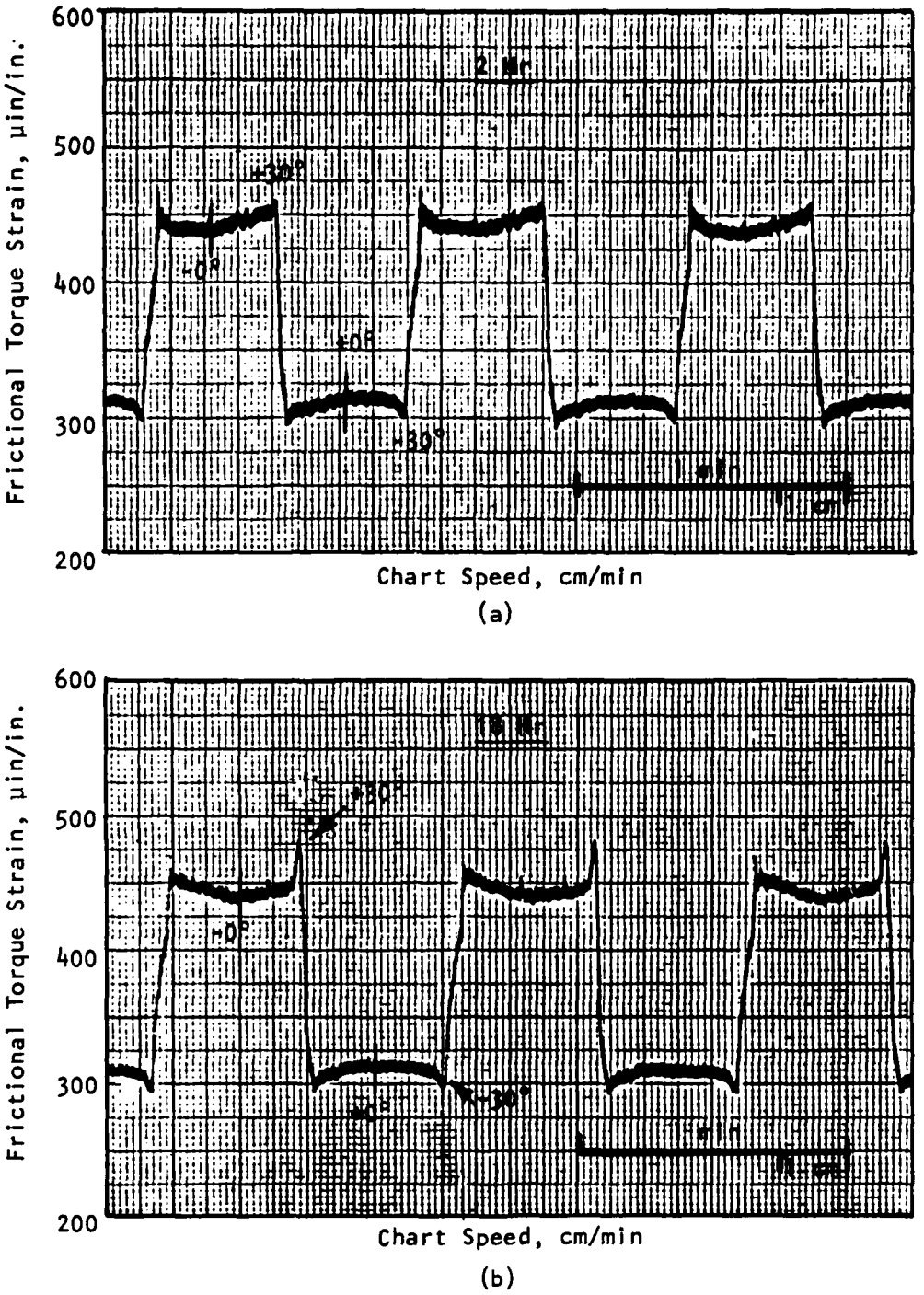

Figure 6. Traces of frictional torque strain observed in various time periods for 52100 steel under 8 lbf (35.6 N) in distilled water (test 202). Amplitude: 60° (π/3 rad); frequency: 1 cpm (17 mHz).

Table 2 data show that, on addition of water after testing for 2 h in air, the coefficient of friction decreased immediately and later increased slightly with time at the +30° and -30° positions, the two end locations where a change in motion direction occurred with a momentary stop. The small strain peaks seen in Fig. 6 at +30° and -30°, and occurring in almost all tests in water, may be attributed to this momentary stoppage with motion reversal, and to breakaway friction which is usually larger than kinetic friction.

Figure 7 shows the frictional torque strain traces in air and water under the very high load of 56 lbf (249 N). Localized adhesions caused significant fluctuation in friction coefficient, as may be seen in Fig. 7a. On addition of water after 2 h of testing in air, the friction coefficient decreased immediately. The inset (Fig. 7c) shows the magnitude of strain due to bearing friction alone which was subtracted from the observed values to obtain the correct strain value for torque and friction coefficient calculations.

In water, the friction coefficient remained virtually unchanged over a long test period, as shown in Fig. 8 for a test under 16 lbf (71.2 N). Earlier, in Fig. 6 for a test under 8 lbf (35.6 N), a similar effect was noted, and it was concluded that the 2-h run-in in the electrolyte would be adequate under all loads for obtaining a steady-state friction coefficient.

5.1.2 Effect of Load and Frequency

The effect of load and frequency on friction coefficient of 52100 and M50 steels was measured under diverse electrochemical and tribological conditions. Friction coefficient data are given in Table D-1, and presented graphically in Fig. 9 for 52100 steel in various conditions--namely, tests 202 through 210 with non-heat treated (softer) pin electrodes.

(a) Load Effect

Tests 202, 203, and 204 (52100 steel). As shown in Fig. 9, in ambient air, the friction coefficient increased as load increased from 8 to 16 lbf (35.6 to 71.2 N), but decreased as load was further increased to 56 lbf (249 N). In distilled water, friction coefficient values for 8 to 16 lbf (35.6 to 71.2 N) loads were very close to each other, and the value of f with 56 lbf (249 N) showed only a very small increase which was within the experimental error.

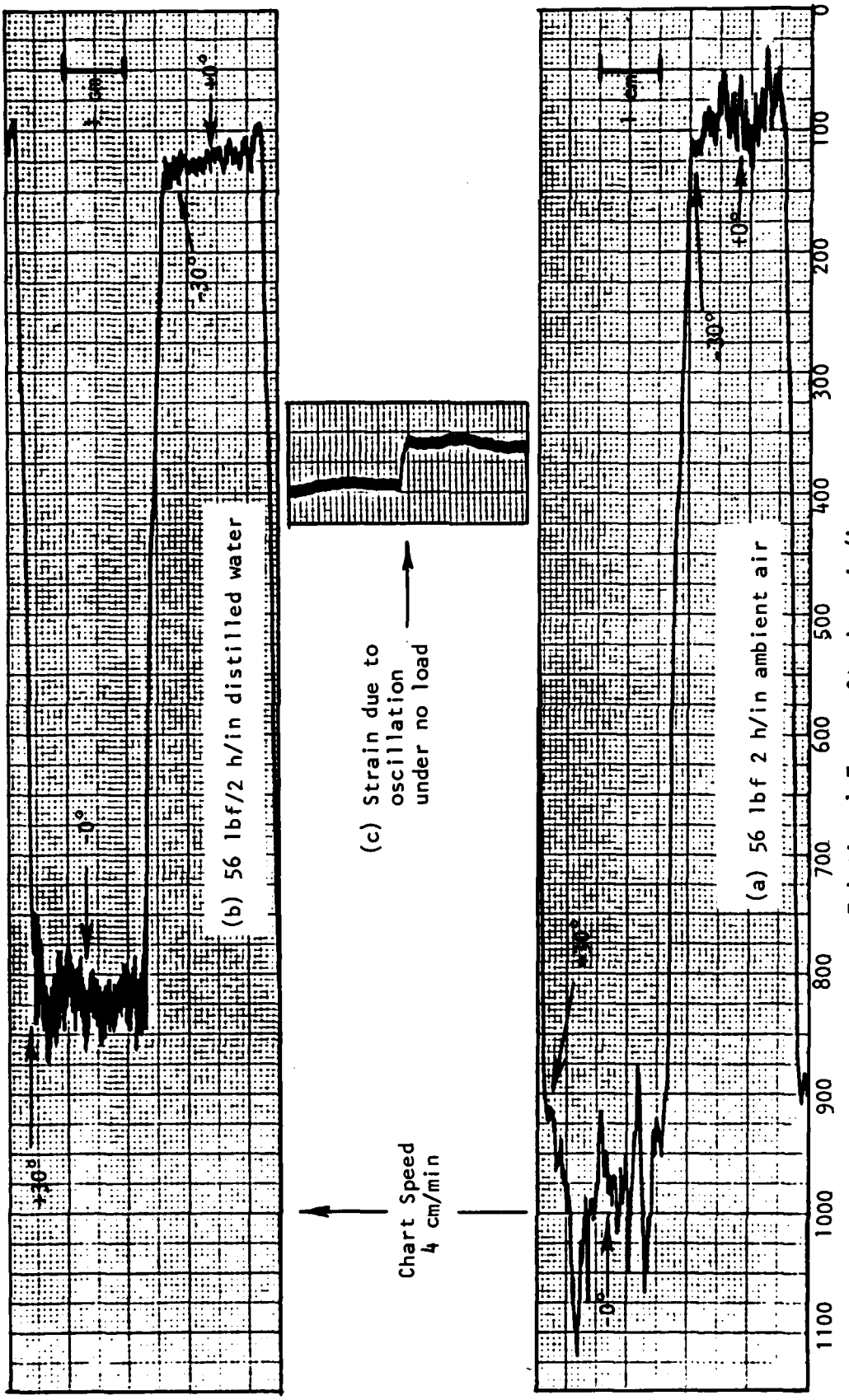

Figure 7. Traces of frictional torque strain observed for 52100 steel under 56 lbf (249 N) in ambient air and in distilled water (test 205). Amplitude: 60° (π/3 rad); frequency: 1 cpm (17 mHz).

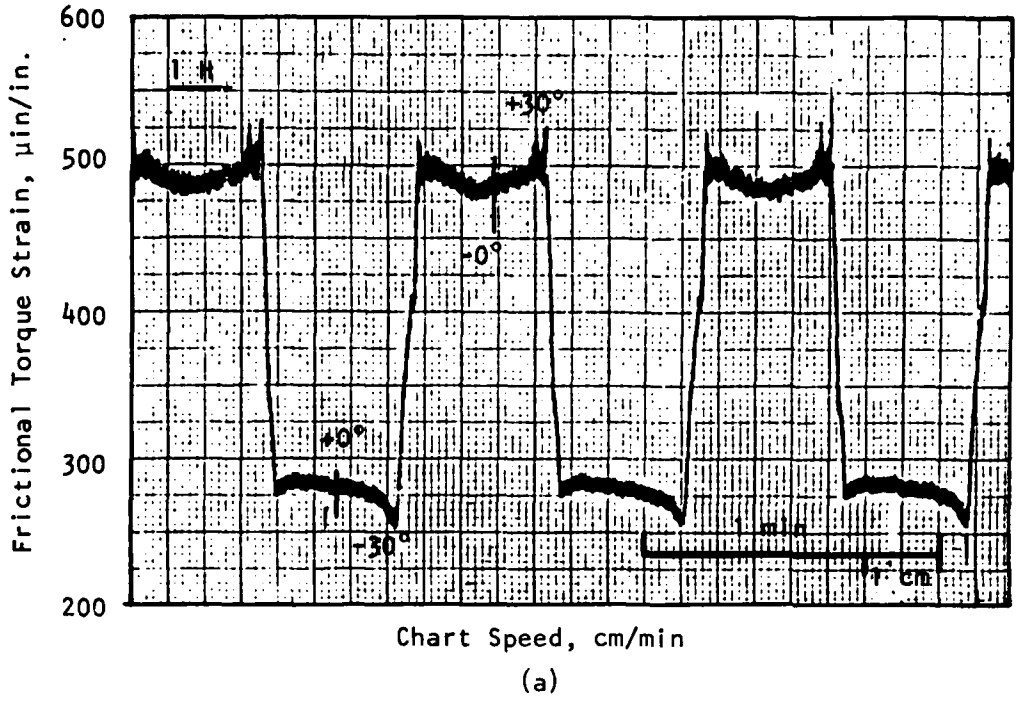

(a)

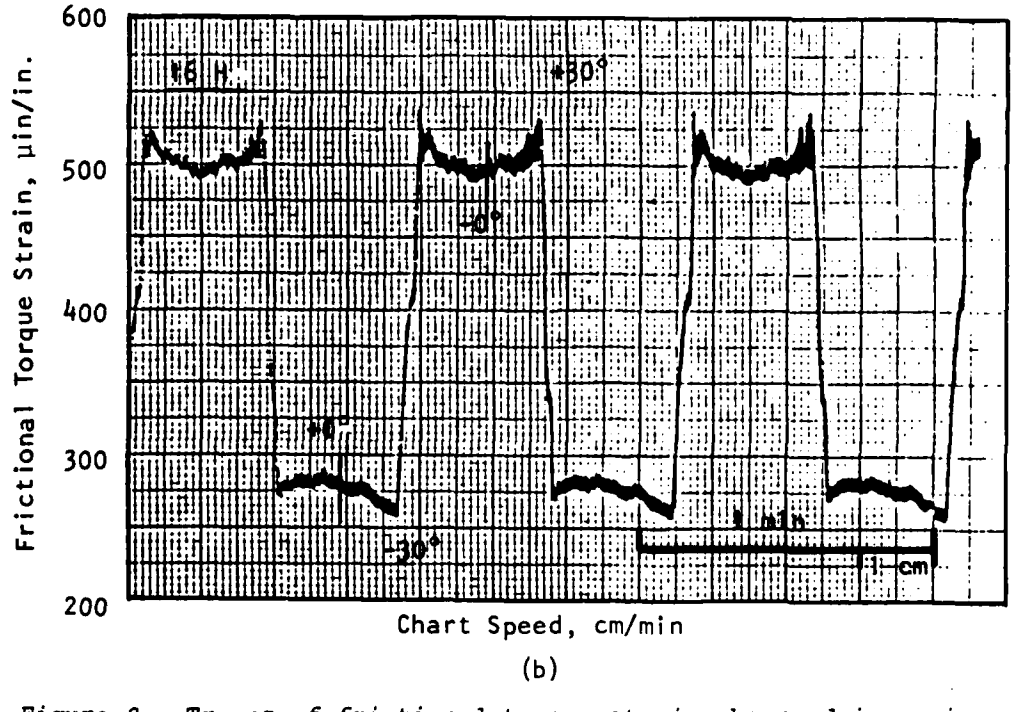

(b)

Figure 8. Traces of frictional torque strain observed in various time periods for 52100 steel under 16 lbf (71.2 N) in distilled water (test 203). Amplitude: 60° (π/3 rad); frequency: 1 cpm (17 mHz).

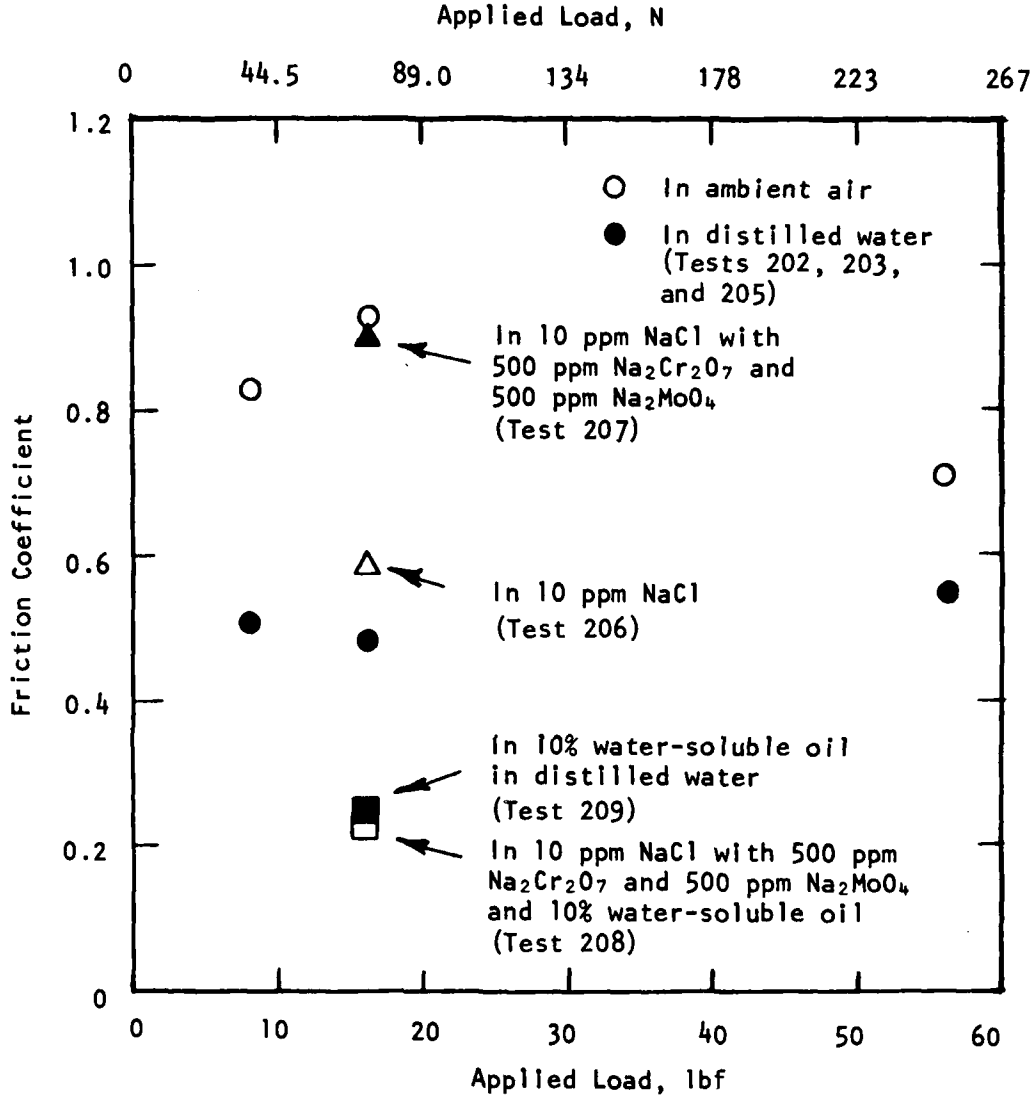

Figure 9. Friction coefficient of 52100 steel disk and pin electrodes with oscillatory motion under various test conditions. (Amplitude: 60° (π/3 rad); frequency: 1 cpm (17 mHz).

Tests 214 and 216 (M50 steel). In 10 ppm NaCl solution with 500 ppm $Na_2Cr_2O_7$ and 500 ppm Na_2MoO_4, an increase in load level from 16 to 56 lbf (71.2 to 249 N) at 1 cpm (17 mHz) decreased the f value significantly from 0.71 to 0.47.

Tests 222 and 225 (M50 steel). In 100 ppm NaCl solution with 0.01M (690 ppm) $NaNO_2$ and 0.01M (2060 ppm) Na_2MoO_4, an increase in load level from 16 to 56 lbf (71.2 to 249 N) at 1 cpm (17 mHz) decreased the f value significantly from 0.59 to 0.35.

Tests 224 and 226 (M50 steel). The electrolyte condition was the same as the one for the above case (tests 222 and 225), but not the oscillating frequency. With oscillating frequency of 10 cpm (170 mHz), an increase in load level from 16 to 56 lbf (71.2 to 249 N) resulted in very small change in f, from 0.50 to 0.53.

Tests 239 and 240 (M50 steel). In 100 ppm NaCl solution with 10% water-soluble oil, an increase in load level from 16 to 56 lbf (71.2 to 249 N) at 10 cpm (170 mHz) resulted in a negligible change in f value, from 0.13 to 0.12. In the presence of lubricant in the electrolyte, the friction coefficient, in general, was not affected by most corrosion-wear parameters used in this program such as load, oscillatory motion, and electrolyte compositions.

(b) Frequency Effect

Tests 222 and 224. In 100 ppm NaCl solution with 0.01M $NaNO_2$ and 0.01M Na_2MoO_4, an increase in oscillating frequency from 1 to 10 cpm (17 to 170 mHz) under 16 lbf (71.2 N) decreased the f value from 0.59 to 0.50.

Tests 225 and 226. The electrolytes of these two tests were the same as the one used for the previous two (tests 222 and 224), but the load was higher. Under 56 lbf (249 N), an increase in oscillating frequency from 1 to 10 cpm (17 to 170 mHz) increased the f value from 0.35 to 0.53.

The measured friction coefficient is the ratio of the observed torque to the applied torque. The observed torque is determined essentially by three factors which are mutually independent of one another: (1) the number of true contacts between surface asperities, (2) the areas of each contact, and (3) the shear strength of each contact junction. Amontons' law indicates that the coefficient of friction is independent of the applied load. However, under

sliding wear condition, frictional force can affect localized asperity temperature which may be responsible for two metallurgical effects on the sliding interfaces. One is enhanced chemical reaction of the surface with the environment which may form surface compounds affecting the frictional resistance, and the other, thermal softening which may cause additional deformation and enlargement of the true contact area.

Frictional force, F, between hard materials such as M50 steel can be expressed by

$$F = A_t \tau$$

where A_t is the true area of contact, and τ is the junction shear strength. Since the applied normal stress, W, is expressed by

$$W = A_t \sigma_y$$

where σ_y is the yield stress of metal, the coefficient of friction, f, can also be expressed by

$$f = F/W = \tau/\sigma_y$$

Since a localized asperity temperature increase under sliding condition may affect both τ and σ_y along with contact area enlargement and enhanced chemical reaction with the environment, the load and frequency effects on the friction coefficient of M50 steel were carefully analyzed also taking into consideration the electrolyte composition.

Table 3 summarizes the effect of load and frequency on friction coefficient with brief phenomenological observations. As discussed above, under sliding wear conditions, frictional forces can cause localized asperity temperature increase which may result in two important effects. If the temperature rise is significant, enhanced chemical reaction with the environment will occur. Also, localized high temperatures at asperity tips may cause additional deformation and enlargement of the true contact area. Contact area enlargement will increase frictional forces while increased metal-environment interaction will tend to decrease metal-to-metal contact and, consequently, frictional forces will decrease.

TABLE 3. EFFECT OF LOAD AND FREQUENCY ON FRICTION COEFFICIENT

Test No.	Load, lbf	Frequency, cpm	Friction Coefficient (f)	Observation
			Effect of Load	
214	16	1	0.71	Higher load more effectively increases metal-environment reaction with minimal effect in enlarging real contact area due to greater opportunity for heat dissipation at low frequency.
216	56	1	0.47	
222	16	1	0.59	
225	56	1	0.35	
224	16	10	0.50	At the higher frequency, a balance between higher heat retention causing real contact area increase (lower asperity strength) with an increase in f is balanced by large increase in reaction product, as was observed.
226	56	10	0.53	
			Effect of Frequency	
222	16	1	0.59	Higher frequency increases heat retention sufficently to cause higher reaction product generation and lowers f, while additional contact area increase was not proportionately high; thereby a net lowering in f was noted.
224	16	10	0.50	
225	56	1	0.35	At higher load and frequency, real contact area enlargement due to higher heat retention will be significant, thereby increasing shear forces and f.
226	56	10	0.53	

1 lbf = 4.45 N; 1 cpm = 17 mHz.

A decrease in the f value with increase in load at 1 cpm (17 mHz) (tests 214 vs. 216 and 222 vs. 225) may be interpreted as follows: Since the system was immersed in an aqueous media, thermal effects sufficiently large to increase real contact area due to an increase in load from 16 to 56 lbf (71.2 to 249 N) at low frequency [1 cpm (17 mHz)] will be minimal due to longer time available for heat dissipation (at the lower frequency). Thus, a total real contact area enlargement due to thermal effect is likely to be negligible and frictional force increase will also be minimal. On the other hand, in the presence of corrosion inhibitors ($NaNO_2$, Na_2MoO_4, and $Na_2Cr_2O_7$) with

passivation assumed by the formation of oxides (γ-Fe_2O_3, MoO_3, and Cr_2O_3), additional formation of oxides due to localized friction heating is likely to occur. An increase in the proportion of oxide in the true contact area will reduce metal-to-metal contact area and will decrease the total shear force to rupture these contact junctions (assuming a lower shear strength of the oxides as compared to metal); consequently, f will decrease, as was observed.

No significant change in the f value of M50 steel with increase in load at 10 cpm (170 mHz) (tests 224 vs. 226) would be due to a balance in these two effects (mentioned above) at the higher frequency.

A small decrease in the f value due to an increase in frequency at low load of 16 lbf (71.2 N) may mean that the localized asperity frictional heat retention (at the higher frequency) might have increased oxide formation which sheared relatively more easily than metal junctions. A low f value at 1 cpm (17 mHz) under 56 lbf (249 N) (test 225) would be due to the greater effectiveness of frictional heat to increase the relative oxide contact area with a reduction in f. On the other hand, at 10 cpm (170 mHz) under 56 lbf (249 N) (test 226), the additional heat retention at a higher frequency may significantly enlarge the true area of contact and increase the frictional forces, as was observed.

5.1.3 Effect of Electrolyte

The effect of elecrolyte on friction coefficient of 52100 and M50 steels was studied in different combinations of NaCl concentration, inhibitor, and lubricant. The friction coefficient data are presented in Table D-1, and a graphical presentation for 52100 steel is given in Fig. 9.

(a) Effect of NaCl Concentration

Tests 203, 206, 211c, 213, 215, and 217. The effect of NaCl concentration on the f value was studied in the range 0-100 ppm NaCl under 16 lbf (71.2 N). No particular change in the f value due to an increase in NaCl concentration was observed using both softer (non-heat-treated) and harder (heat-treated) pin electrodes. In 100 ppm NaCl solution (test 217), M50 steel corroded moderately with several pits along the wear track. However, no effect of corrosion product and/or localized pits on the f value was detected.

(b) Effect of Inhibitor

Tests 206, 207, and 211a; 211b and 211c; and 214 and 215. Addition of 500 ppm $Na_2Cr_2O_7$ and 500 ppm Na_2MoO_4 in 10 ppm NaCl solution significantly increased the f values of 52100 and M50 steels. Such increases were observed while using both soft (non-heat-treated) and hard (heat-treated) pin electrodes. Repeated test results confirmed that dichromate and molybdate had increased the friction coefficient. It may be assumed that surface reaction and formation of chromic and molybdic oxides may contribute to the increase in area of contact and thus increase the f values because the oxides, unlike sulfides, are not friction modifiers. Other factors modifying the number of contacts and junction shear strength will also affect the overall f value.

Tests 217, 218, 219, 220, and 222. All tests were conducted with M50 steel in 100 ppm NaCl solution with 16 lbf (71.2 N) at 1 cpm (17 mHz) with different combinations of corrosion inhibitors and lubricant. Without any corrosion inhibitor and lubricant, the f value was 0.52 (test 217). An addition of 500 ppm of Na_2CrO_4 (test 218) increased the f value from 0.52 to 0.69, while an addition of 500 ppm Na_2MoO_4 (test 219) changed it from 0.52 to 0.61. However, an addition of $NaNO_2$ (test 220) showed no indication of a change in the f value obtained with no inhibitor (test 217). With a combined addition of two inhibitors, 0.01M (690 ppm) $NaNO_2$ and 0.01M (2060 ppm) Na_2MoO_4 (test 222), the f value increased from 0.52 to 0.59. A similar increment was observed with the addition of molybdate alone. These observations also suggest that addition of $NaNO_2$ to NaCl solution did not modify the frictional forces.

When chromate (or dichromate) and molybdate were present, it was assumed that surface reaction and formation of chromic and molybdic oxides may contribute to an enlargement in the true area of contact with an increase in the f value because the oxides, unlike the sulfides, have generally higher friction coefficients. Other factors modifying the number of contacts and junction shear strength will also affect the overall f value. When nitrite is present, it is known that formation of γ-Fe_2O_3 is responsible for passivation of steel. It is believed that formation of iron oxide is possible in low concentration of NaCl solution under dynamic wear condition due to frictional heat at contact interfaces. Therefore, addition of $NaNO_2$ to low concentration NaCl

solutions did not modify the friction reaction any further and showed values observed without the addition.

(c) Effect of Lubricant

Tests 208, 209, and 210 (52100 steel). Electrolytes for all three tests contained 10% water-soluble oil. Friction coefficients observed with the water-soluble oil were almost the same (0.23) regardless of the presence of 10 ppm NaCl and corrosion inhibitors. Lubricating oil effect was dominant in decreasing f as may be seen in comparing with the results obtained without the water-soluble oil (tests 203, 206, and 207).

Tests 221, 238 to 244, and 247 to 250 (M50 steel). Addition of 10% water-soluble oil to 100 ppm NaCl solution with various combinations of corrosion inhibitors decreased the f value significantly in all cases. The f value ranged between 0.11 and 0.47. In general, the friction coefficient value was consistently low when no corrosion inhibitor was used (tests 239, 240, 244, and 248), whereas the friction coefficient value showed quite a scatter when corrosion inhibitors were used (tests 242 vs. 247, and 250). As discussed in the previous section, the presence of $Na_2Cr_2O_7$ (or Na_2CrO_4) and Na_2MoO_4 in the corrosion-wear system may develop chromic and molybdic oxides which could contribute to an enlargement in the true area of contact with an increase in the f value. Under severe wear conditions, even in a lubricated system, it is possible that formation of such oxides would tend to increase the f value.

5.1.4 Effect of Wear Time

Dependence of friction coefficient on wear time varied primarily with corrosion-wear conditions including load and frequency levels and electrolyte composition. At 1 cpm (17 mHz), a 2-h run-in under load up to 16 lbf (71.2 N) both in distilled water and in NaCl solutions with concentration up to 100 ppm, yielded a stable friction coefficient value, and only a negligible increase was observed over a 24-h period. Hence, all the f values reported were obtained after a 2-h run-in under given wear conditions. However, an increase in load and frequency levels and the presence of corrosion inhibitors in the electrolyte revealed a significant effect of wear time on friction coefficient.

Table 4 shows the change in the value of friction coefficient of M50 steel with time in relation to various corrosion-wear test conditions. In

TABLE 4. CHANGE IN FRICTION COEFFICIENT OF M50 STEEL WITH TIME

Test No.	Wear Condition[a] Load, lbf	Frequency, cpm	Friction Coefficient (f) for Given Wear Time 2 h	4 h	8 h	24 h	48 h
224	16	10	0.50	-	-	0.85	-
225	56	1	0.35	-	-	0.59	-
226	56	10	0.53	-	-	0.81	-
229	16	1	0.59	-	0.69	0.82	0.92
230	16	1	0.48	-	-	-	0.51
231	16	1	0.59	0.65	0.72	0.76	0.86

1 lbf = 4.45 N; 1 cpm = 17 mHz.

[a]Oscillatory amplitude for all tests was 60° (π/3 rad).

test 225, an increase in load level to 56 lbf (249 N) at 1 cpm (17 mHz) resulted in an increase in f value from 0.35 to 0.59 for wear time from 2 to 24 h. At 10 cpm (170 mHz), both load levels of 16 and 56 lbf (71.2 and 249 N) showed significant increases in f values with time over a 24-h period (tests 224 and 226). Data for tests 229, 230, and 231 are presented graphically in Fig. 10. At 16 lbf (71.2 N) and 1 cpm (17 mHz), the friction coefficient of M50 steel tested in 100 ppm NaCl solution showed only a negligible increase over a 48-h period (test 230). At the same load and frequency level, the presence of corrosion inhibitor in 100 ppm NaCl solution resulted in a different behavior of friction coefficient with wear time. Addition of 0.01M $NaNO_2$ and 0.01M Na_2MoO_4 (test 229) and of 0.01M $NaNO_2$ and 0.01M Na_2MoO_4 (test 231) to 100 ppm NaCl solution increased the friction coefficient of M50 steel with time significantly over a 48-h period. From Fig. 10, one may assume that the presence of chromate and molybdate was contributing to the increase in f value with wear time and that nitrite was not affecting f values.

The absolute increase in f with wear time may indicate a continuing smoothing of the surface due to wear and corrosion, and a consequent enlargement of total asperity contact area. Also, the surface reaction products formed with different inhibitors will be different and might have different shear properties contributing to f values. The relative increase in f value

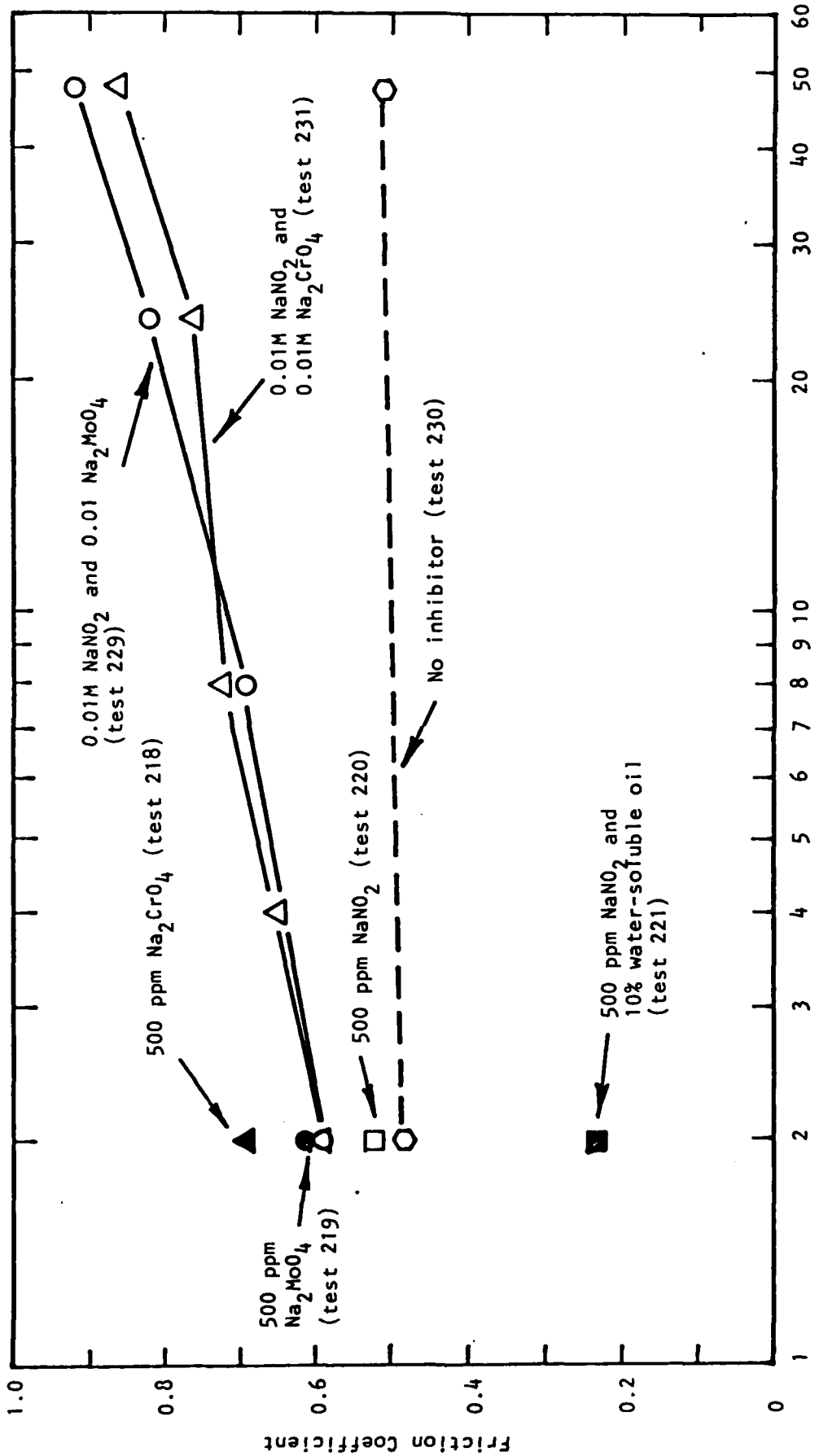

Figure 10. Effect of wear time on the friction coefficient of M50 steel in 100 ppm NaCl solution with various corrosion inhibitors under 16 lbf (71.2 N) at 1 cpm (17 mHz) and 60° (π/3 rad) amplitude.

between different test conditions will also depend on the relative contact areas composed of metal-to-metal and oxide-to-oxide or mixed metal-to-oxide.

5.1.5 Effect of Overpotential

The effect of overpotential on the f values was observed by holding the sample under wear condition at either anodic or cathodic overpotential. The sample was held under a given condition for sufficiently long time to allow surface modification, if any, to occur. Table 5 compares the f values of 52100 and M50 steels obtained at different overpotentials with those obtained their respective open-circuit potentials. In general, it was observed that the f values obtained at overpotentials were slightly less than those obtained at the open-circuit potentials. It may be assumed that at high anodic overpotentials, the true area of contact may increase because of high random distribution of corrosion products between the rubbing surfaces due to a high rate of metal dissolution. On the other hand, f may decrease if the presence of corrosion products at the rubbing interface lowers the shearing force and/or if development of many localized pits reduces the true area of contact. Figure 11 shows the wear tracks of disk and pin electrodes for test 213. The disk electrode corroded severely with many pits in the wear track, but no pit

TABLE 5. FRICTION COEFFICIENT MEASURED AT DIFFERENT POTENTIALS

Test No.	Material	Friction Coefficient (f)	Measured Potential, mV	Holding Time at the Potential, h
213	52100 steel	0.52	Open-circuit	-
		0.41	+600	17
214	M50 steel	0.71	Open-circuit	-
		0.68	-1400	16
215	M50 steel	0.54	Open-circuit	-
		0.47	-1200	16
216	M50 steel	0.47	Open-circuit	-
		0.49	a	-

[a]Measured right after anodic polarization to +700 mV.

SEM No. 9684 25X SEM No. 9685 500X

(a) (b)

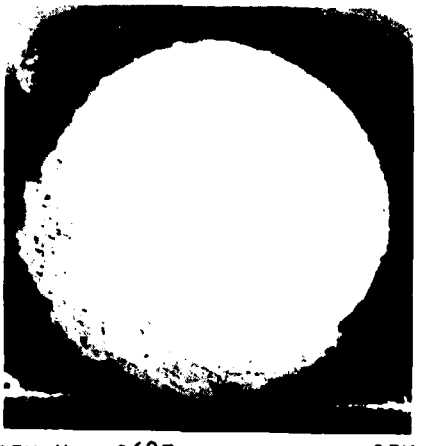

SEM No. 9687 25X

(c)

Figure 11. SEM micrographs of 52100 steel disk and pin electrodes (test 213); (a) general surface morphology of wear track on the disk, (b) a pit on the disk, and (c) wear scar of the pin.

was observed on the wear scar of the pin. It appears that the decrease in f value observed at high anodic potential is due to the presence of corrosion products at the interface, and development of corrosion-wear pits would be an additional effect.

At high cathodic overpotentials, if generation of hydrogen causes an embrittlement problem (decrease in junction shear strength), the f value will be affected and further aggravated by additional surface irregularity caused by removal of metal from the rubbing surfaces. From tests 214 and 215, no such effects were observed. However, the f value decreased slightly in both cases when compared with the f values obtained at the open-circuit potential. It appears that the decrease in the f value may be related to the "polishing effect" due to long exposure under wear.

5.2 ELECTROCHEMICAL BEHAVIOR

Electrochemical behavior of 52100 and M50 steels was studied under various corrosion-wear conditions through open-circuit potential and electrode polarization measurements. The factor effects on electrochemical behavior (including presence/absence of inhibitors and/or a lubricant, load, and frequency) were extensively studied. Table D-2 in Appendix D summarizes the electrochemical data on open-circuit potential and corrosion current density; test conditions for each test are given in Table D-1. For M50 steel, only a part of the results are presented in this section; the rest are presented in Section 5.6 under statistical analysis.

The oscillatory amplitude was kept constant at 60° ($\pi/3$ rad) in all tests, but oscillatory frequency varied from 1 to 10 cpm (.7 to 170 mHz). The disk electrodes were coated with epoxy resin except for the contact area and its immediate vicinity, as shown earlier in Fig. 4. The uncoated areas of the disk electrode were 0.25 and 0.20 $in.^2$ (1.6 and 1.3 cm^2) for tests 206-220, and tests 221-250, respectively. Therefore, the approximate ratio of the corrosion-wear scar area to the corroded non-wear area was 1 to 4 for the former, and 1 to 3 for the latter tests. The pin electrodes for all the tests were completely coated except for the actual contact area. Detailed descriptions of the potential scanning methods for polarization measurements are given in Appendix C.

5.2.1 Open-Circuit Potential Behavior

The open-circuit potential of the test materials varied with time depending on the corrosivity of the electrode. In general, the open-circuit potential of bearing steels under no-wear condition became more electronegative when corroded, and more electropositive when passivated. Both M50 and 52100 steels corroded in NaCl solution with concentration as low as 10 ppm. However, addition of various corrosion inhibitors effectively passivated the materials, and the amount of corrosion inhibitor added was determined according to test material/electrolyte combination.

Figure 12 shows a typical transitional behavior of open-circuit potential and frictional torque strain of a passivated material upon loading. An addition of 500 ppm $Na_2Cr_2O_7$ and 500 ppm Na_2MoO_4 completely passivated 52100 steel in 10 ppm NaCl solution (test 207), and the open-cirucit potential under no-load condition was -115 mV. The oscillatory motion was 60° (π3 /rad) amplitude and 1 cpm (17 mHz). With 16 lbf (71.2 N) loading, the potential dropped immediately to -185 mV due to disruption of the passive film. As the surface motion under wear continued, the open-circuit potential gradually decreased and the frictional torque strain gradually increased. Under wear conditions, the potential reading was not stable but fluctuating, in general, approximately ±20 mV from the average value. Most likely, the fluctuations were related to the passive film disruption in one area with simultaneous reformation in another area. The range of potential fluctuations usually increased with the degree of wear with values as high as ±40 mV from the mean value. The potential also changed with time, and reached a steady-state value approximately 2-6 h after loading depending on the corrosion-wear conditions. Figure 13 shows traces of open-circuit potential and frictional torque strain observed 2 h after loading (test 207). It is to be noted that both the open-circuit potential and the frictional torque strain had reached steady-state values; however, the open-circuit potential fluctuated in the range between -205 and -225 mV as the electrode oscillated.

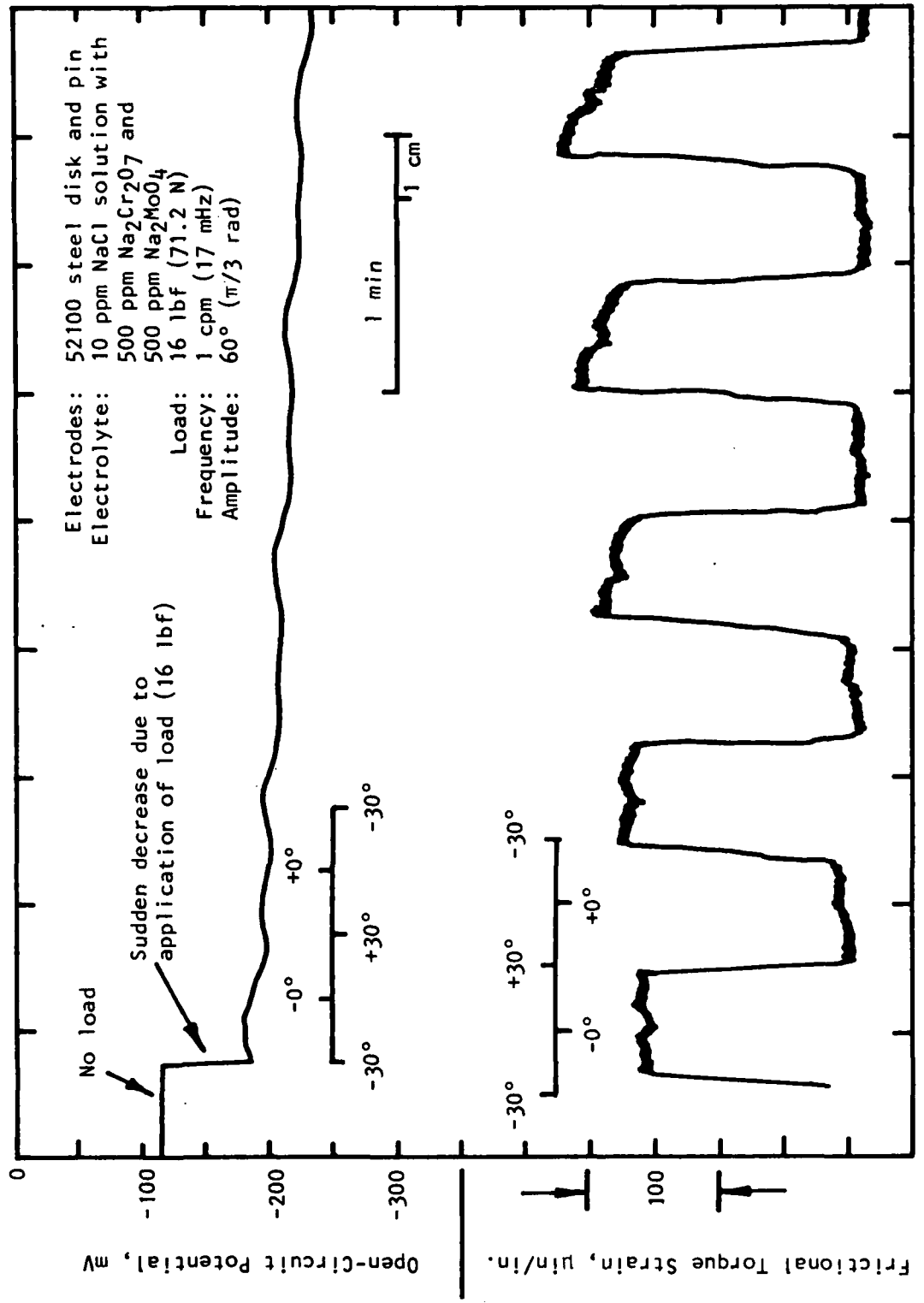

Figure 12. Traces of open-circuit potential and frictional torque strain upon loading (test 207).

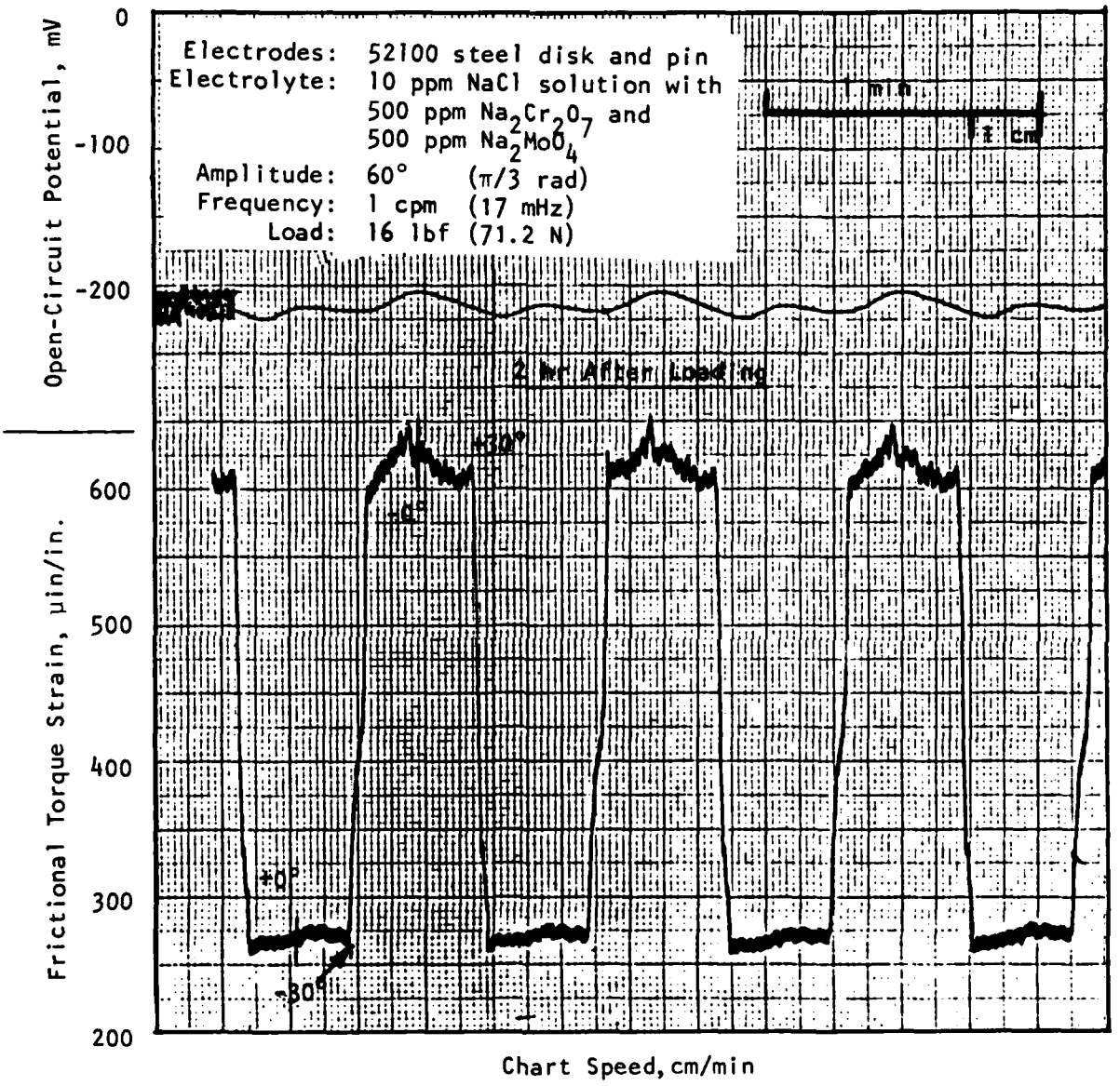

Figure 13. Traces of open-circuit potential and frictional torque strain after 2 h (test 207).

The effect of wear on the open-circuit potential was discussed extensively in prior studies[2,3] for both protective and non-protective film forming conditions. It was shown that the effect of continuous wear provided by full rotational motion was very significant when a protective film could be formed in air or in solution, but almost negligible when non-protective film was formed. Initial disruption of the protective film was the principal factor in decreasing the open-circuit potential to the more electronegative direction. The additional surface deformation by subsequent increments of load did not significantly change the open-circuit potential.

In the present study with oscillatory motion, observations on the effect of wear on open-circuit potential were similar to those observed with full rotational motion. One interesting observation, however, was the effect of oscillatory frequency. Table 6 lists the values of open-circuit potentials of M50 steel observed under various combinations of load and oscillatory frequencies. The electrolyte condition for the four tests was 100 ppm NaCl solution with 0.01M $NaNO_2$ and 0.01M Na_2MoO_4. In this electrolyte, M50 steel was passivated and the open-circuit potential under no-wear condition was between -160 and -180 mV. An examination of the open-circuit potential values shown in Table 6 indicates that an increase in oscillatory frequency under a constant load decreased the open-circuit potential, whereas an increase in load at a constant oscillatory frequency had no significant effect. This indicates that a highly active surface is obtained by increasing interfacial motion under constant load rather than by increasing load at constant interfacial motion. A further decrease in the open-circuit potential by increasing oscillatory frequency after an initial potential drop by disruption of passive film also resulted in an increase in corrosion rate as discussed in the next section.

---

[2]K. Y. Kim, S. Bhattacharyya, and V. Agarwala, in Wear of Materials, p. 772, Proc. 3rd Int. Conf. on Wear of Materials, ASME, San Francisco, CA (1981).

[3]V. Agarwala, K. Y. Kim, and S. Bhattacharyya, in Materials Evaluation Under Fretting Conditions,, S. R. Brown (Ed.), p. 106, ASTM STP 780 (1982).

TABLE 6. OPEN-CIRCUIT POTENTIAL OF M50 STEEL AS A FUNCTION OF LOAD AND FREQUENCY

Test No.	Wear Condition[a] Load, lbf (N)	Oscillatory Frequency, cpm (mHz)	Open-Circuit Potential, mV
223	16 (71.2)	1 (17)	-320 ± 20
224	16 (71.2)	10 (170)	-500 ± 30
225	56 (249)	1 (17)	-320 ± 20
226	56 (249)	10 (170)	-480 ± 20

[a]Electrolyte: 100 ppm NaCl with 0.01M $NaNO_2$ and 0.01M Na_2MoO_4.

5.2.2 Polarization Measurements

(a) Effect of Corrosion Inhibitor and Lubricant

52100 Steel. Polarization behavior of 52100 steel was observed in different electrolyte conditions under 16 lbf (71.2 N) at 1 cpm (17 mHz), and is presented in Figs. 14 to 18. The polarization curve of 52100 steel tested in the electrolyte without inhibitor (tests 206 and 213) showed a simple iron dissolution curve and an oxygen reduction curve, but both curves also showed strong indications of resistance polarization due to the low conductivity of 10 ppm NaCl solution. Addition of 500 ppm $Na_2Cr_2O_7$ and 500 ppm Na_2MoO_4 in 10 ppm NaCl solution (tests 207 and 211) resulted in passivation of the anodic component; however, an indication of pitting occurred at higher anodic potentials. A significant increase in the open-circuit potential (approximately 200 mV) resulted from the addition of corrosion inhibitors.

An addition of 10% water-soluble oil to the 10 ppm NaCl solution also passivated 52100 steel (test 210). A similar result was observed when the water-soluble oil was introduced in distilled water (test 209) and in 10 ppm NaCl solution with inhibitors (test 207), as shown in Figs. 17 and 18, respectively. Polarization curves observed under lubricated condition showed no indication of pitting even at +1200 mV. When compared with the polarization curves for test 211 (and test 207 in Fig. 16), the current density in the passive region decreased by almost one-half order of magnitude. It seems that

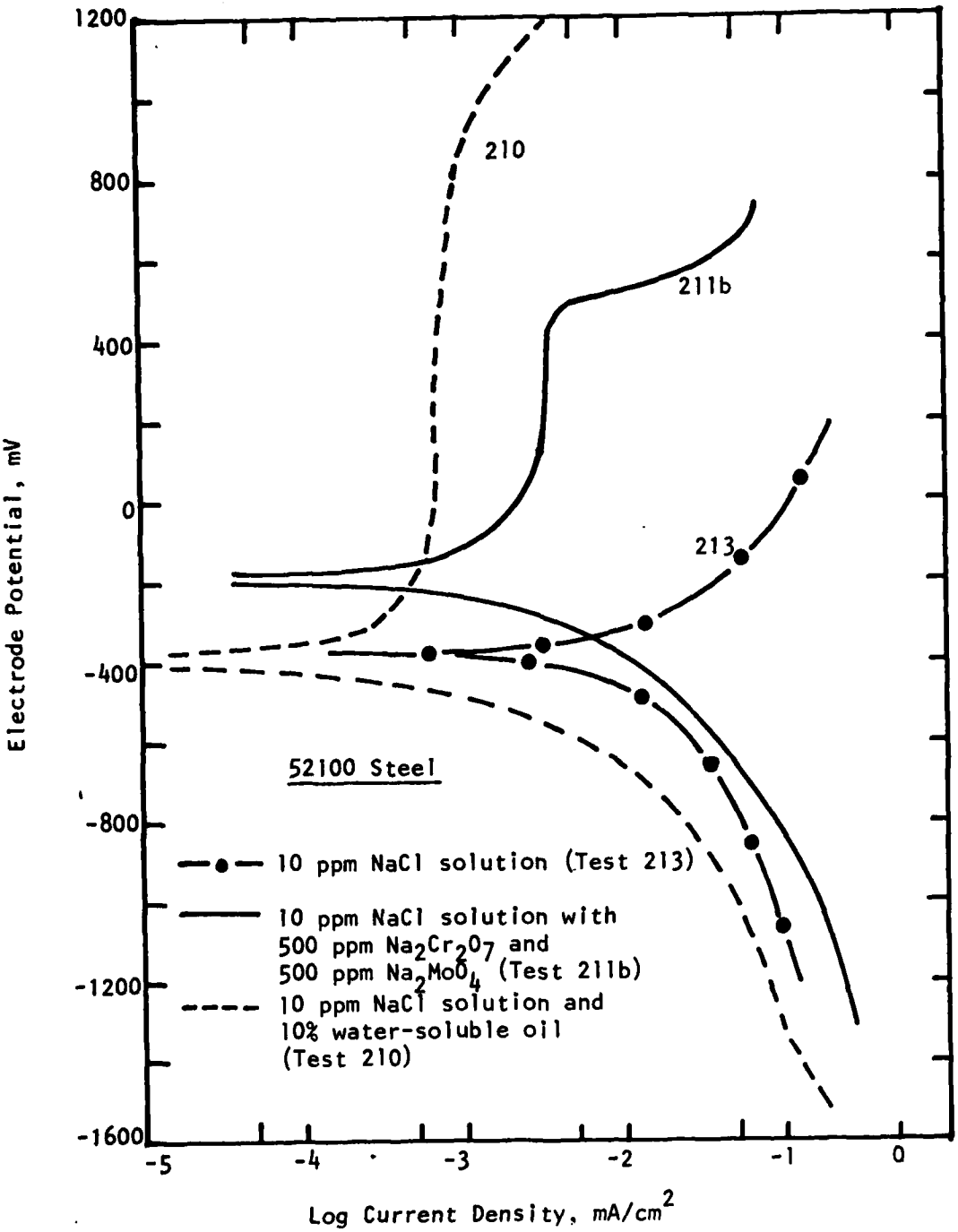

Figure 14. Polarization behavior of 52100 steel in different electrolytes with oscillatory motion under 16 lbf (71.2 N) load, 60° (π/3 rad) amplitude, 1 cpm (17 mHz) (tests 210, 211, and 213).

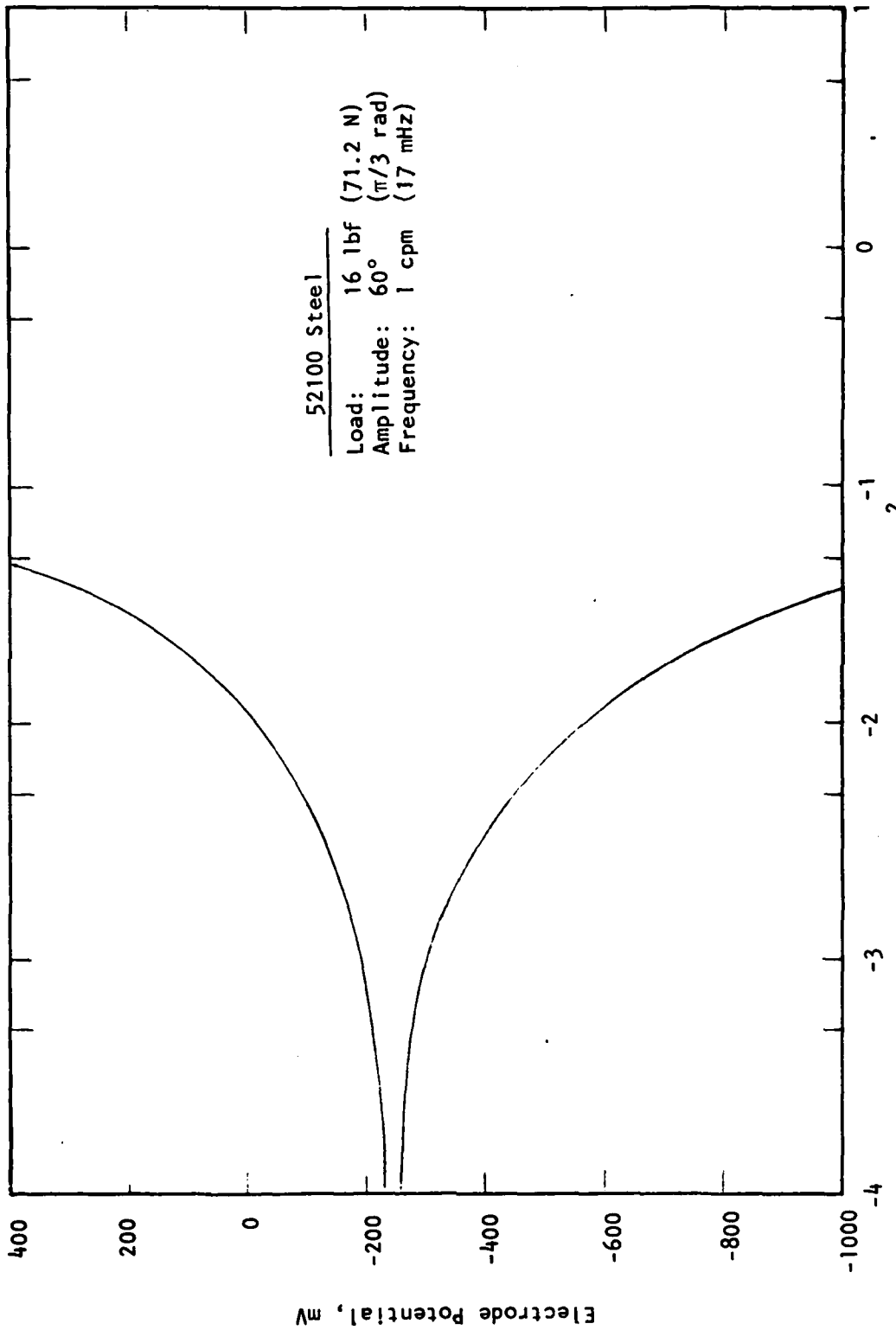

Figure 15. Polarization behavior of 52100 steel in 10 ppm NaCl solution (test 206).

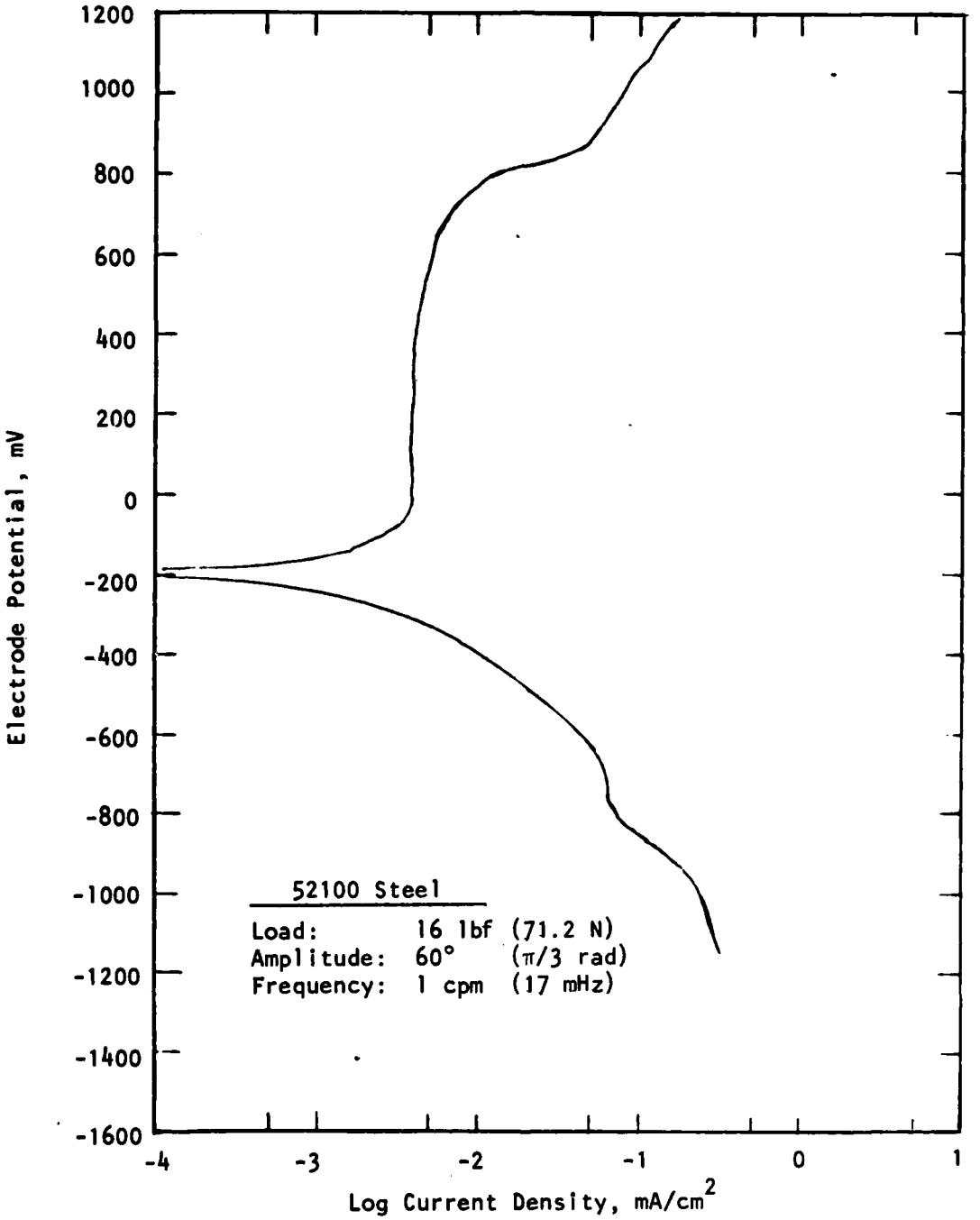

Figure 16. Polarization behavior of 52100 steel in 10 ppm NaCl solution with 500 ppm $Na_2Cr_2O_7$ and 500 ppm Na_2MoO_4 (test 207).

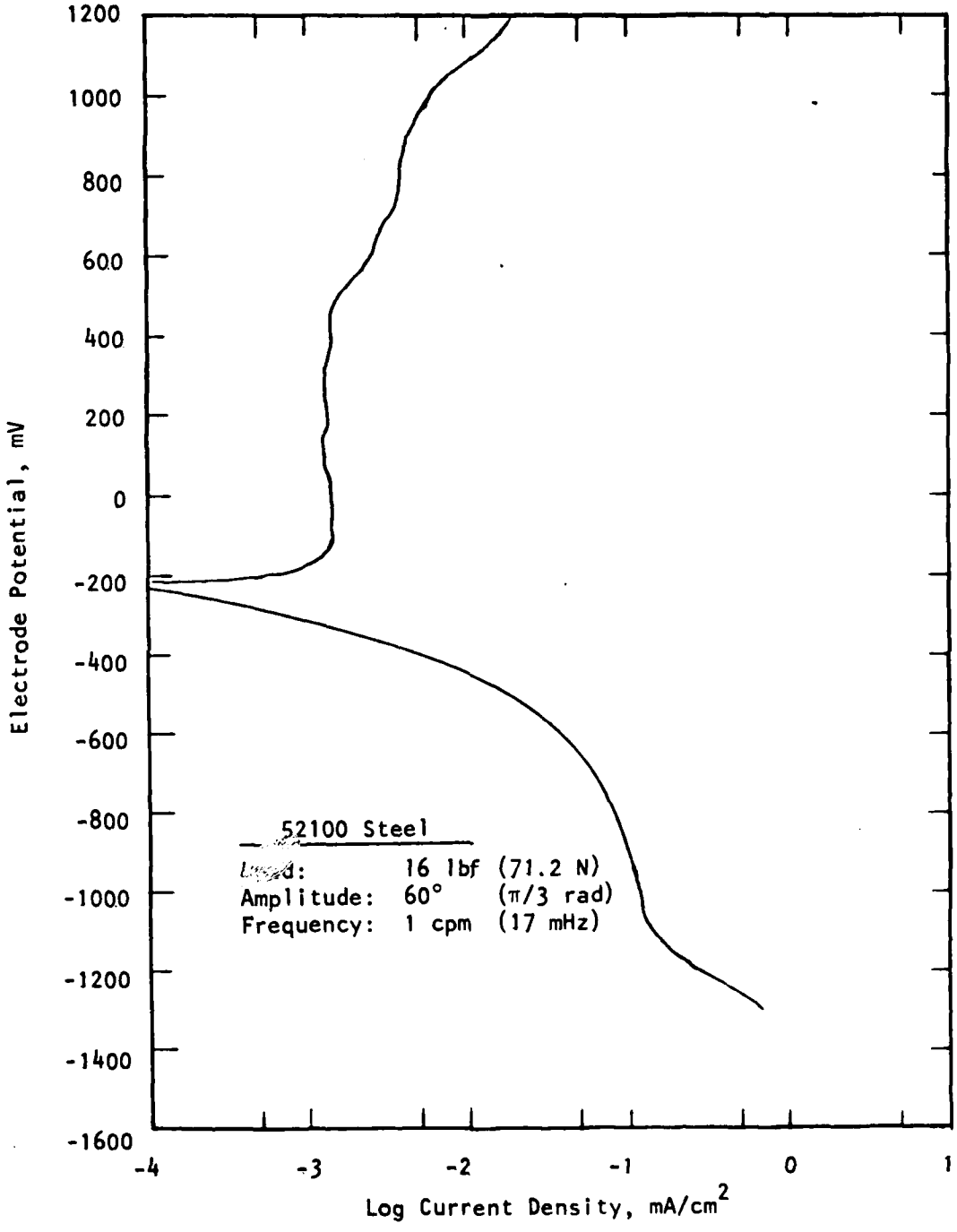

Figure 17. Polarization behavior of 52100 steel in 10 ppm NaCl solution with 500 ppm $Na_2Cr_2O_7$, 500 ppm Na_2MoO_4, and 10% water-soluble oil (test 208).

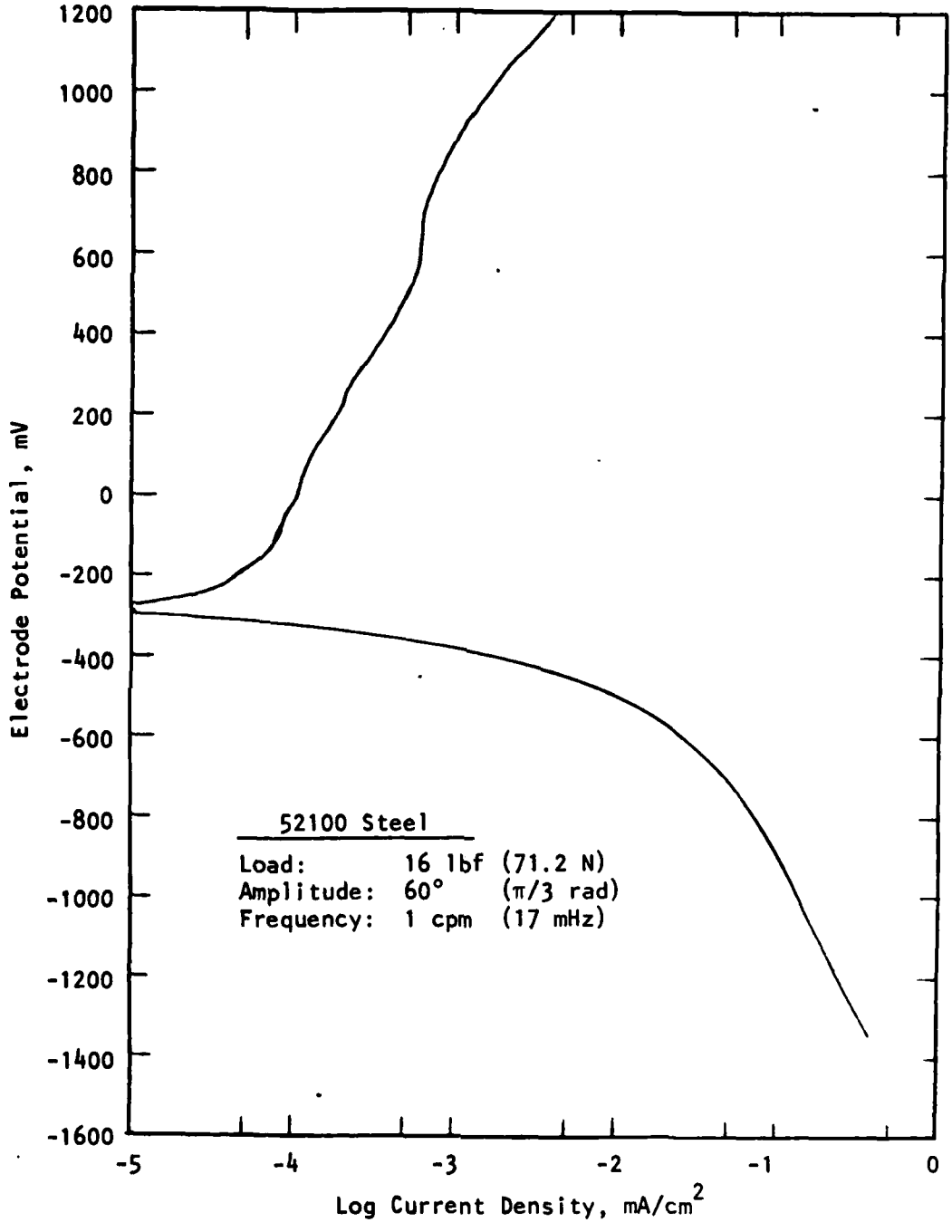

Figure 18. Polarization behavior of 52100 steel in distilled water and 10% water-soluble oil (test 209).

water-soluble oil had affected the corrosion-wear process by acting as a lubricant as well as a catalyst for corrosion inhibition, or by behaving by itself as a corrosion inhibitor to a certain degree.

M50 Steel. Figure 19 shows the individual effects of chromate, molybdate, and nitrite on the polarization behavior of M50 steel electrodes under no-wear condition. Polarization measurements were made without load after the pin electrode was tested under 16 lbf (71.2 N) at 1 cpm (17 mHz). This means that the surface of the disk electrode was subjected to wear prior to polarization measurements.

The M50 steel in 100 ppm NaCl solution without corrosion inhibitor (test 217) shows a simple anodic dissolution and high concentration polarization by oxygen reduction. The open-circuit potential and corrosion rate ($I_{corr.}$) were -360 mV and 1.0×10^{-2} mA/cm^2 (4.58 mpy), respectively. With the addition of 500 ppm Na_2CrO_4 in 100 ppm NaCl solution (test 218), the M50 steel electrode was passivated and the oxygen reduction rate was significantly suppressed. The net effect of these two electrode reactions was a significant decrease in the open-circuit potential and the corrosion current density which became -600 mV and 6.0×10^{-4} mA/cm^2 (0.27 mpy), respectively. With the addition of 500 ppm Na_2MoO_4 in 10 ppm NaCl solution (test 219), the M50 steel was also passivated; however, the oxygen reduction reaction was little affected. The open-circuit potential increased to -200 mV, but the corrosion current density decreased to 4.0×10^{-4} mA/cm^2 (0.18 mpy).

With the addition of 500 ppm $NaNO_2$ to 100 ppm NaCl solution (test 220), M50 steel was passivated; however, the oxygen reduction reaction was little affected, as was observed with addition of molybdate. The open-circuit potential and the corrosion current density were -180 mV and 5.0×10^{-4} mA/cm^2 (0.23 mpy), respectively. The overall polarization behavior was similar to the one observed with the addition of molybdate except at high anodic potentials where pitting was indicated with molybdate but not with nitrite.

Although all three corrosion inhibitors passivated M50 steel in 100 ppm NaCl solution, the potential range of passivation region was much larger with chromate than with either molybdate or nitrite. However, the current density in the passive region was slightly lower with either molybdate or nitrite than

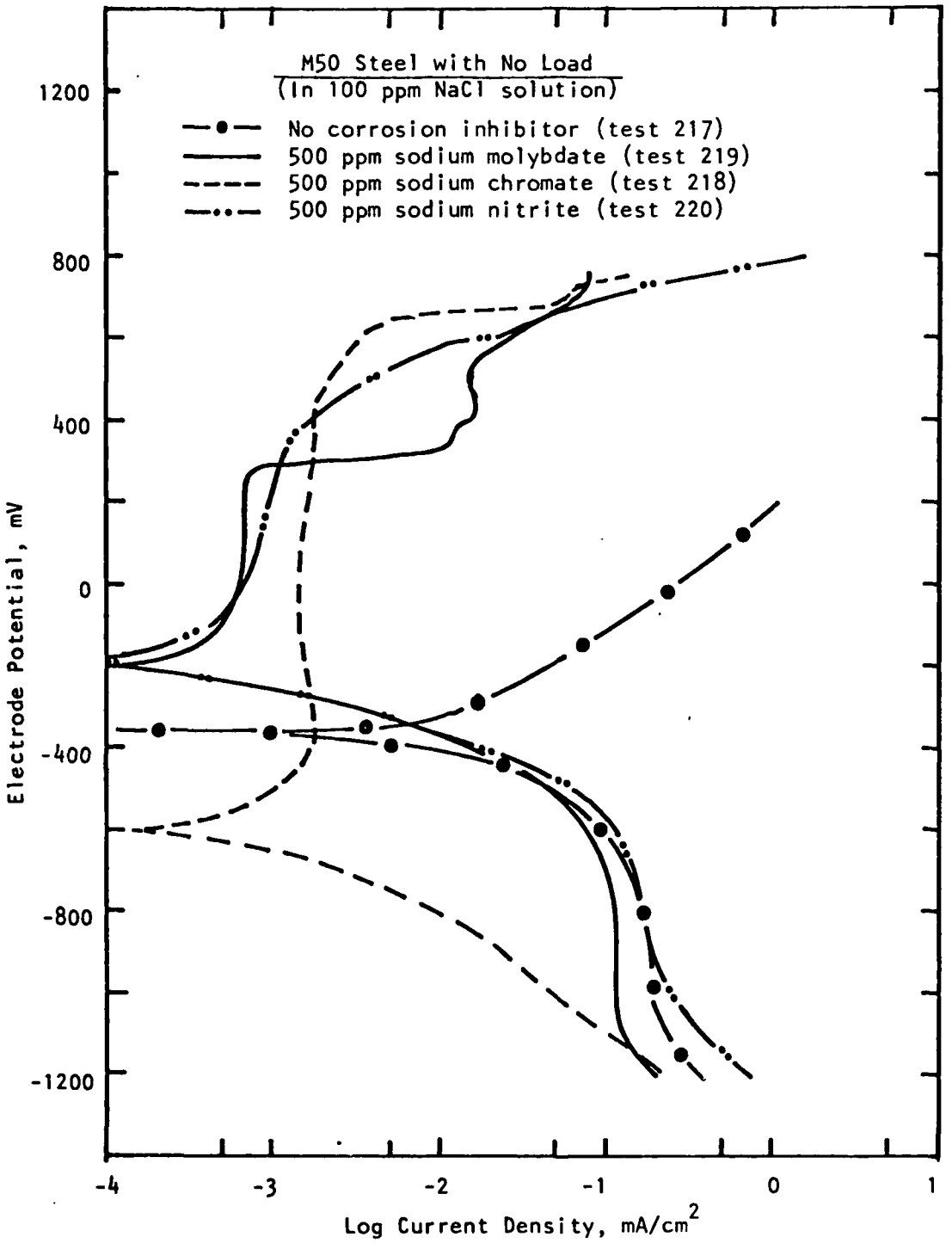

Figure 19. Effect of corrosion inhibitor on the polarization behavior of M50 steel under no-load conditions, 60° (π/3 rad) amplitude, 1 cpm (17 mHz) (tests 217, 218, 219, and 220).

with chromate. Pitting was indicated with molybdate and chromate at +300 and +600 mV, respectively, but not clearly with nitrite.

Figure 20 compares the polarization behavior of M50 steel in 100 ppm NaCl solution when different combinations of corrosion inhibitors and lubricant were used as follows:

- 500 ppm $NaNO_2$ (test 220)
- 500 ppm $NaNO_2$ and 10% water-soluble oil (test 221)
- 690 ppm (0.01M) $NaNO_2$ and 2060 ppm (0.01M) Na_2MoO_4 (test 222).

Prior to polarization measurements, the disk electrodes for all three tests were subjected to wear conditions as shown in Table D-1. The cathodic reactions of all three combinations seemed to be essentially the same governed by oxygen reduction reaction at low cathodic potentials and by hydrogen reduction reaction at high cathodic potentials. However, the cathodic cell current of test 221 with a water-soluble oil was significantly smaller through all cathodic potential ranges than that of the other two tests. It may be due to the resistance polarization effect caused by the presence of water-soluble oil which reduced the conductivity of the electrolyte.

During anodic polarization, all three tests showed passivation behavior; however, at high anodic potentials, test 221 with water-soluble oil showed a secondary passivation effect while the other two tests showed a steady increase in the cell current density up to +800 and +600 mV for tests 220 and 222, respectively. The favorable effect of lubricant was clearly observed. At lower anodic potentials, the cell current in the passive region was greater with molybdate addition (test 222) than with nitrite alone (test 220). It was somewhat contrary to expectation and two more tests (tests 223 and 227) were performed and the results compared with those of tests 220 and 222 to clarify the effect of molybdate addition to NaCl solution with nitrite.

The polarization curves for tests 222, 223 and 227 are shown in Fig. 21. The differences in test conditions among four comparative tests were as follows:

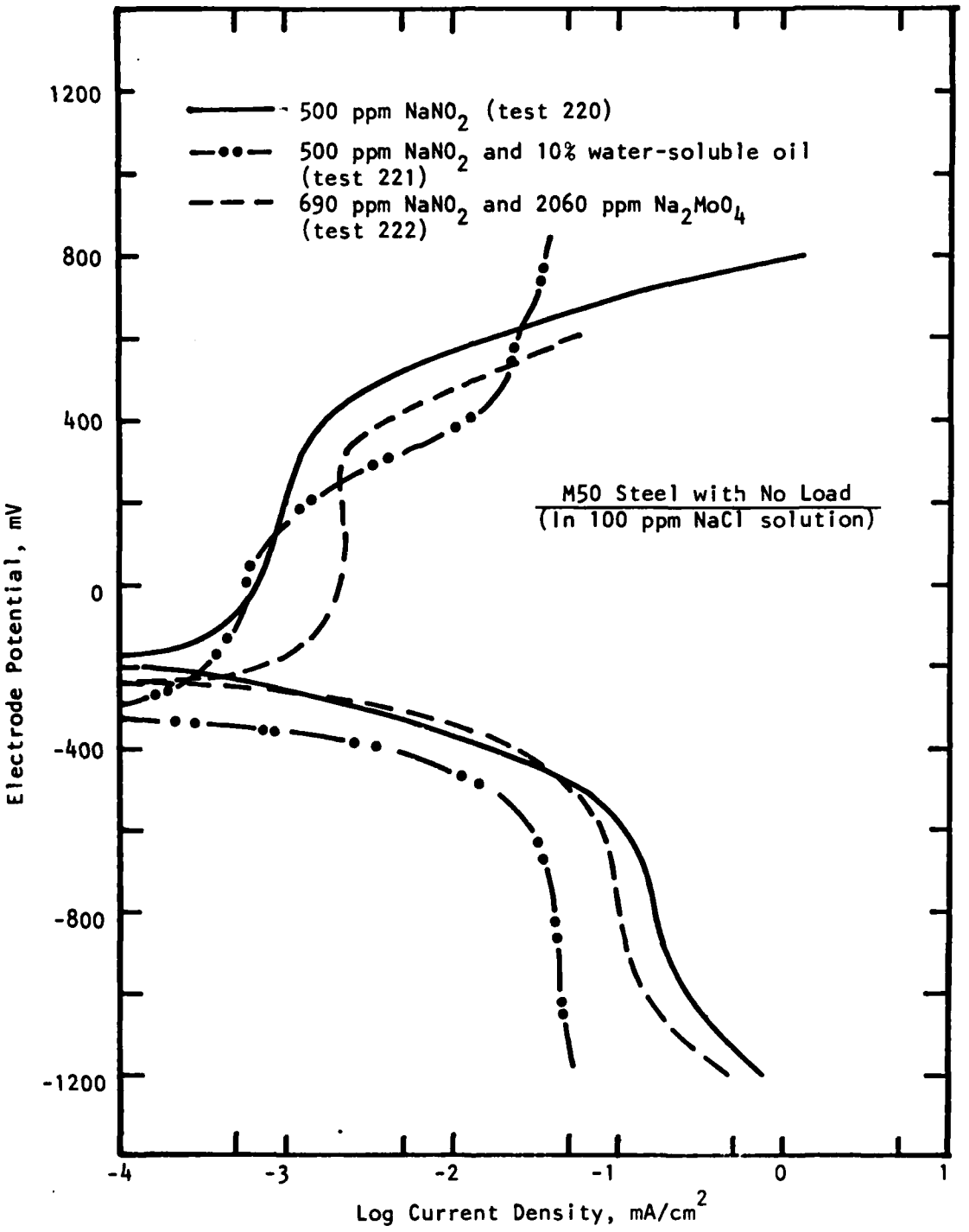

Figure 20. Effect of corrosion inhibitor and lubricant on the polarization behavior of M50 steel under no-load condition, 60° (π/3 rad) amplitude, 1 cpm (17 mHz) (tests 220, 221, and 222).

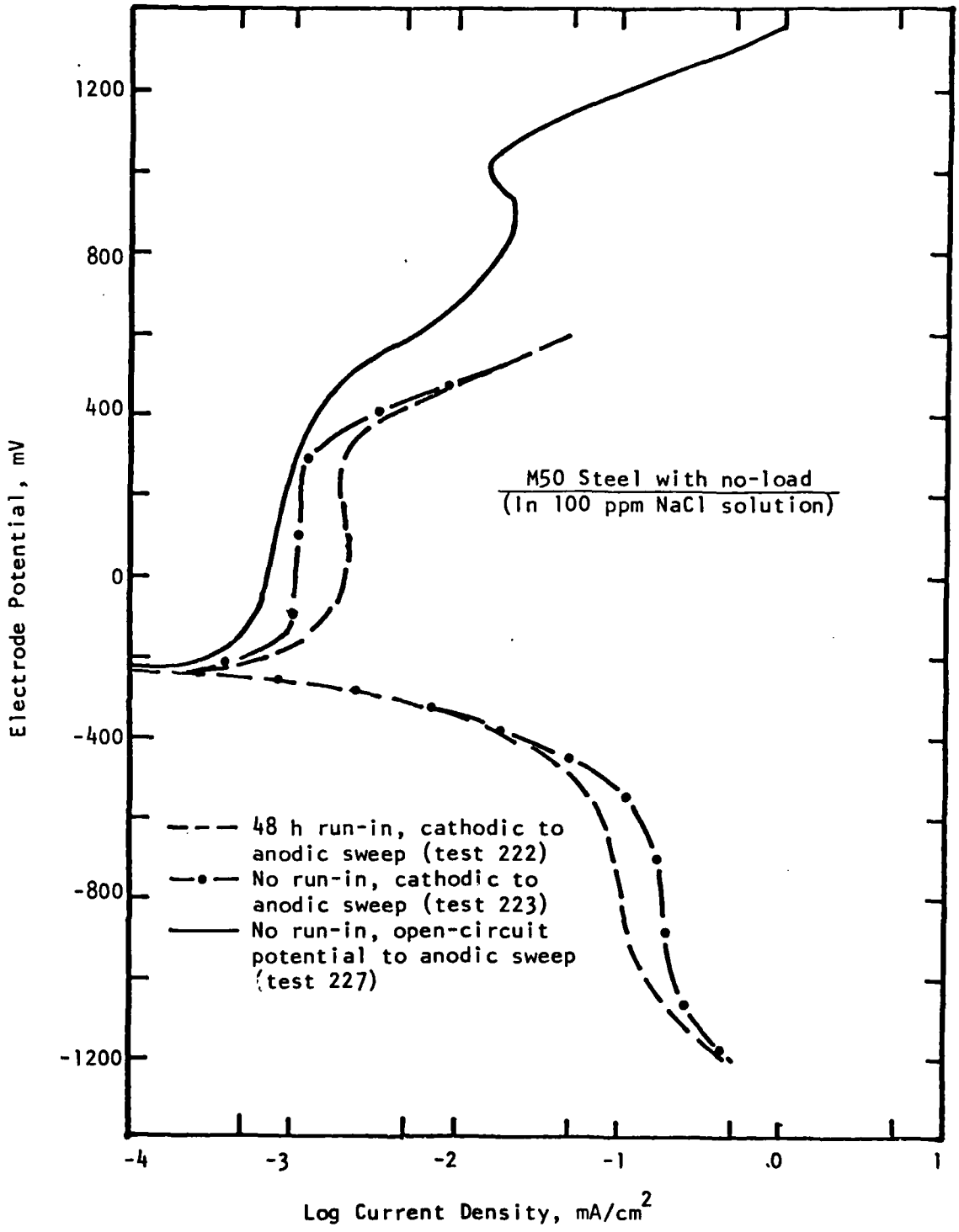

Figure 21. Effect of run-in and potential sweep on the polarization behavior of M50 steel under no-load condition, 60° (π/3 rad) amplitude, 1 cpm (17 mHz) (tests 222, 223, and 227).

Test	Run-in	Potential Sweep	Corrosion Inhibitors
220	Yes	Cathodic to anodic	Nitrite alone
222	Yes	Cathodic to anodic	Nitrite and molybdate
223	No	Cathodic to anodic	Nitrite and molybdate
227	No	Open-circuit to anodic	Nitrite and molybdate

- Tests 220, 222, 223, and 227. The effect of molybdate addition was more clearly observed at high anodic potentials than at low anodic potentials. A comparison between tests 220 (Fig. 20) and 227 (Fig. 21) shows that at +800 mV, the cell current density in test 220 (nitrite alone) was almost two orders of magnitude higher than that of test 227 (nitrite plus molybdate). With the addition of molybdate, a secondary passivation was observed at high anodic potentials up to +1000 mV where oxygen evolution became apparent; but no secondary passivation was observed with nitrite alone.
- Tests 222 and 223. An effect of run-in on the polarization behavior was observed on the cell current density in the passive region. The cell current density of the disk electrode with run-in prior to polarization measurement (test 222) showed a little higher value than that for the other: 2 vs. 1 $\mu A/cm^2$.
- Tests 223 and 227. The effect of potential sweep on the polarization behavior was studied. Potential sweep from the open-circuit to anodic potential showed lower cell current densities throughout all the anodic potential regions than potential sweep all the way from cathodic to anodic potential. Difference in the cell current value between them increased as the anodic potential increased. However, the open-circuit potential was the same for both tests, -220 mV.

Figure 22 shows polarization behavior of M50 steel tested in different electrolytes and under different loads. The effect of corrosion inhibitors was clearly demonstrated in the anodic component of tests 214, 216a, and 216b

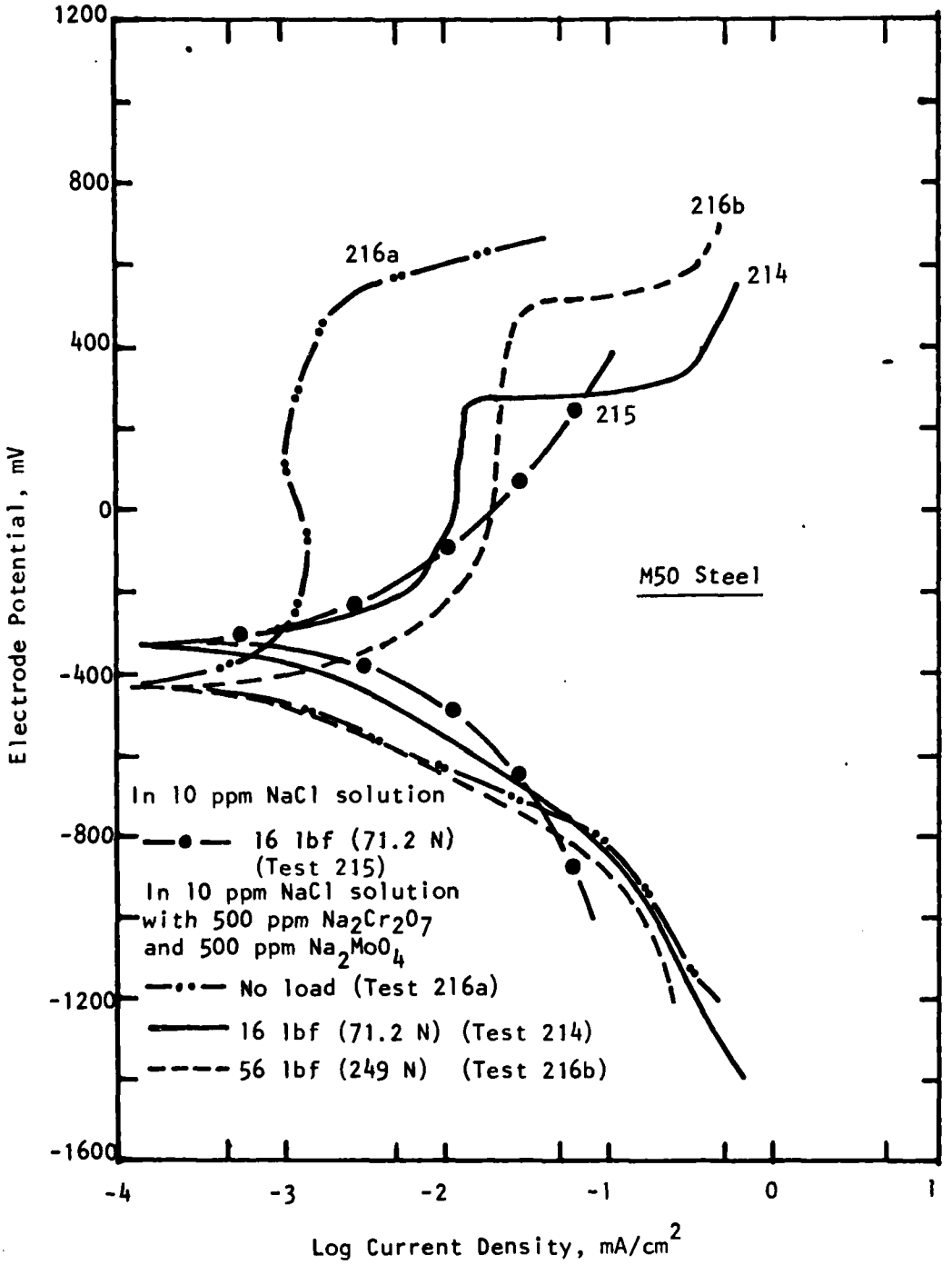

Figure 22. Polarization behavior of M50 steel in different electrolytes with oscillatory motion under various loads, 60° (π/3 rad) amplitude, 1 cpm (17 mHz) (tests 214, 215, 216a, and 216b).

when compared with the anodic component of test 215. In tests 216a and 216b, all the corrosion-wear test conditions except load condition were the same; however, the polarization measurement was performed with no-load for test 216a and with 56 lbf (249 N) for test 216b. The M50 steel in 10 ppm NaCl solution showed a simple metal dissolution curve; however, when 500 ppm $Na_2Cr_2O_7$ and 500 ppm Na_2MoO_4 were added, the M50 steel showed a clear passive region.

In tests 214, 216a, and 216b where corrosion inhibitors were used, load was observed to affect current density in the passive region. The current density in the passive region was the least for no-load, and the largest for 56 lbf (249 N). It increased almost one order of magnitude when load increased from 0 to 16 lbf (71.2 N); however, a negligible increase was indicated when load increased from 16 to 56 lbf (71.2 to 249 N).

The M50 steel electrodes passivated by corrosion inhibitors had undergone pitting at high anodic potential. Pitting occurred at approximately +260 mV for test 214, and at +500 mV for tests 216a and 216b. It was surmised from later test results that pitting was possibly due to insufficient amount of $Na_2Cr_2O_7$ which was consumed during the interface motion, i.e., by forming chromic oxide.

(b) Effect of Load and Frequency

The effect of load and oscillatory frequency on polarization behavior of M50 steel was examined in 100 ppm NaCl solution with 0.01M $NaNO_2$ and 0.01M Na_2MoO_4. Figure 23 compares the effect of load from 0 to 56 lbf (249 N) at 1 cpm (17 mHz), and the effect of load between 16 and 56 lbf (71.2 and 249 N) at 10 cpm (170 mHz).

Tests 223, 225, and 227. The effect of load was clearly observed on open-circuit potential and anodic behavior, but not on the cathodic behavior. The open-circuit potential decreased with the application of 16 lbf (71.2 N), from -220 to -320 mV. A further increase in load to 56 lbf (249 N) did not change the open-circuit potential which remained virtually unaffected at -320 mV. At lower anodic potentials, the anodic cell current density with no-load condition was almost one order of magnitude lower than those of the loaded conditions, 16 and 56 lbf (71.2 and 249 N), between which only a nonsignificant difference was observed. As the anodic potential increased to extremely high values, the difference in the cell current densities between no-load and

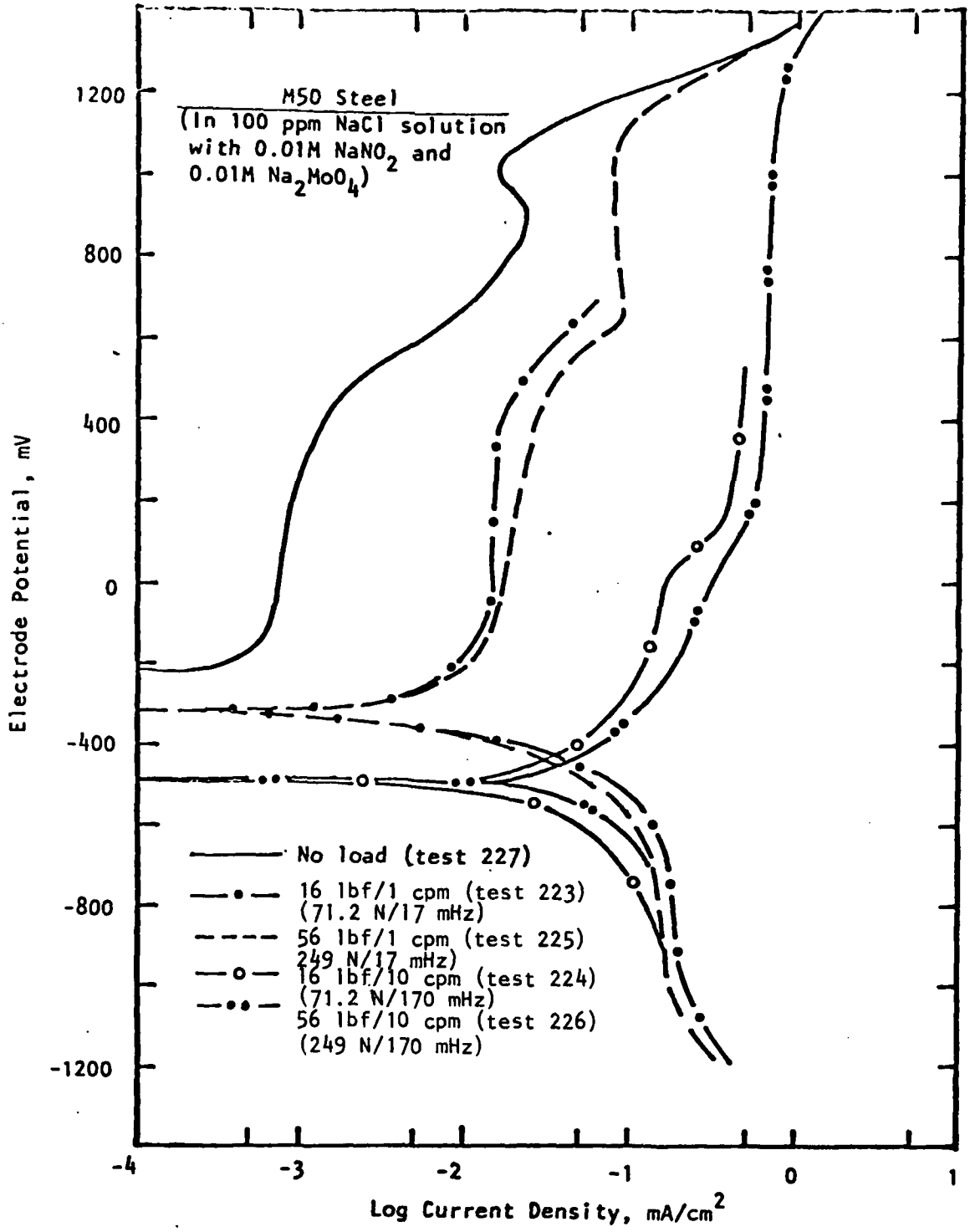

Figure 23. Effect of load and oscillatory frequency on the polarization behavior of M50 steel, 60° (π/3 rad) amplitude (tests 223, 224, 225, 226, and 227).

load conditions became smaller and finally merged at the potential ranges where oxygen evolution was significant. This observation indicated that, at 1 cpm (17 mHz) level, disruption of passive film was the prime factor affecting the polarization behavior while surface deformation leading to asperity contact enlargement was a secondary factor, as observed previously with full rotational motion.[1]

Tests 224 and 226. At 10 cpm (170 mHz), the polarization behavior was essentially the same for both load conditions of 16 and 56 lbf (71.2 and 249 N) throughout all potential ranges. Due to severe wear at high oscillating frequency, the surface of the disk electrode was highly activated, so that the open-circuit potential shifted in the active direction to -500 mV, and the anodic dissolution rate increased significantly when compared with the anodic curve of test 227. At high anodic potentials (greater than about +200 mV), however, a rate-limiting reaction was observed. This implied that corrosion rate could not be increased beyond this limit, no matter how severe the wear condition was. The anodic cell current increase observed in the extremely high potential region (over +1000 mV) was due to oxygen evolution. Between two different load levels, there was an appreciable difference in the cell current density except at extremely low cathodic potentials where hydrogen evolution became significant.

Test 223 and 224. At 16 lbf (71.2 N), the effect of oscillatory frequency on polarization behavior was clearly observed on open-circuit potential and cell current density. An increase in frequency level from 1 to 10 cpm (17 to 170 mHz) shifted the open-circuit potential from -320 to -500 mV. At 16 lbf (71.2 N) and 1 cpm (17 mHz), a potential decrease from no-load condition was primarily due to disruption of passive film, so that a further decrease in potential with an increase in frequency would be associated with an enlargement of asperity contact areas and the associated damage factors of localized deformation, heat, and structural alterations. It is clearly shown that anodic cell current is greatly dependent on frequency. An increase in frequency from 1 to 10 cpm (17 to 170 mHz) increased the anodic cell current density by almost one order of magnitude up to +600 mV.

Tests 225 and 226. At 56 lbf (249 N), the effect of oscillatory frequency on polarization behavior was shown to be similar to that observed at 16 lbf

(71.2 N). In addition to disruption of passive film, the enhanced asperity contact area caused by high frequency clearly affected the anodic reaction processes occurring at the wear interface.

It is interesting to note that an increase in load at a constant frequency [either 1 or 10 cpm (17 or 170 mHz)] did not affect the anodic reaction process as much as an increase in frequency did at constant load [either 16 or 56 lbf (71.2 or 249 N)]. The significant difference between the two observed effects was most likely due to a combination of several damaging factors which included additional wear due to longer sliding distance, increased true asperity contact area, and heat effects on localized deformation and structural alterations.

(c) Effect of Wear on Polarization Reaction Processes

The effect of wear on polarization reaction processes was observed by measuring the cell current response at controlled potentials with alternate application of wear and no-wear condition. The sample electrode was in the active state when the oscillatory motion was applied under load, whereas the sample electrode was allowed to be in the passive state when the oscillatory motion was stopped. Figure 24 compares the polarization curve obtained by continuous scan under no-wear condition (solid line) with the polarization curve obtained by alternate application of motion under load (dashed line) for M50 steel in 100 ppm NaCl solution with 0.01M $NaNO_2$ and 0.01M Na_2MoO_4. The wear condition was 16 lbf (71.2 N) at 1 cpm (17 mHz) and 60° ($\pi/3$ rad) amplitude. The small dotted lines shown on both sides of the dashed line in the anodic region represent the current fluctuation caused by wear. During cathodic polarization, the current fluctuation by wear was negligible. Under no-load (no surface contact) oscillatory motion, current fluctuations were not present.

The interconnected solid circles shown on both curves indicate the shift and reduction in cell current from dynamic wear condition to no-wear condition when motion was stopped under load. For current readings after oscillatory motion was stopped, 5 min were given to reach a passive state. Beyond 5 min, virtually no detectable change in the cell current was observed.

During cathodic polarization, stoppage of motion (no wear) did not change the cathodic cell current at all. This meant that the cathodic reaction was

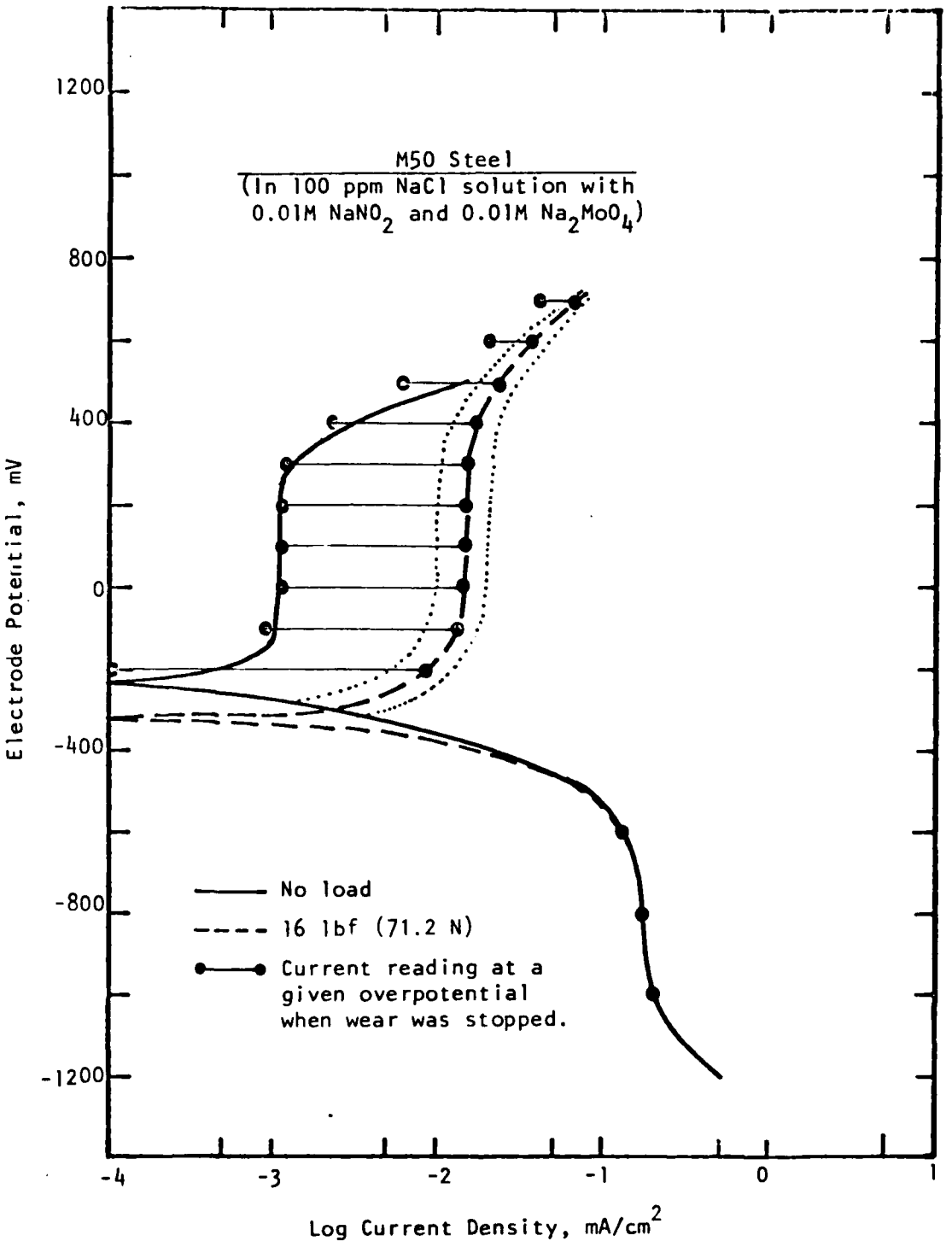

Figure 24. Effect of wear on the polarization reaction process of M50 steel, 60° (π/3 rad) amplitude at 1 cpm (17 mHz). Cell current behavior at controlled overpotential with and without wear is illustrated (test 223).

not affected by wear. On the other hand, during anodic polarization, no-wear condition caused by motion stoppage decreased the anodic cell current density to the value obtained under no-load (no-wear) condition within 5 min. As shown in Fig. 24, stepwise measurement of anodic cell current density at every 100 mV increment followed approximately the value obtained under no-wear condition. With reapplication of oscillatory motion, the anodic cell current instantly reached the original value observed under wear.

These observations clearly indicated that electrode polarization of M50 steel was controlled anodically under wear, not cathodically. A similar observation was made with M2 steel in NaOH solution previously with full rotational motion.[1] This mechanism of anodic control under wear can be used to interpret such phenomena as the open-circuit potential decrease, net cathodic current decrease, and net anodic current increase in the vicinity of the open-circuit potential where the effect of the mixed potential was significant. This understanding of the tribochemical wear mechanism also advances the opportunity and possibility of controlling tribochemical wear through modification of the anodic segment.

5.3 WEIGHT LOSS MEASUREMENTS

Weight loss of fully hardened 52100 and M50 steel disk electrodes under oscillatory motion was generally too little to measure. However, weight loss of pin electrodes can be determined by measuring the scar diameter, from which the volume loss can be calculated and, in turn, the weight loss. It was observed that on the pin electrodes, unlike the disk electrodes, polarization had negligible or no effect. Therefore, the effect of wear alone can be examined, in principle, from the weight loss measurements of pin electrodes after polarization measurement. However, it was difficult to obtain consistent weight-loss data for a thorough analysis since test conditions were set up primarily to obtain the electrochemical polarization data. In this section, weight-loss data obtained without polarization tests are discussed in detail. For reference, the weight-loss data obtained after polarization measurements are presented in Table D-3 in Appendix D.

The pin electrode was modified by grinding a flat on one side for positioning a setscrew. This setscrew kept the pin electrode in an identical

orientation when a pin was reinserted into the holder. The pin electrode was used to obtain weight-loss data for long-term tests with intermittent measurements during a test. At each measurement, the pin weight and wear-scar diameter were measured. From the pin wear-scar diameter, weight loss was determined by calculation. Figure 25 illustrates the pin electrode geometry and the formula used for calculation of weight loss.

Tables 7, 8, and 9 summarize the calculated weight loss and wear rate data (from wear-scar measurements) of pin electrodes from tests 229, 230, and 231, respectively. Initially, wear developed a circular scar which then changed to a slightly elliptical shape with a small difference between the major and minor diameters. However, as the wear time prolonged, the wear scar usually took a more circular shape rather than an elliptical one. For calculation of weight loss from wear-scar measurements, a circular geometry was used because the maximum difference between the diameters was less than 8%.

The equation relating weight loss (ΔW) and wear time (t) [or equivalent sliding distance (D)] may be given by

$$\Delta W = kt^n$$

or

$$\log \Delta W = n \log t + \log k$$

where k and n are constants. When $n = 1$, the wear rate ($d\Delta W/dt$) is constant; when $n > 1$, the wear rate continually increases; and when $n < 1$, the wear rate continually decreases. It is also generally established that wear rate is principally affected by the applied load and not by the apparent contact pressure (based on apparent contact area).

Figure 26 shows a log-log plot of weight loss vs. wear time for tests 229, 230, and 231. The weight-loss data determined from wear-scar measurements were used for this plot. The relationship between weight loss and wear time for each test fits very well in the general equation shown above. The values of n determined from a linear regression analysis were 1.12, 1.00, and 1.19 for tests 229, 230, and 231, respectively. For tests 229 and 231, where corrosion inhibitors were used, the n values were slightly greater than unity; in test 230, where no corrosion inhibitor was used, n equalled unity. In test

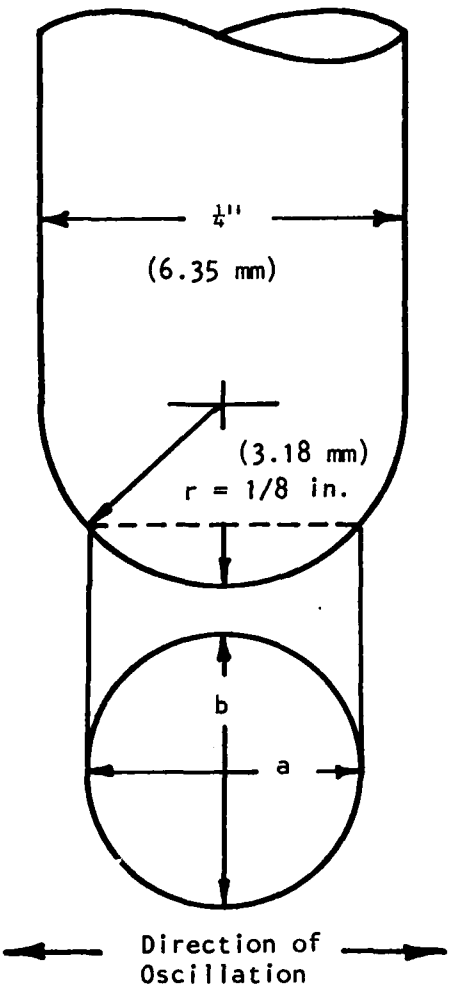

$$h = r - (r^2 - x^2/4)^{\frac{1}{2}}$$

where

$$x = \frac{a + b}{2}$$

Volume Loss = $(1/3)\pi h^2(3r - h)$

Weight Loss = (Volume loss) · (Density)

Figure 25. Spherical pin-end geometry and the formula used to calculate weight loss.

TABLE 7. WEIGHT LOSS DATA OF M50 STEEL PIN ELECTRODE TESTED IN 100 ppm NaCl SOLUTION WITH 0.01M $NaNO_2$ AND 0.01M Na_2MoO_4 UNDER WEAR CONDITION[a] (TEST 229)

Wear Time, h	Measured Wear Scar Diameter,[b] cm		Calculated Data	
	Major	Minor	Weight Loss, µg	Wear Rate, mg/y[c]
0	-	-	-	-
1	0.025	0.025	0.5	4.2
2	0.064	0.059	17.4	76.3
4	0.076	0.071	35.6	77.9
8	0.096	0.089	89.5	98.0
24	0.123	0.123	282	103
48	0.148	0.148	594	108

[a]Wear condition: 16 lbf (71.2 N), 1 cpm (17 mHz), and 60° (π/3 rad) amplitude.

[b]Major and minor diameters are at right angles to each other; in most cases, the major diameter is in the direction of motion.

[c]Linear extrapolation.

TABLE 8. WEIGHT LOSS DATA OF M50 STEEL PIN ELECTRODE TESTED IN 100 ppm NaCl SOLUTION UNDER WEAR CONDITION[a] (TEST 230)

Wear Time, h	Measured Wear Scar Diameter,[b] cm		Calculated Data	
	Major	Minor	Weight Loss, µg	Wear Rate, mg/y[c]
0	-	-	-	-
1	0.056	0.0505	9.6	84.1
2	0.061	0.061	16.3	71.5
4	0.078	0.074	40.7	89.1
8	0.093	0.091	87.6	95.9
24	0.113	0.112	179	71.7
48	0.142	0.135	454	82.9

[a]Wear condition: 16 lbf (71.2 N), 1 cpm (17 mHz), and 60° (π/3 rad) amplitude.

[b]Major and minor diameters are at right angles to each other; in most cases, the major diameter is in the direction of motion.

[c]Linear extrapolation.

TABLE 9. WEIGHT LOSS DATA OF M50 STEEL PIN ELECTRODE TESTED IN 100 ppm NaCl SOLUTION WITH 0.01M $NaNO_2$ AND 0.01M Na_2CrO_4 UNDER WEAR CONDITION[a] (TEST 231)

Wear Time, h	Measured Wear Scar Diameter,[b] cm		Calculated Data	
	Major	Minor	Weight Loss, µg	Wear Rate, mg/y[c]
0	-	-	-	-
1	0.046	0.050	4.3	38.1
2	0.054	0.050	8.9	38.9
4	0.064	0.061	18.6	40.7
8	0.080	0.076	45.2	49.5
24	0.108	0.107	164	59.7
48	0.133	0.133	386	70.4

[a]Wear condition: 16 lbf(71.2 N), 1 cpm (17 mHz), and 60° (π/3 rad) amplitude.

[b]Major and minor diameters are at right angles to each other; in most cases, the major diameter is in the direction of motion.

[c]Linear extrapolation.

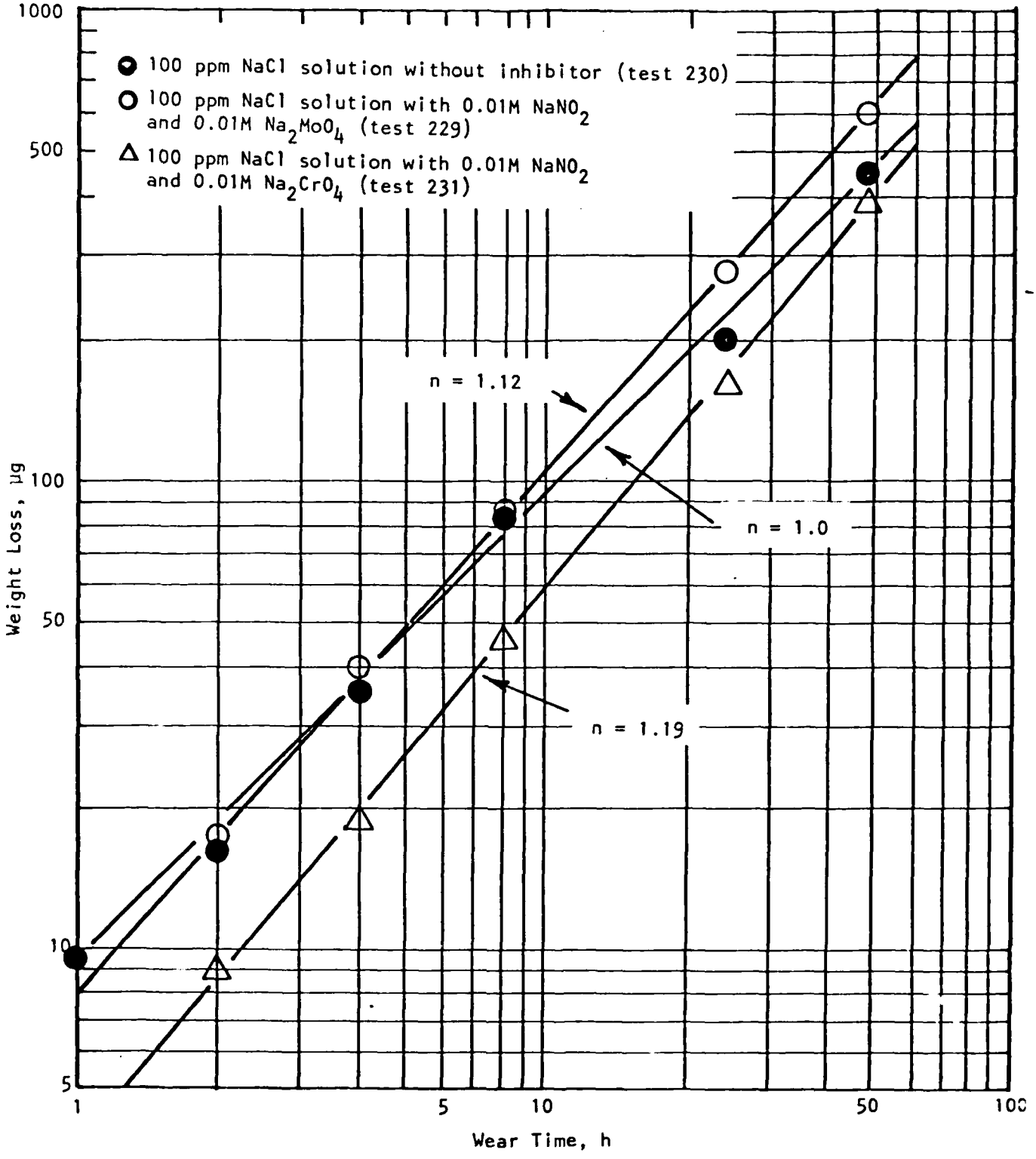

Figure 26. Weight loss vs. wear time plot for M50 steel tested under 16 lbf (71.2 N) at 1 cpm (17 mHz) and 60° (π/3 rad) amplitude in various electrolyte conditions.

229, 0.01M $NaNO_2$ and 0.01M Na_2MoO_4 were used; and in test 231, 0.01M $NaNO_2$ and 0.01M Na_2MoO_4 were used. The higher n for test 231 suggests that formation of chromic oxide at the interface may be contributing to a higher n, with molybdic oxide at the interface in test 229 showing a lower n value.

A comparison between the n values and the wear rates (given in Tables 7 to 9) shows the following:

Test	n	Behavior of Wear Rate
229	>1	The wear rate increases continually.
230	1	The wear rate shows approximate linearity with small fluctuations.
231	>1	The wear rate increases continually.

The higher n values in tests with inhibitors indicate the possibility that surface corrosion products, formed in the presence of inhibitors, have certain properties such as strength (shear), hardness, and brittleness which differ from those of corrosion products formed in the absence of inhibitors, and the former had promoted wear. Between the two inhibitors, chromic oxide products may be different from the molybdic oxide products in terms of wear-promoting effects related to their differing crystalline morphologies and their affinity to form hydrated oxide complexes.

These test results also indicated that the presence of corrosion inhibitors, while reducing the corrosion rate, may tend to increase wear rate depending on the property of corrosion-wear products at the interface. More information is needed in this regard, and if found to be significant, additional inhibitor complexes must be added to counteract this tendency so that these inhibitors can be used effectively to reduce corrosion without promoting wear.

Phenomenological analysis of wear data listed in Table D-3, Appendix D, based on one-to-one comparison, is given below. (Also, see Table D-1 for test details.)

Tests 210 and 211a. Between two soft pin electrodes of 52100 steel, the wear rate of test 210 was much lower than that of test 211a. In test 210, a water-soluble oil was used with no inhibitors, while corrosion inhibitors were used without oil addition in test 211a. Also, the wear time was 55.3 and 3 h

for tests 210 and 211a, respectively. The overwhelming lubricating effect was observed in the much lower wear rate and friction coefficient of test 210 (see Table D-1).

Tests 211c and 216. Between the fully hardened 52100 and M50 steel pin electrodes with approximately the same order of wear time, the wear rate of test 216 was much higher than that of test 211c. The load levels were 16 and 56 lbf (71.2 and 249 N) for tests 211c and 216, respectively, and the effect of load on wear rate was clearly observed.

Tests 211b and 213. The wear times for these two tests were very similar (i.e., 23.5 and 21 h), with corrosion-wear test conditions differing in electrolyte and high anodic overpotential effect. The wear rate for test 213 was much less than that of test 211b although the system for test 213 was held at +600 mV for 17 h under wear condition. The effect of high anodic overpotential was found to be negligible or nil on the wear rate of pin electrodes, unlike that observed on disk electrodes where severe corrosion and pitting had occurred, as shown in Fig. 11. The relatively higher wear rate of test 211b over test 213 could be due to the effect of corrosion inhibitors. It is also to be noted that friction coefficient, too, had increased (in test 211b) in the presence of corrosion inhibitors. However, in a tribological system, wear rate and friction coefficient are not uniquely related.

Tests 214 and 215. The corrosion-wear test conditions, except for the presence of corrosion inhibitor (in test 214), were approximately in the same range for these two tests. The wear rate of test 215 was about five times higher than that of test 214. This comparison suggests that corrosion inhibitor may reduce the wear rate while increasing the friction coefficient.

Tests 217, 218, 220, 221, and 222. The wear condition was the same for all the tests [16 lbf (71.2 N) at 1 cpm (17 mHz)] for 48 h, but the electrolyte conditions were different. The wear rates obtained by both measurement and calculation were between 70 and 111 mg/y except for test 222 (from measurement data only). The wear rate of test 221 was the lowest in this group indicating the lubricating effect of the water-soluble oil. Among tests 217, 218, 221, and 222, the electrolyte of test 217 did not contain any corrosion inhibitor. The wear rate of test 217 (by calculation) was relatively low. Thus the effect of corrosion inhibitor on the wear rate was observed to

differ from tests 214 and 215. However, there was a difference in test time between these two sets of tests, and a clear understanding of the effect of corrosion inhibitor on wear rate would require further testing and analysis.

Test 219 vs. Tests 217, 218, 221, 222 and 223. Though wear time varied, the load, 16 lbf (71.2 N), was the same for all. With 24 h of wear time, the wear rate in test 219 was almost twice as high as the wear rates in the other tests with a wear time of 48 h. This indicated that wear rate of M50 steel pin electrodes tended to decrease with time. When tests 219 and 223 were compared, the higher wear rate with the shorter test time was further manifested. Also, a comparison of tests 215 and 217 indicated a similar time effect.

Tests 224 and 226. The corrosion-wear conditions, except for load level, were the same for both tests. It was observed that the wear rate of test 226 (under 56 lbf [249 N]) was only slightly greater than that of test 224 (under 16 lbf [71.2 N]), and the effect of the much higher load on wear was not noted. Additional tests will be required to clarify this small effect of load on wear rate at the high oscillatory frequency level.

Tests 225 and 226. The corrosion-wear conditions, except for oscillatory frequency, were the same for both tests. It was observed that the weight loss of test 226 [at 10 cpm (170 mHz)] was approximately 8.5 times greater than that of test 225 [at 1 cpm (17 mHz)]. The sliding distance of test 226 was 10 times longer than that of test 225, so that the weight loss of the former was supposed to be 10 times greater than that of the latter as well if no effect other than sliding distance was considered. However, the observed wear rate ratio of test 226 to test 225 was 8.5:10. This meant that secondary effects other than sliding distance affected weight loss by wear. One possible effect would be that of the frictional heat sink which may arise from the oscillatory frequency difference. At high frequency under high load [10 cpm (170 mHz), 56 lbf (249 N)], frictional heat may modify the microstructure of asperities before the heat is absorbed by the electrolyte, and, hence, the asperities, and possibly the immediate subsurface, may locally yield to enlarge the real asperity contact area. As a result, the area of each contact may increase and new contacts may be established. The heat effect will also promote more intense surface-environment interaction, and a higher corrosion rate may

emerge. It is to be noted that both these effects on wear reinforce each other while they oppose in the resulting friction effects, mentioned earlier.

5.4 SCANNING ELECTRON MICROSCOPY

The surface morphology of corrosion-wear specimens was characterized using scanning electron microscopy. Figure 11 and Figs. 27 to 34 represent typical macro and microphotographs of disk and pin electrodes of 52100 and M50 steels. The test conditions for these specimens are listed in Table D-1. Polarization measurements were performed in tests 207 and 210 (Figs. 27 and 28) and 213 to 216 (Figs. 11, 29 to 31), but not in tests 229 to 231 (Figs. 32 to 34). Anodic and cathodic potential limits of each polarization test may be noted from polarization curves presented in Section 5.2. The specimens in tests 213 to 215, after polarization, were held at either anodic or cathodic overpotential for a reasonably long time as described in Table 5. In tests 229 to 231, during corrosion-wear testing, no polarization measurement was performed; thus, the corrosion reaction was only due to the electrochemical property of electrolyte and not due to any externally applied potential.

5.4.1 Specimens after Polarization Measurements

Both 52100 and M50 steel disk electrodes polarized without the water-soluble oil (tests 207, 213, 214, 215, 216) generally displayed two different zones in the wear track, with pits, and with a smooth surface of non-wear area. But no pit was observed on the pin wear scar in any of these tests. The pits on the disk electrodes ran parallel with the oscillating direction (Fig. 27a). At higher magnifications, many significant cracks inside the pits were observed (Fig. 27b). In tests 207 and 213, the pits were distributed evenly. However, in tests 214, 215, and 216 the pits were more heavily distributed near both edges of the wear track (Figs. 29 to 31). It was clearly noted that the pit size of the test 213 specimen (see Fig. 11b) was much bigger than that of other specimens. This larger pit size was related to the effect of anodic overpotential. The specimen for test 213 was held at +600 mV for 17 h after polarization testing.

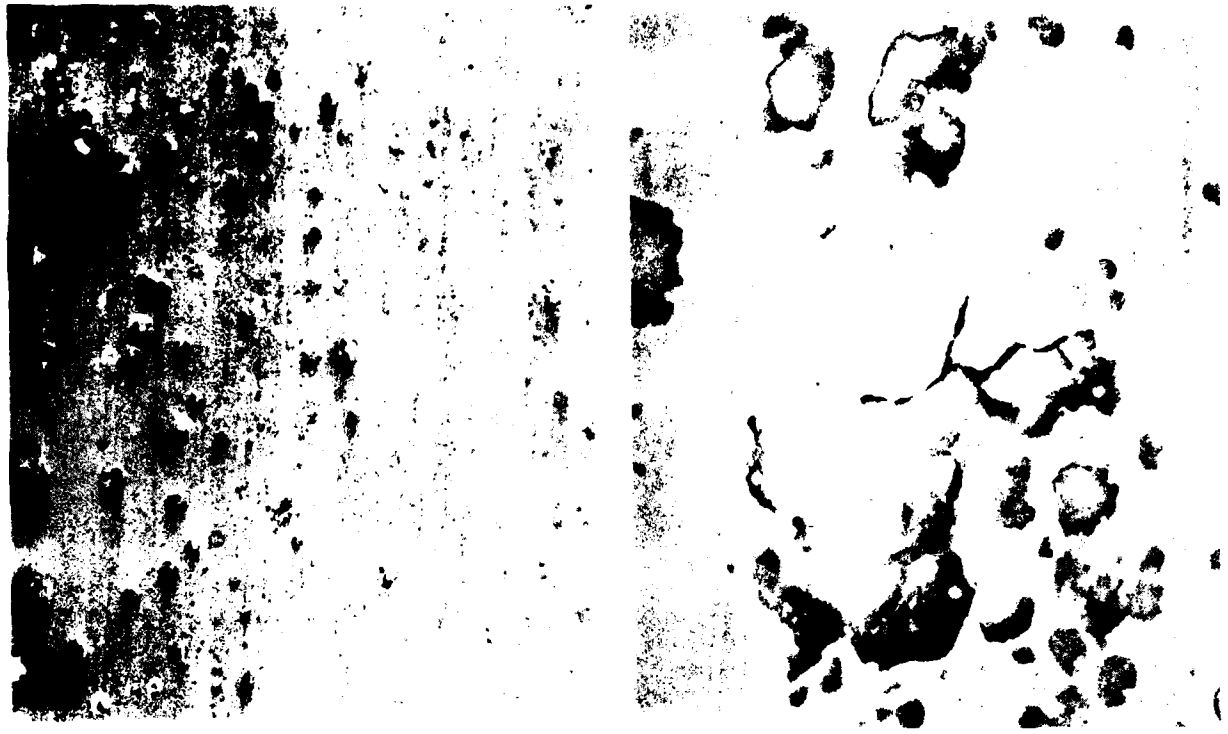

Figure 27. SEM micrographs of 52100 steel disk and pin electrodes (test 207): (a) general surface morphology of wear track on the disk showing many pits, (b) detail view of a pit on the disk, and (c) wear scar of the pin.

SEM No. 9682 25X

(a)

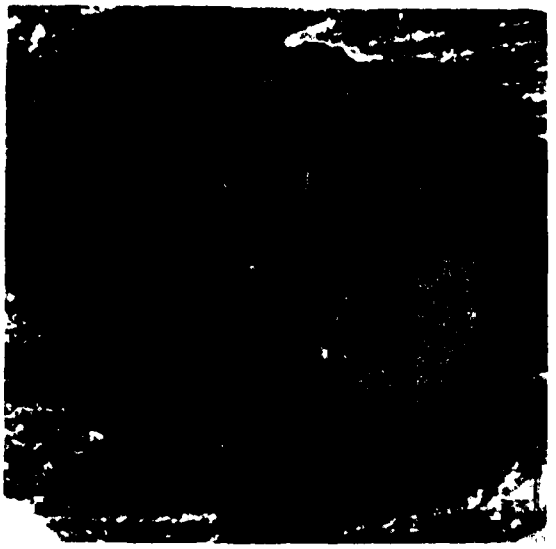

SEM No. 9683 25X

(b)

Figure 28. SEM micrographs of 52100 steel disk and pin electrodes (test 210). A water-soluble oil was used as lubricant. (a) Wear track on disk, (b) wear scar on pin.

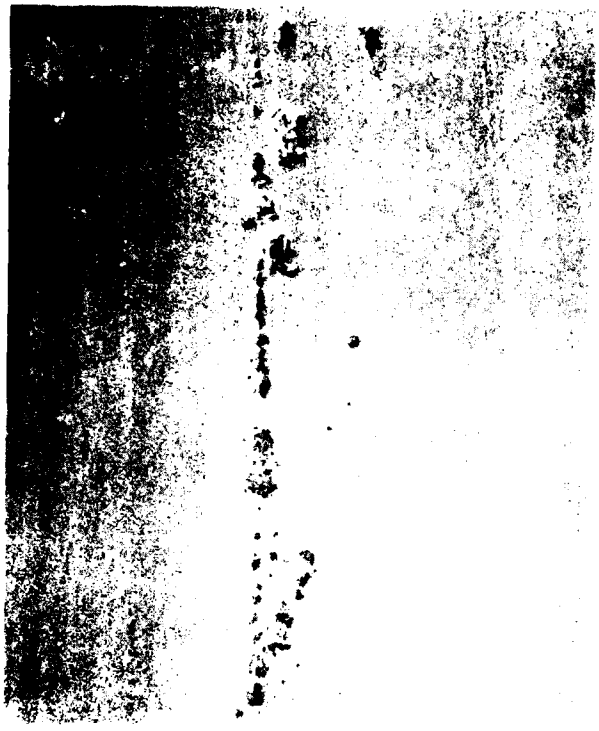

SEM No. 9677 50X

(a)

SEM No. 9679 500X

(b)

SEM No. 9681 50X

(c)

Figure 29. SEM micrographs of M50 steel disk and pin electrodes (test 214): (a) general surface morphology of wear track on the disk with many pits, (b) detail view of a pit on the disk, and (c) wear scar on the pin.

SEM No. 9674 25X

(a)

SEM No. 9673 1000X

(b)

SEM No. 9676 50X

(c)

Figure 30. SEM micrographs of M50 steel disk and pin electrodes (test 215): (a) general surface morphology of wear track on the disk with several pits, (b) detail view of a pit on the disk, and (c) wear scar on the pin.

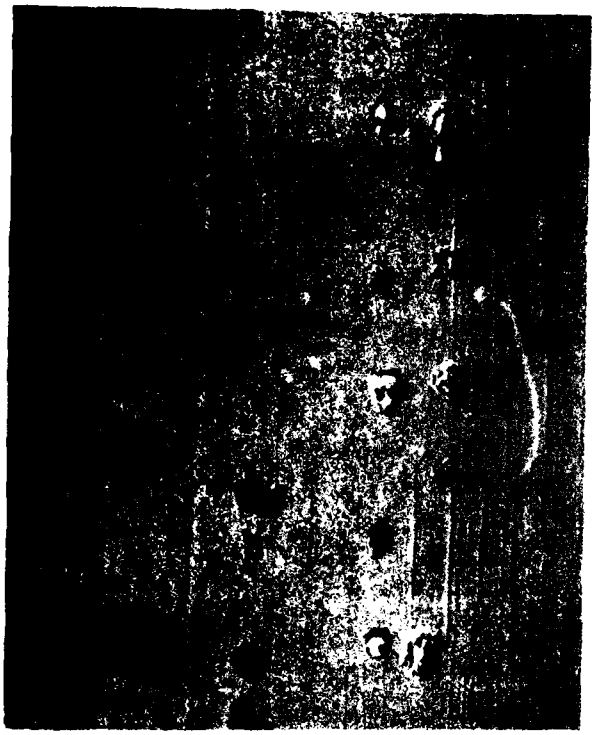

SEM No. 9671 50X

(a)

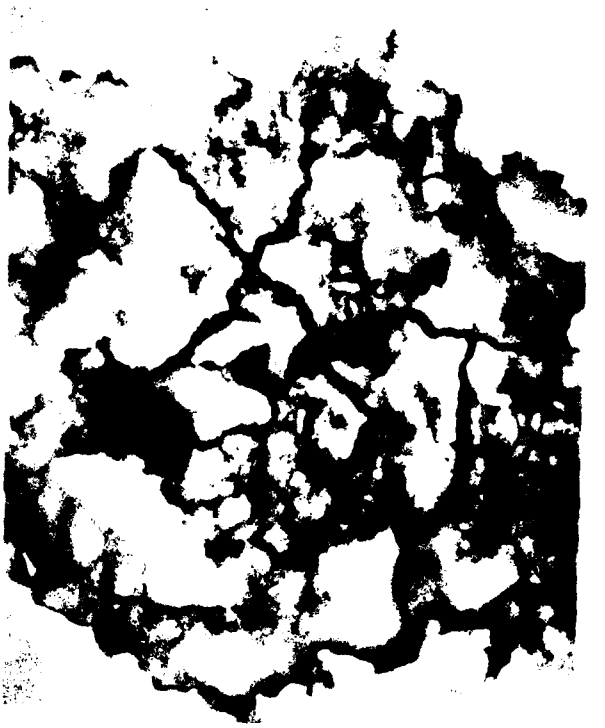

SEM No. 9670 1000X

(b)

SEM No. 9672 50X

(c)

Figure 31. SEM micrographs of M50 steel disk and pin electrodes (test 216): (a) general surface morphology of wear track on the disk with several pits, (b) detail view of a pit on the disk, and (c) wear scar on the pin.

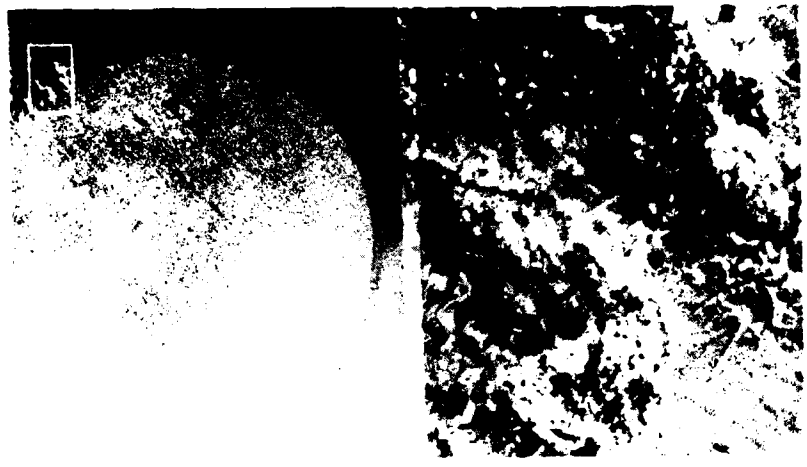

SEM No. 601 36X 360X

(a) (b)

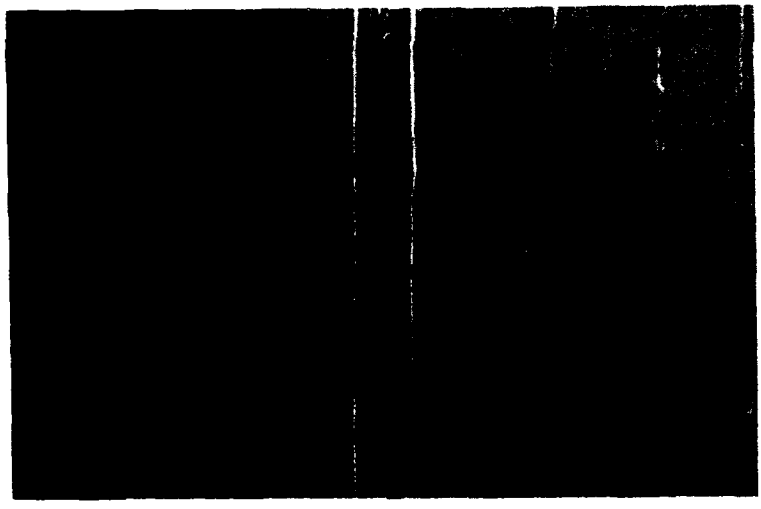

SEM No. 557 510X

(c)

Figure 32. SEM photomicrographs of M50 steel pin and disk electrodes (test 229): (a, b) Wear scar of the pin at low and high magnifications, (c) detail view of wear track on the disk.

SEM No. 604 50X

(a)

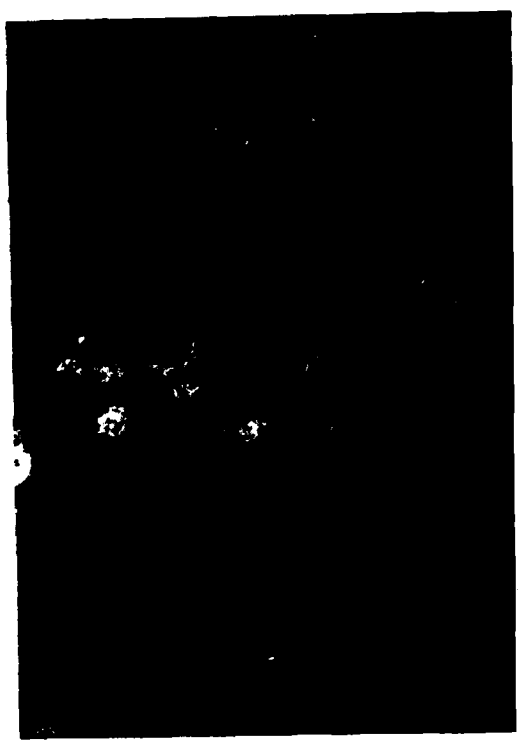

SEM No. 561 17X

(b)

SEM No. 562 170X

(c)

Figure 33. SEM photomicrographs of M50 steel pin and disk electrodes (test 230): (a) Wear scar of the pin, (b) general surface morphology of wear track on the disk showing many pits, and (c) detail view of a pit on the disk.

SEM No. 600 30X 300X

(a) (b)

SEM No. 570 510X

(c)

Figure 34. SEM photomicrographs of M50 steel pin and disk electrodes (test 231): (a, b) Wear scar of the pin at low and high magnifications, respectively, and (c) detail view of wear track on the disk.

Specimens for both tests 214 and 215 were held at high cathodic overpotential after polarization testing. Test 214 had the corrosion inhibitors whereas test 215 did not. The effect of corrosion inhibitors on pit nucleation during anodic polarization can be observed in the pit distribution of these two specimens. Pits were confined inside the wear track in test 214, while pits were found both inside and outside of the wear track in test 215. It suggests that the surface passivated by corrosion inhibition would be much less susceptible to pitting than the nonpassivated surface if there were no wear. However, no particular effect of cathodic overpotential, such as metal removal due to hydrogen embrittlement, was observed.

Examination of surface morphology of all of the disk electrodes suggested that pits nucleated exclusively inside the wear track zone. The wear-assisted pit initiation can be observed in Fig. 11b (test 213), in the vicinity of preexisting pits. It seems that microcracks developed by interfacial motion under load were the precursors of the pits. Once a pit is initiated, numerous microcracks develop inside the pit, with some along the grain boundaries.

Figure 28 shows the surface appearance of 52100 steel disk and pin electrodes polarized in the electrolyte with a water-soluble oil (test 210). Although this specimen was anodically polarized up to 1200 mV, no pits at all were observed. Both sliding surfaces of the disk and pin electrodes were very smooth and shiny. This observation suggests that water-soluble oil acts as a lubricant as well as a corrosion inhibitor.

5.4.2 Specimens With No Polarization Measurements

The surface features of both pin and disk electrodes for tests 229 and 231 indicated certain similarities in corrosion-wear behavior. In these two tests, the corrosion inhibitors used were: $NaNO_2$ and Na_2MoO_4 for test 229, and $NaNO_2$ and Na_2CrO_4 for test 231. No significant corrosion attack was detectable on the pin and disk electrodes by both visual and microscopic observations. As shown in Figs. 32a and 34a, light wear tracks, with their orientation parallel to the oscillating direction, were observed on the pins. Figures 32b and 34b show, at a higher magnification, the areas indicated with a rectangle on Figs. 32a and 34a, respectively. It was observed that wear resulted in a smoothing of the corroding wear surface at the wear track boundary. This type of smoothing effect was also observed on the wear track of

disk electrodes. Magnified views of wear tracks of disk electrodes for both tests 229 and 231 shown in Figs. 32c and 34c, respectively, indicate a mild corrosion/wear condition. On the wear track area of disk electrodes in both tests, no indication of wear-assisted corrosion was observed. This observation was distinctly different from wear-assisted corrosion observed on the wear track area of a disk electrode which was subjected to electrode polarization during corrosion-wear testing (e.g., Fig. 29 for test 214 in which corrosion inhibitors were also used).

In test 230, no corrosion inhibitor was used. Wear-assisted localized corrosion was observed on wear track areas of both pin and disk electrodes, as shown in Figs. 33a and b. On the free surface area (outside the wear track) of the disk electrode, a pattern of uniform corrosion was observed. No corrosion pits were observed on the free surface. The pits developed exclusively inside the wear track zone. The wear-assisted pit initiation can be observed in Fig. 33c, in the vicinity of preexisting pits. As observed previously on M50 steel under different corrosion-wear conditions (Fig. 11 for test 213), the present examination of surface morphology also seemed to indicate that microcracks developing from interfacial motion under load are the precursors of the pits. Once a pit is initiated, numerous cracks develop inside the pit, as may be seen in Fig. 33c.

Observations on surface morphology of corrosion-wear specimens clearly indicated a beneficial effect of corrosion inhibitors on the localized corrosion attack which would otherwise take place on the wear track area. Nonpolarization of the electrodes manifested itself in the absence of localized corrosion in the wear track area.

5.5 SURFACE ROUGHNESS MEASUREMENTS

The surface roughnesses of several disk electrodes of 52100 and M50 steels were measured before and after corrosion-wear tests with a profilometer and a Proficorder. Table 10 lists the surface roughness data taken with the profilometer; all roughness numbers are root mean square (rms) values. The roughness data for wear track include about 0.2 cm of free surface (no wear) on both sides of the wear track since the width of the wear track itself for all the specimens was too small for the profilometer to determine the root

TABLE 10. SURFACE ROUGHNESS OF 52100 AND M50 STEEL AND M50 STEEL DISK ELECTRODES UNDER VARIOUS WEAR CONDITIONS[a]

Test No.	Disk Material	Load, lbf (N)	Surface Roughness, μin.[b] Before Test	After Test
207	52100 steel	16 (71.2)	7-10	7-9
210	52100 steel	16 (71.2)	8-10	8-10
213	52100 steel	16 (71.2)	8-10	138-142
214	M50 steel	16 (71.2)	7-10	7-9
215	M50 steel	16 (71.2)	7-10	16-20
216	M50 steel	56 (249)	8-10	9-11

[a]See Table D-1, in Appendix D, for details.

[b]Bendix profilometer, Pilotor Model VEB; 39.4 μin. = 1 μm.

mean square value. The width of wear track fell between 0.05 and 0.15 cm. The traces of wear track on the disk electrodes listed in Table 10 are presented in Figs. 35 and 36.

In general, the surface roughness of fully hardened 52100 and M50 steels changed negligibly because of wear; and in some cases (tests 207 and 214) the wear resulted in a "polishing effect" reducing the surface roughness. When water-soluble oil was used in test 210, the surface roughness virtually remained the same after the test. No change in the surface profile of the test 210 disk electrode was observed in Fig. 35b. The surface roughness of test 213 electrode increased almost 14-fold after the test in which an anodic overpotential of +600 mV was applied for 17 h under wear. This significant change in surface roughness was most likely due to the effect of anodic overpotential. The deep valleys observed on the surface profile shown in Fig. 35c represent pits that had developed in the wear track. It seems that for fully hardened steels, surface roughness was more significantly affected by corrosion than by wear. In tests 214 and 215, the sample electrodes were held at high cathodic overpotential for 16 h; however, corrosion inhibitors were used for test 214, but not for test 215. The surface roughness for test 214 (Fig. 36a) remained almost the same before and after the corrosion-wear test, whereas the surface roughness of test 215 (Fig. 36b) after the test increased

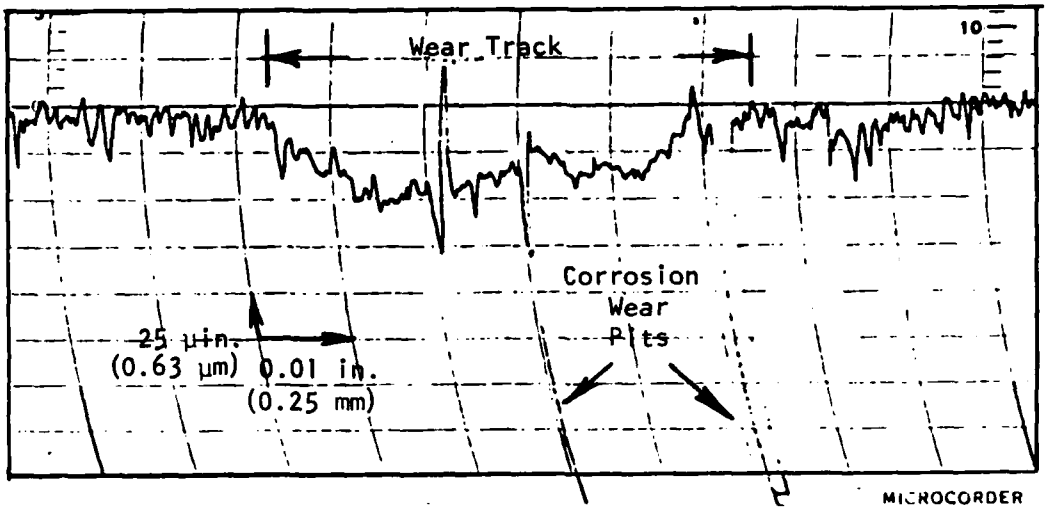

(a)

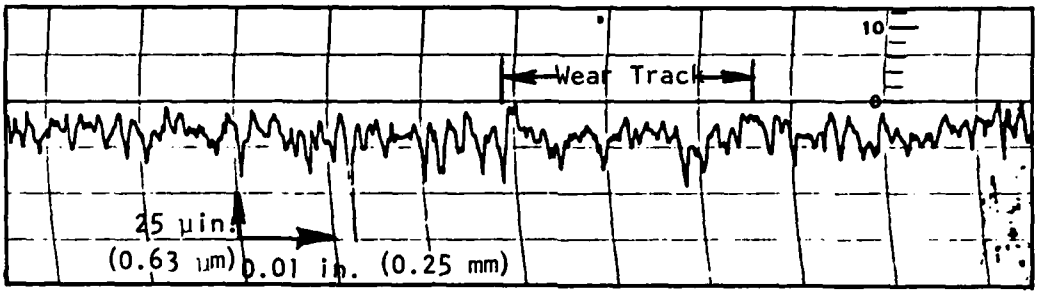

(b)

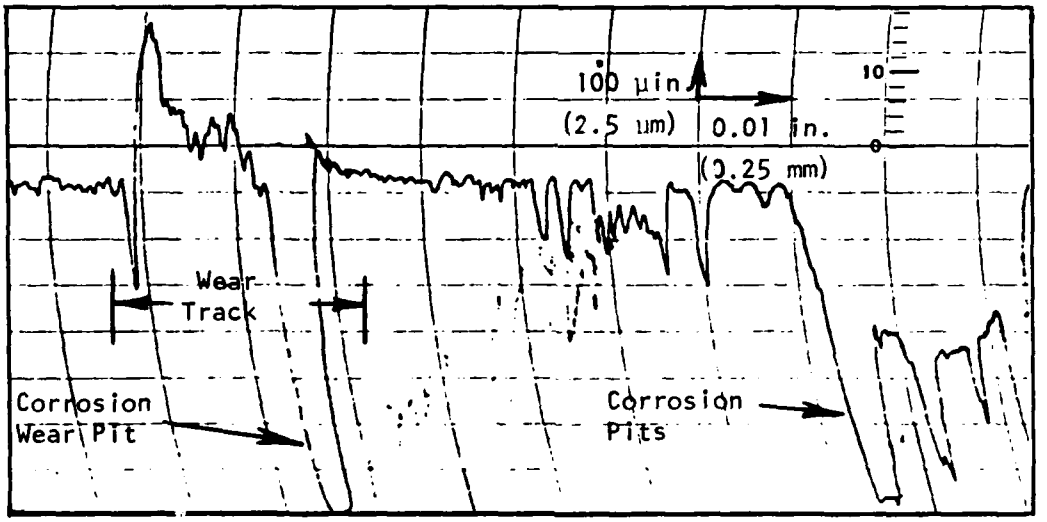

(c)

Figure 35. Surface profiles of 52100 steel disk electrodes tested under 16 lbf (71.2 N). (a) Corrosion inhibitors were used (test 213); (b) a water-soluble oil was used (test 210); (c) no inhibitor or lubricant was used (test 213).

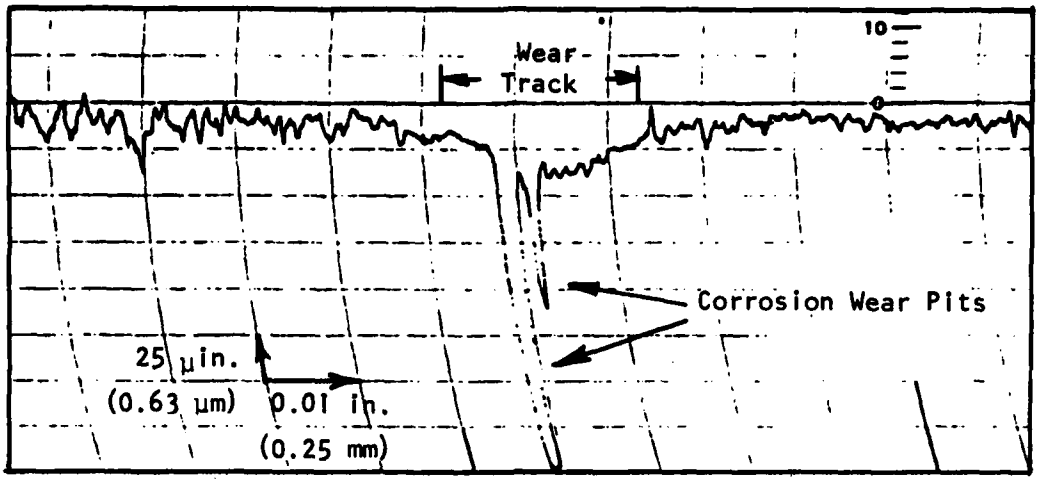

(a)

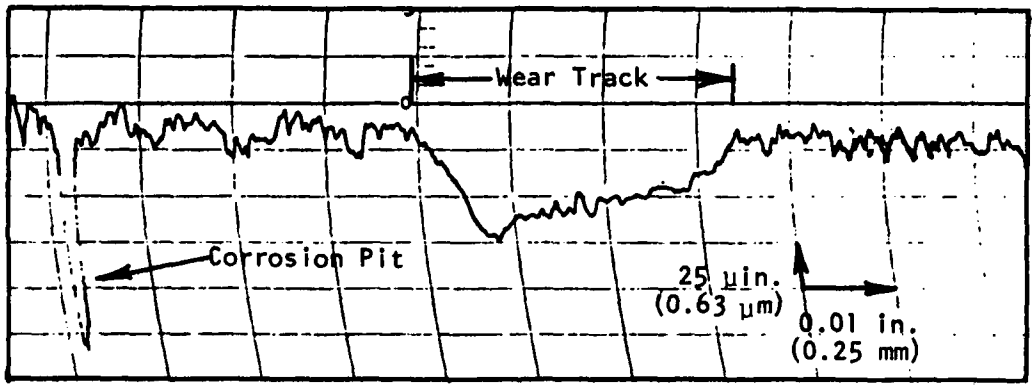

(b)

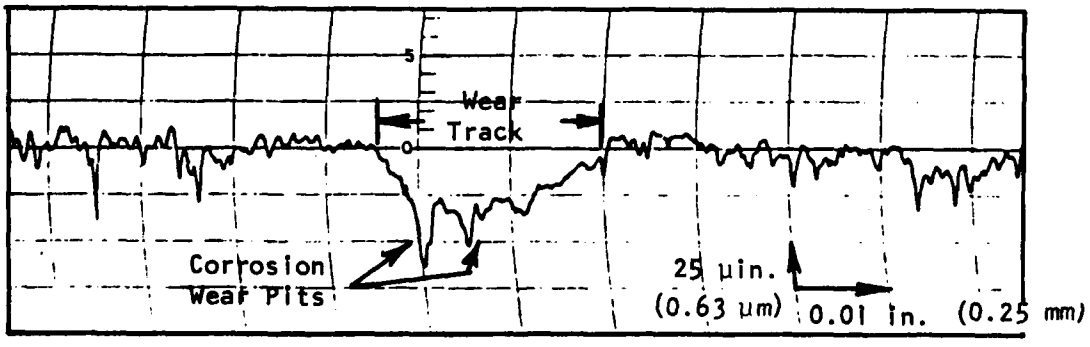

(c)

Figure 36. Surface profiles of M50 steel disk electrodes. (a) Corrosion inhibitors were used, with 16 lbf (71.2 N) (test 214); (b) No inhibitor or lubricant was used, with 16 lbf (71.2 N) (test 215); (c) Corrosion inhibitors were used, with 56 lbf (249 N) (test 216).

about twice as much as the one observed before the test. The difference in the surface roughness between tests 214 and 215 may be due to the effect of corrosion inhibitors in the system. Figure 36c shows the effect of higher load in test 216 when compared with Fig. 36a (test 214); inhibitors were used in both tests.

5.6 STATISTICAL CORROSION-WEAR TESTS

A set of statistically designed corrosion-wear tests (based on a Plackett-Burman test matrix[4]) was performed to clearly demonstrate the effectiveness of inhibitors, load, etc., on the observed corrosion-wear and friction performances. Table 11 shows the designed test matrix used for the statistical corrosion-wear tests. In this test design, a set of five independently controlled variables at two levels was chosen for the assigned variables, which included corrosion inhibitors of two different combinations (X1, X5), lubricant (X4), load (X6), and frequency (X10). The test was exclusively conducted with M50 steel in 100 ppm NaCl solution with air saturation at room temperature. A detailed description of potential scanning methods for these statistical tests is given in Appendix C. A total of 19 tests including 7 replicate tests were performed.

The test variables and their levels were carefully assigned so that the results could be analyzed phenomenologically as well as statistically. Phenomenological analysis of the significant corrosion-wear parameters is presented prior to statistical analysis. Several analyses of corrosion-wear surface morphologies are also given.

5.6.1 Phenomenological Analysis

Nine sets of polarization curves compare the effects of the respective factors on the polarization behavior of M50 steel in 12 tests (tests 232 to 243) under different corrosion-wear conditions. The observed values of the open-circuit potential, corrosion current density, and friction coefficient are summarized on each diagram for a more effective analysis. Seven replicate

---

[4]J. W. Dini, and H. R. Johnson, "Use of Strategy of Experimentation in Gold Plating Studies," Plating and Surface Finishing, Vol. 68 (2), p. 52 (1981).

TABLE 11. TWELVE-TEST STATISTICAL DESIGN AND TEST MATRIX

Trial	Mean	X1	X2	X3	X4	X5	X6	X7	X8	X9	X10	X11	Test No.	$\bar{Y}$
1	+	+	+	-	+	+	+	-	-	-	+	-		
2	+	+	-	+	+	+	-	-	-	+	-	+		
3	+	-	+	+	+	-	-	-	+	-	+	+		
4	+	+	+	+	-	-	-	+	-	+	+	-		
5	+	+	+	-	-	-	+	-	+	+	-	+		
6	+	+	-	-	-	+	-	+	+	-	+	+		
7	+	-	-	-	+	-	+	+	-	+	+	+		
8	+	-	-	+	-	+	+	-	+	+	+	-		
9	+	-	+	-	+	+	-	+	+	+	-	-		
10	+	+	-	+	+	-	+	+	+	-	-	-		
11	+	-	+	+	-	+	+	+	-	-	-	+		
12	+	-	-	-	-	-	-	-	-	-	-	-		

1. Five assigned variables and their levels:

	Variables	(+)	(-)	Observation
X1	$Na_2Cr_2O_7$	Yes	No	$\bar{Y}$ = Open-circuit potential
X4	Lubricant*	Yes	No	= Corrosion current density
X5	$NaNO_2$ and Na_2MoO_4	Yes	No	= Friction coefficient
X6	Load, lbf (N)	56 (249)	16 (71.2)	
X10	Frequency, cpm (mHz)	10 (170)	1 (17)	

*10% water-soluble oil

2. Fixed test parameters:
   a) Electrode materials - M50 steel
   b) Electrolyte - 100 ppm NaCl solution
   c) Environment - Air saturation
   d) Test temperature - Room temperature [70°F(21°C)]
   e) Oscillatory amplitude - 60° (π/3 rad)

tests (tests 244 to 250) were performed to confirm the reproducibility and to explain more fully some of the unusual behavior observed in the initial 12 statistical tests. These results are presented in five additional sets of polarization curves where a comparison between the original and replicate tests made. Fourteen sets of curves and typical corrosion-wear surface morphologies are presented in Figs. 37 to 57.

(a) Effect of Lubricant (Tests 233 and 245 vs. 242)

Figure 37 compares the effect of lubricant on the polarization of M50 steel in 100 ppm NaCl solution with 0.01M $Na_2Cr_2O_7$ under 56 lbf (249 N) at 1 cpm (17 mHz) (tests 233 vs. 242). The effect of lubricant on the open-circuit potential was marginal. However, the presence of water-soluble oil decreased the corrosion current density by an appreciable amount. Without lubricant, a sudden increase in the anodic cell current at approximately +300 mV was observed, indicating severe pit development. To confirm this pitting behavior, a replicate test (test 245) was performed and the result is given in Fig. 38. A sharp increase in the cell current density was observed again at +300 mV. General polarization behavior in the two tests was similar although a noticeable difference in the current density was observed at lower anodic potentials below the pitting potential.

Figure 39 shows the corrosion-wear surface morphology of the disk electrode of test 233 where very severe pits on the wear track (but not outside it) may be noted. A similar corrosion-wear surface morphology was observed on the disk electrode of test 245. Pit initiation on the wear track was likely due to local deficiency in $Na_2Cr_2O_7$ at the disk and pin interface. Since $Na_2Cr_2O_7$ is a strong oxidant, insufficient amount of $Na_2Cr_2O_7$ may permit the development of pits while otherwise protecting the metal surface from general corrosion. It may be speculated that the consumption rate of dichromate which promoted formation of chromic oxide resulting from a higher localized frictional heating might be greater than the dichromate transport rate at this high load. This condition would cause localized dichromate insufficiency, hence pitting. The presence of water-soluble oil in test 242 decreased the friction coefficient significantly from 0.41 (test 233) and 0.44 (test 245) to 0.12 (test 242).

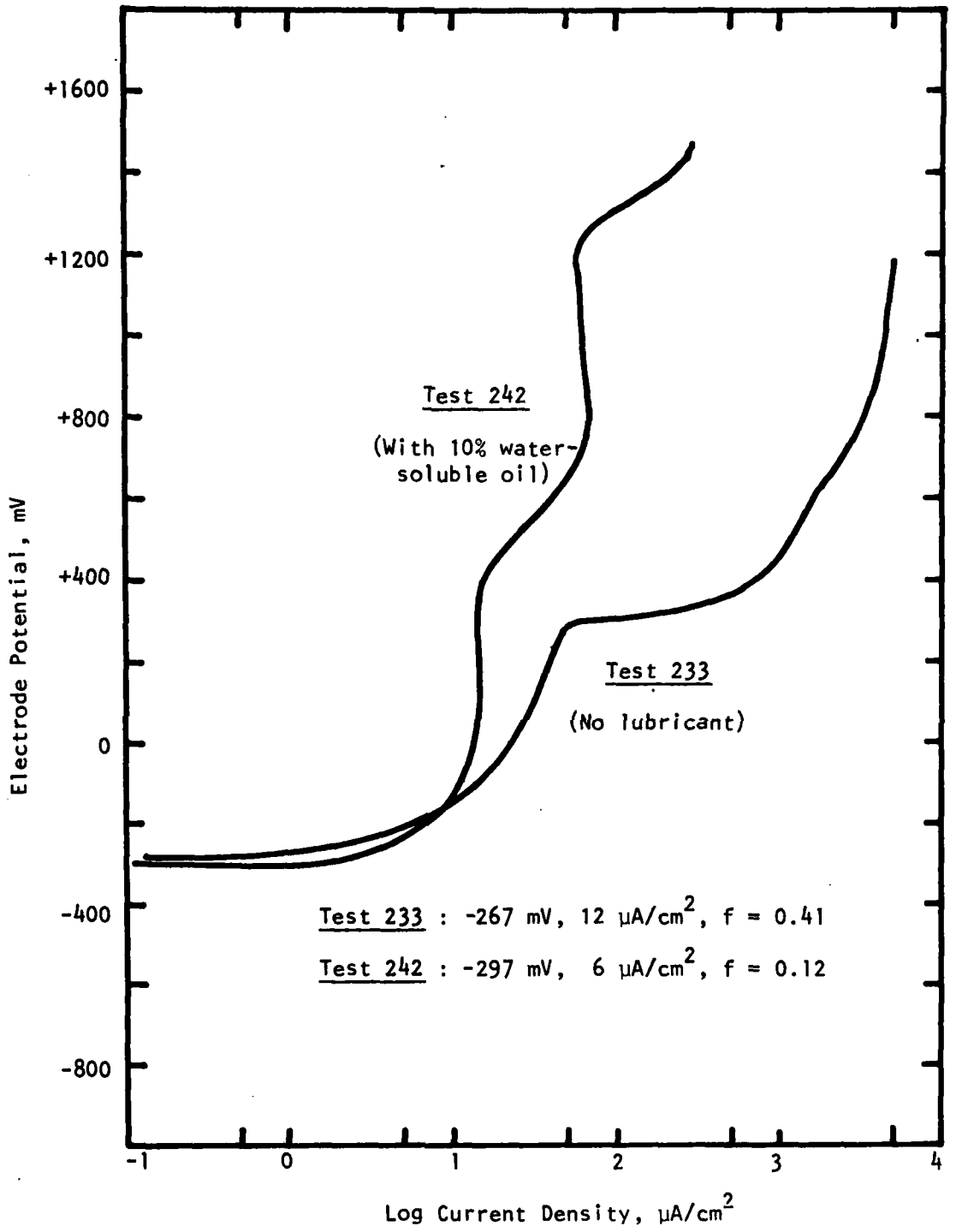

Figure 37. Effect of lubricant on the polarization behavior of M50 steel in 100 ppm NaCl solution with 0.01M $Na_2Cr_2O_7$ under 56 lbf (249 N) at 1 cpm (17 mHz).

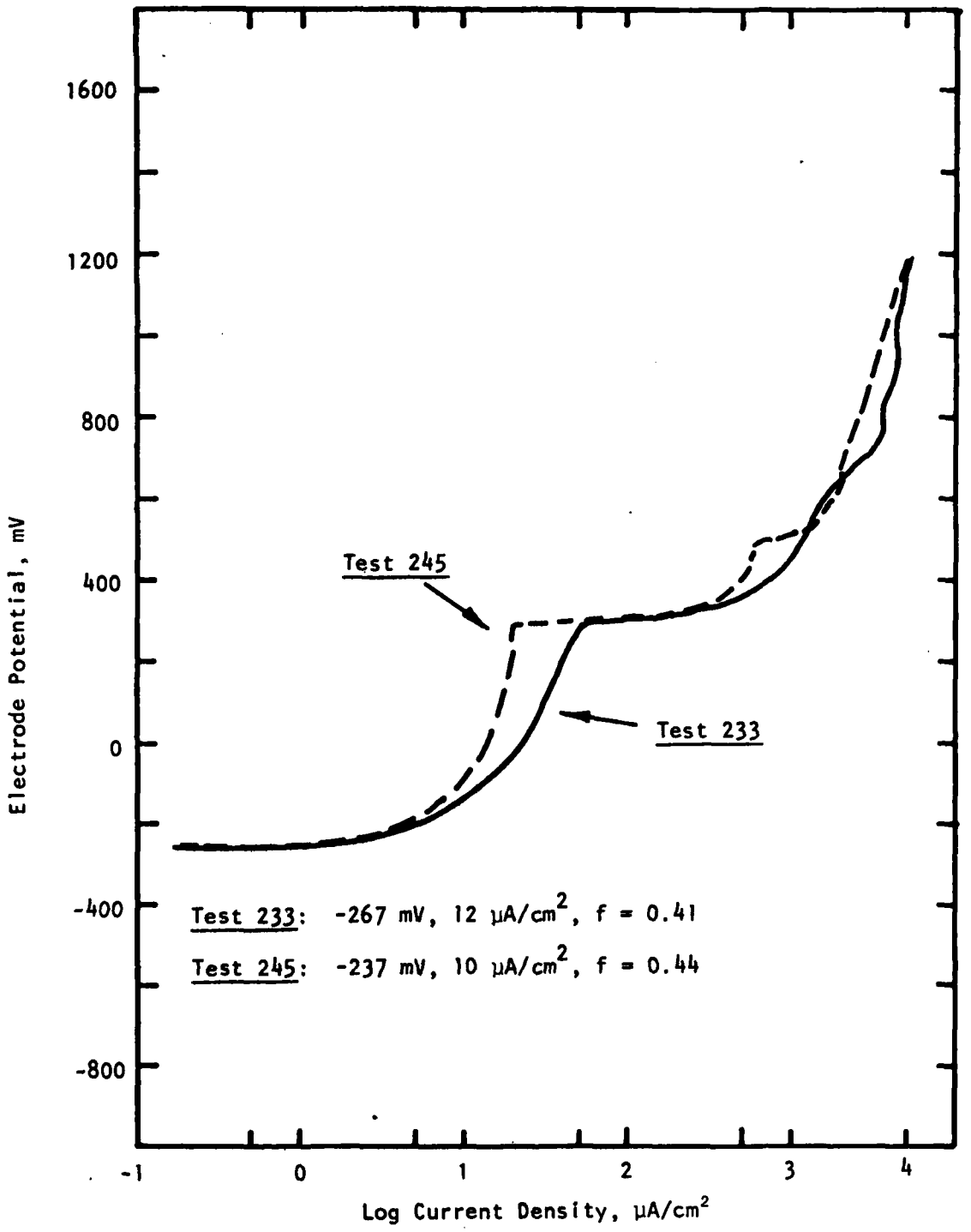

Figure 38. Polarization behavior of M50 steel tested in 100 ppm NaCl solution with 0.01M $Na_2Cr_2O_7$ under 56 lbf (249 N) at 1 cpm (17 mHz).

Neg. No. 55307 25X

Figure 39. Corrosion-wear surface morphology of M50 steel disk tested in 100 ppm NaCl solution with 0.01M $Na_2Cr_2O_7$ under 56 lbf (249 N) at 1 cpm (17 mHz) (test 233).

(b) Effect of Sodium Nitrite and Sodium Molybdate (Tests 232 and 246 vs. 234)

Figure 40 compares the effect of nitrite and molybdate on the polarization behavior of M50 steel in 100 ppm NaCl solution with 0.01M $Na_2Cr_2O_7$ under 16 lbf (71.2 N) at 10 cpm (170 mHz) (tests 232 and 234). Both polarization curves show similar behavior in the open-circuit potential and cell current density except at high anodic potentials. Without nitrite and molybdate, the cell current at high anodic potential (950 mV) showed a sudden increase, indicating severe pit development; however, addition of nitrite and molybdate suppressed the pitting current significantly.

Figure 40 also shows the polarization curve obtained from test 246. Tests 246 and 232 conditions were identical except for the run-in time before polarization measurement: 19 h run-in for test 232 vs. 2 h run-in for test 246. In a strict sense, test 246 was not a true replicate of test 232, but it showed the effect of run-in time on the polarization behavior and friction coefficient. An increase in run-in time (test 232) resulted in an increase in the anodic cell current density and friction coefficient when compared with test 246. General polarization behavior showed a similar trend, in both cases a sharp increase occurred in the cell current at a high anodic potential due to pit formation. Pitting potential was lower for test 246 for which run-in time was substantially shorter than that for test 232.

Figure 41 shows corrosion-wear surface morphology of the disk electrode in test 246. Pits were observed on the wear track zone but not on the free surfaces. Similar morphology was observed on the test 232 specimen. Pit formation would be due to the local deficiency in $Na_2Cr_2O_7$, as discussed previously. Test results of this set show that run-in time affects polarization behavior and friction coefficient significantly, and the results for test 246 were used for statistical analysis since all other tests were done with a 2 h run-in before polarization measurements.

Tests 233 and 245 had the same corrosive environment (electrolyte conditions) as tests 232 and 246, but differed in wear conditions--high load/low frequency for the former and low load/high frequency for the latter--and it was observed that pitting had occurred at a lower potential under high load/low frequency conditions in the presence of dichromate. It seems that

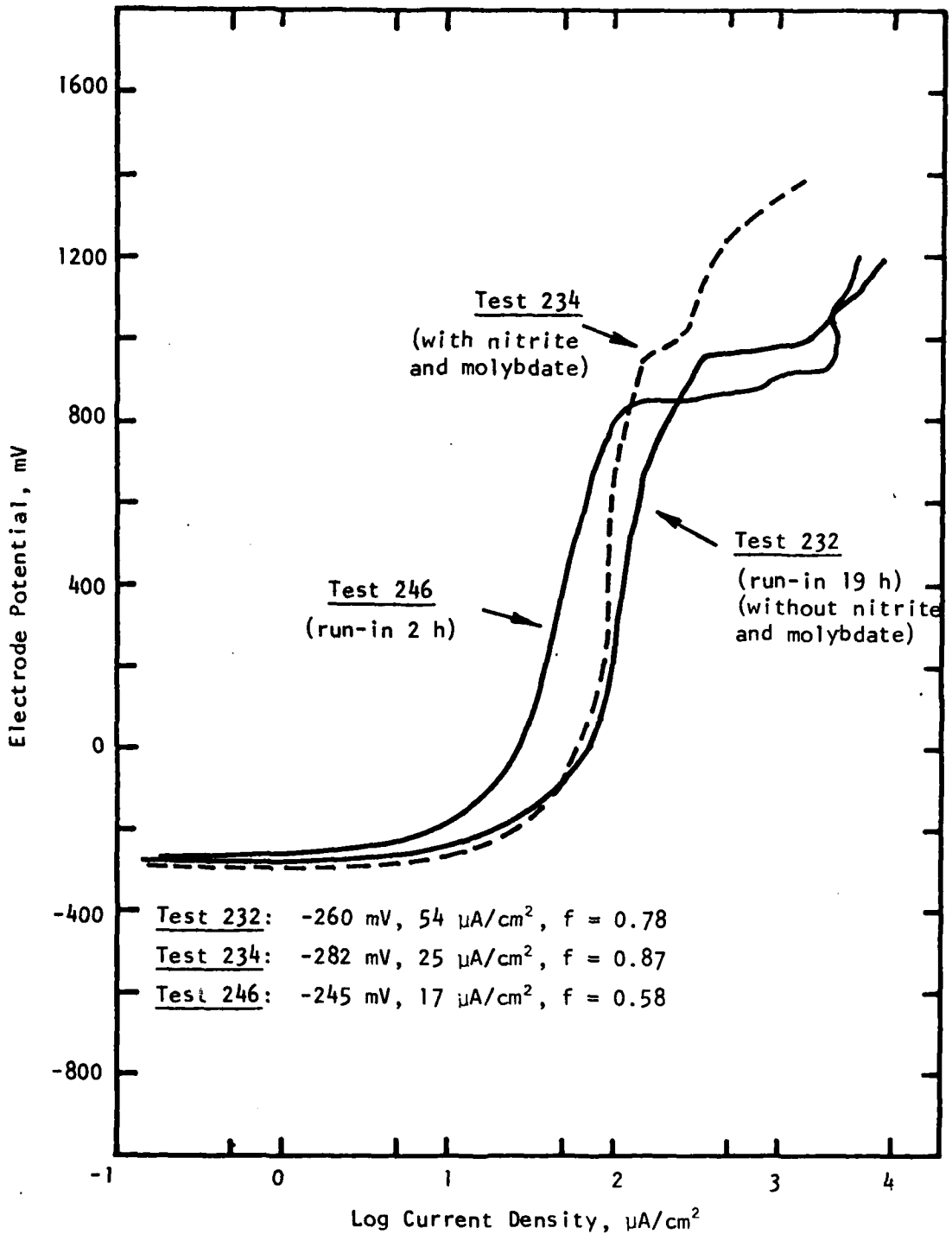

Figure 40. Polarization behavior of M50 steel tested in 100 ppm NaCl solution with 0.01M $Na_2Cr_2O_7$ under 16 lbf (71.2 N) at 10 cpm (170 mHz).

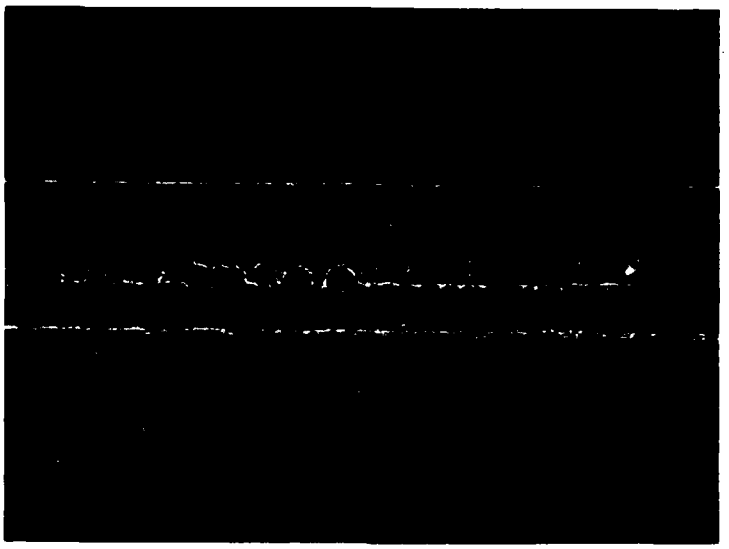

Neg. No. 55316 25X

Figure 41. Corrosion-wear surface morphology of M50 steel disk tested in 100 ppm NaCl solution with 0.01M $Na_2Cr_2O_7$ under 16 lbf (71.2 N) at 10 cpm (170 mHz) (test 246).

AD-A145 781 WEAR AND CORROSION OF COMPONENTS UNDER STRESS AND SUBJECTED TO MOTION(U) IIT RESEARCH INST CHICAGO IL K Y KIM ET AL. 05 MAR 84 IITRI-M06060-16 NADC-79137-60 2/2

UNCLASSIFIED N62269-79-C-0702 F/G 20/11 NL

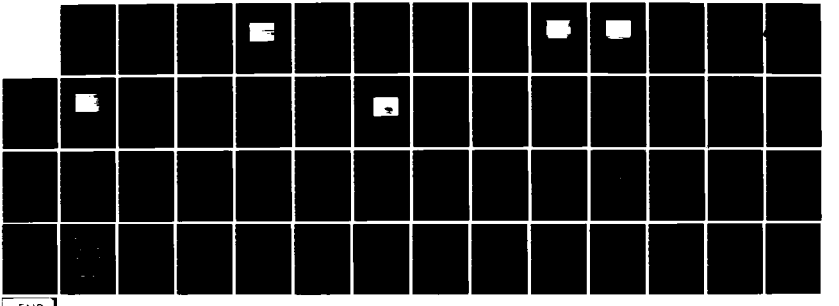

END

FILMED

DTIC

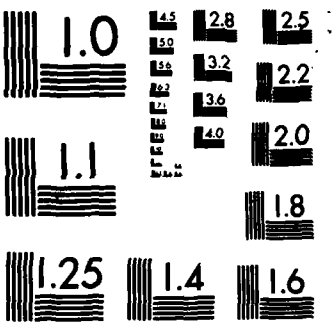

pitting potential was not significantly affected by run-in time since pitting potential of test 232 was much higher than those of tests 233 and 245 although run-in time was substantially longer for test 232 than for the other two.

(c) Effect of Frequency (Tests 235 vs. 236 and 247)

Figure 42 compares the effect of frequency on the polarization behavior of M50 steel in 100 ppm NaCl solution with 0.01M $NaNO_2$ and 0.01M Na_2MoO_4 under 56 lbf (249 N). The effect of frequency was clearly demonstrated on all three corrosion-wear parameters--the open-circuit potential, corrosion current density, and friction coefficient. As observed previously (Fig. 23), an increase in frequency at constant load shifted the open-circuit potential in the more electronegative direction, and increased the cell current density significantly.

Test 247 is a replicate test of test 236, and these results are compared in Fig. 42. General polarization behavior showed the same trend in both tests. Polarization behavior was identical up to approximately 500 mV, beyond which a difference in the anodic cell potential became noticeable. However, the cell current density had the same value at high anodic potentials (above 1200 mV).

Figure 43 shows the corrosion-wear surface morphology of the disk electrode in test 236. Light wear tracks with their orientation parallel to the oscillating direction were observed. Free surfaces were completely passivated, and no indication of wear-assisted corrosion was observed. Similar corrosion-wear surface morphology was observed from test 247 disk electrode. A comparison of Figs. 39 (without nitrite and molybdate) and 43 (with nitrite and molybdate) clearly indicates the role of additional inhibitors in suppressing pitting.

(d) Effect of Load (Tests 239 and 244 vs. 240 and 248)

Figure 44 compares the effect of load on the polarization behavior of M50 steel in 100 ppm NaCl solution with 10% water-soluble oil (tests 239 vs. 240). An increase in load from 16 to 56 lbf (71.2 to 249 N) at 10 cpm (170 mHz) resulted in virtually no change in the open-circuit potential and a slight increase in the corrosion current density. This is in good agreement with the previous observation (Fig. 23) that an increase in load at a constant

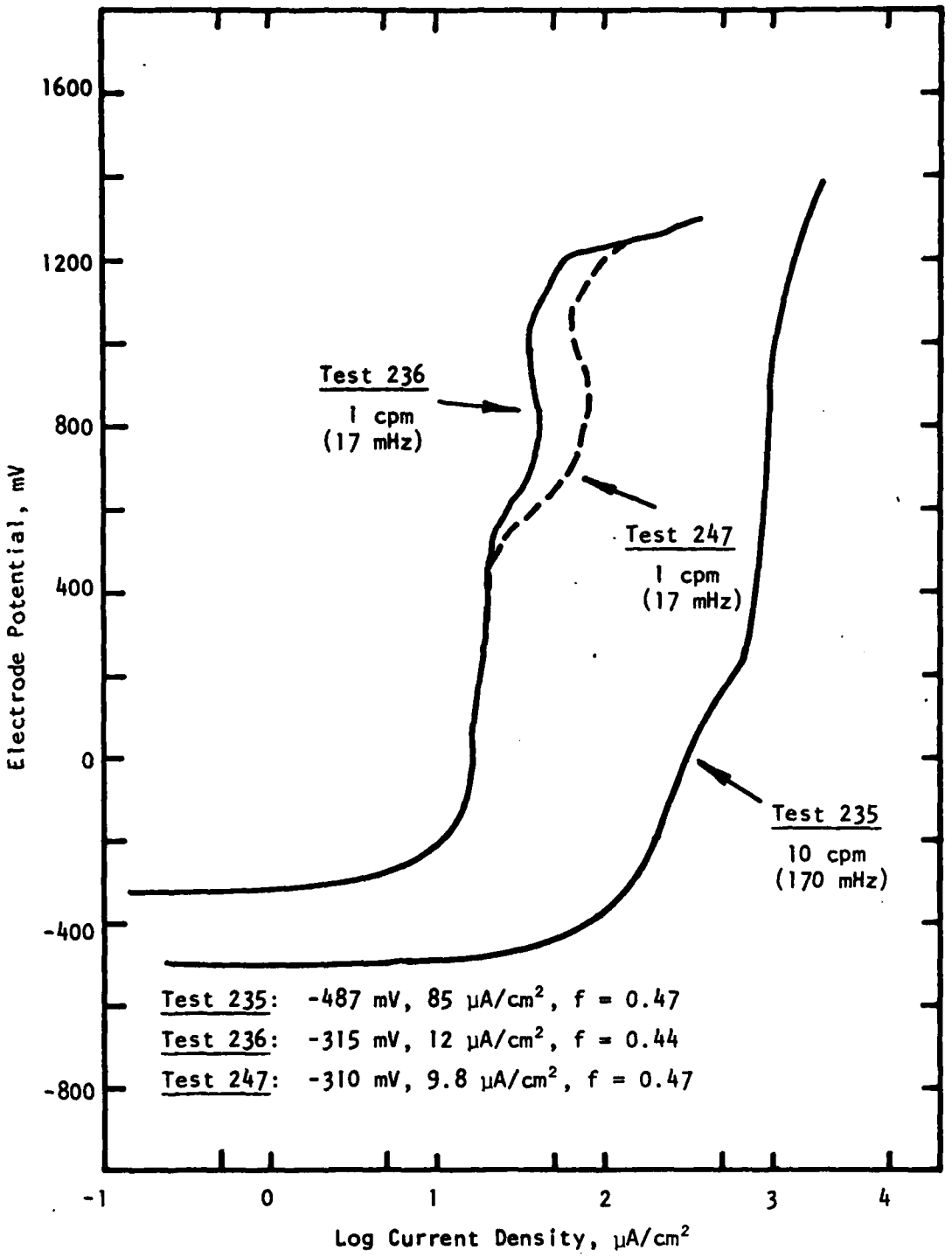

Figure 42. Polarization behavior of M50 steel tested in 100 ppm NaCl solution with 0.01M $NaNO_2$ and 0.01M Na_2MoO_4 under 56 lbf (249 N).

Neg. No. 55310 25X

Figure 43. Corrosion-wear surface morphology of M50 steel disk tested in 100 ppm NaCl solution with 0.01M $NaNO_2$ and 0.01M Na_2MoO_4 under 56 lbf (249 N) at 1 cpm (17 mHz) (test 236).

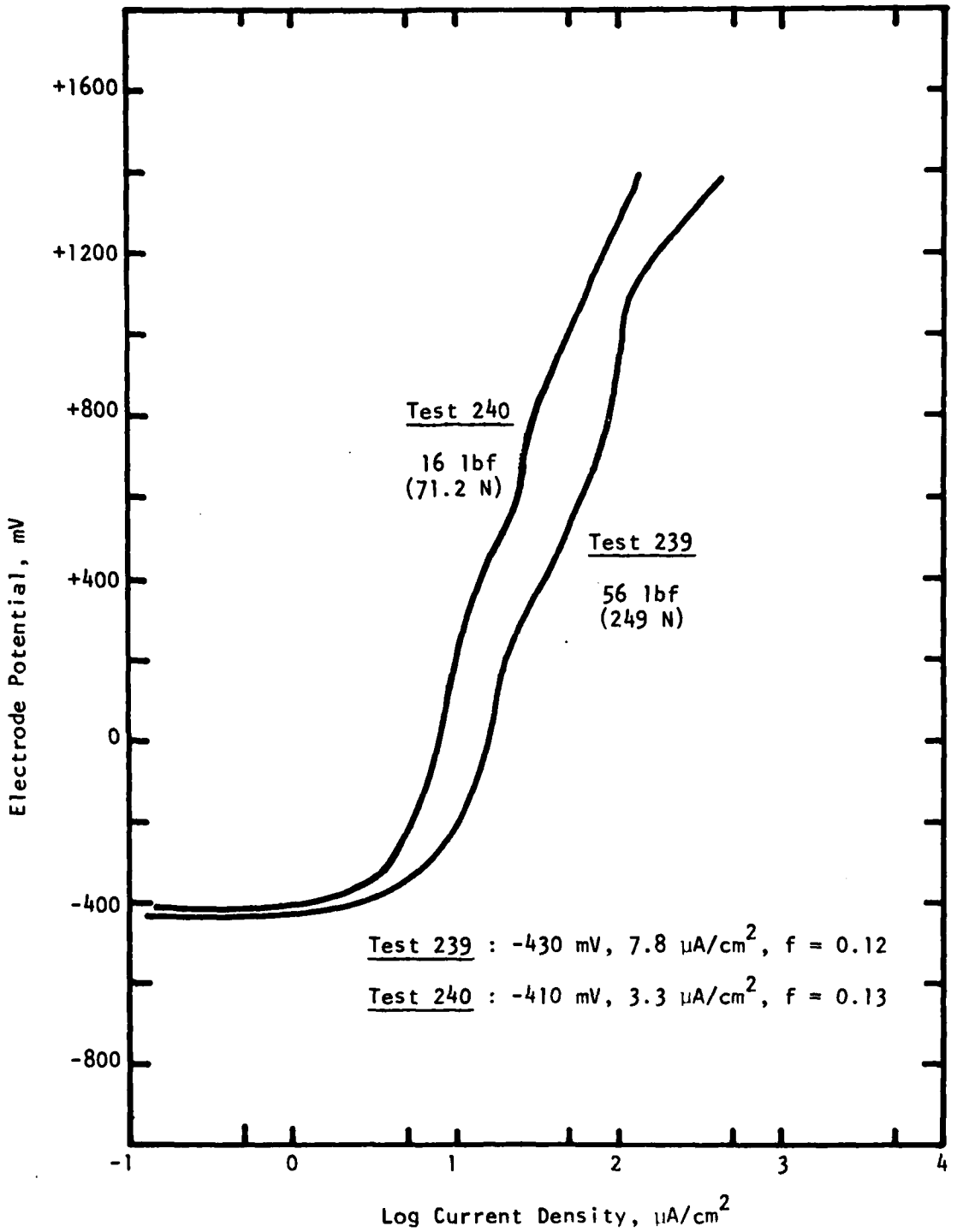

Figure 44. Effect of load on the polarization behavior of M50 steel in 100 ppm NaCl solution with 10% water-soluble oil at 10 cpm (170 mHz).

frequency did not affect the open-circuit potential but increased the anodic cell current slightly. There was no change in the f value due to an increase in load at 10 cpm (170 mHz).

Reproducibility was demonstrated in Figs. 45 (tests 239 vs. 244) and 46 (tests 240 vs. 248) for both loading conditions. In each set of polarization curves, the similarity in polarization behavior is to be noted with a satisfactory reproducibility of polarization measurements and friction coefficient values.

Figures 47 and 48 show the corrosion-wear surface morphology of the disk electrodes of tests 244 and 240, respectively. Light wear tracks with orientation parallel to oscillation direction were observed on both the surfaces. In the presence of lubricant, both disks showed neither pits nor wear-assisted corrosion. Free surfaces of both disks were effectively passivated.

(e) Combined Effect of Corrosion Inhibitors and Lubricant (Tests 237 vs. 243)

Figure 49 compares the combined effect of corrosion inhibitors and lubricant on the polarization behavior of M50 steel in 100 ppm NaCl solution under 16 lbf (71.2 N) at 1 cpm (170 mHz). No corrosion inhibitor or lubricant was used for test 237, whereas 0.01M $Na_2Cr_2O_7$, 0.01M $NaNO_2$, 0.01M Na_2MoO_4, and 10% water-soluble oil were used for test 243. The beneficial effects of corrosion inhibitors and lubricant were clearly observed on all three corrosion-wear parameters of open-circuit potential, corrosion current density, and friction coefficient. Test 237 showed only simple dissolution of iron, while test 243 showed a limited effect of partial passivation. The partial passivation could arise from an effective inhibiting of worn area due to the presence of corrosion inhibitors and lubricant. Significant decrease in friction coefficient for test 243 was due to the presence of water-soluble oil.

(f) Combined Effect of Load and Frequency (Tests 238 and 250 vs. 243)

Figure 50 compares the combined effect of load and frequency on the polarization behavior of M50 steel in 100 ppm NaCl solution with 0.01M $NaNO_2$, 0.01M Na_2MoO_4, and 10% water-soluble oil (tests 238 vs. 243). The load and frequency level was 56 lbf/10 cpm (249 N/170 mHz) and 16 lbf/1 cpm (71.2 N/17 mHz) for tests 238 and 243, respectively. An increase in load and frequency shifted the open-circuit potential in the active direction, and increased the

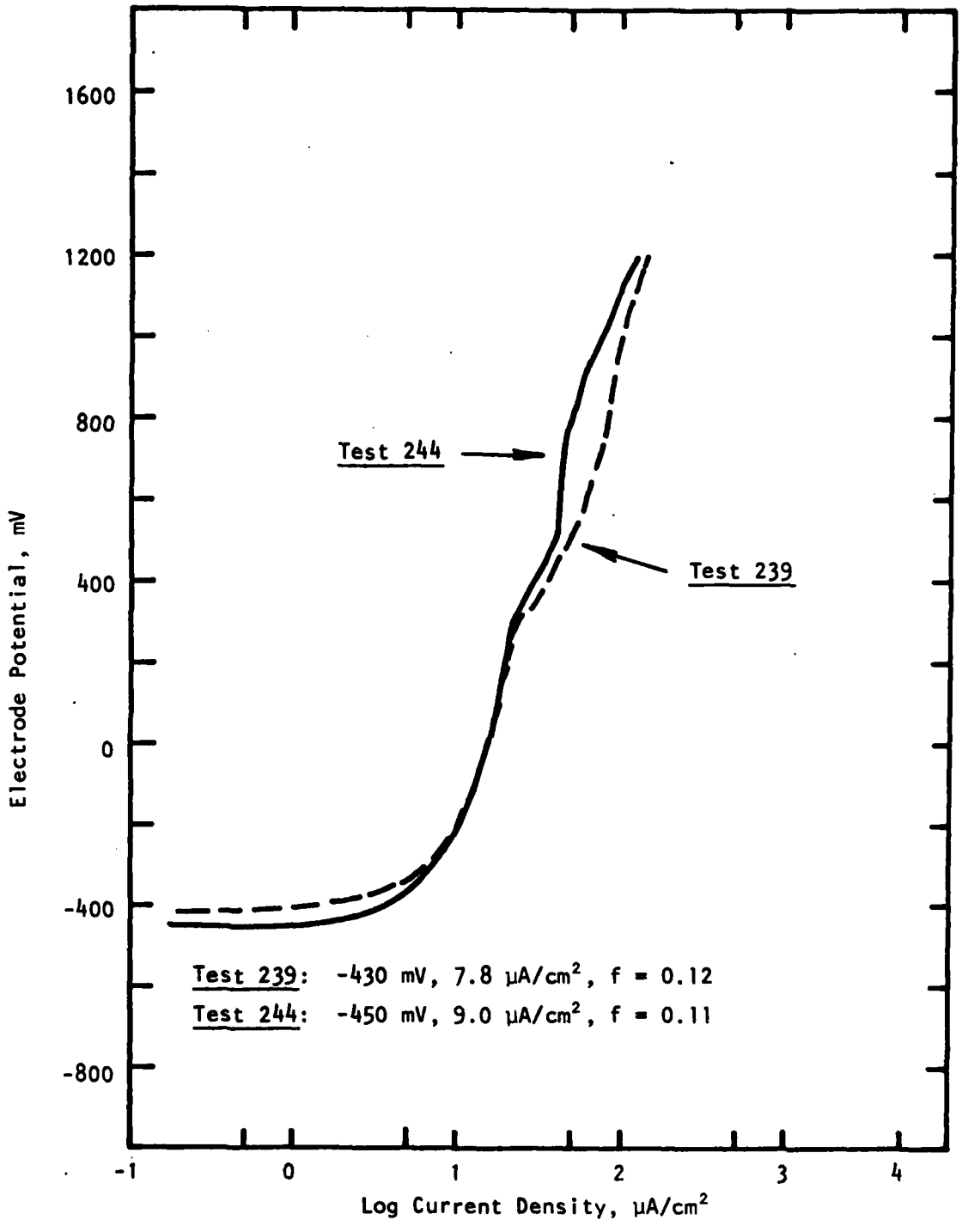

Figure 45. Polarization behavior of M50 steel tested in 100 ppm NaCl solution with 10% water-soluble oil under 56 lbf (249 N) at 10 cpm (170 mHz).

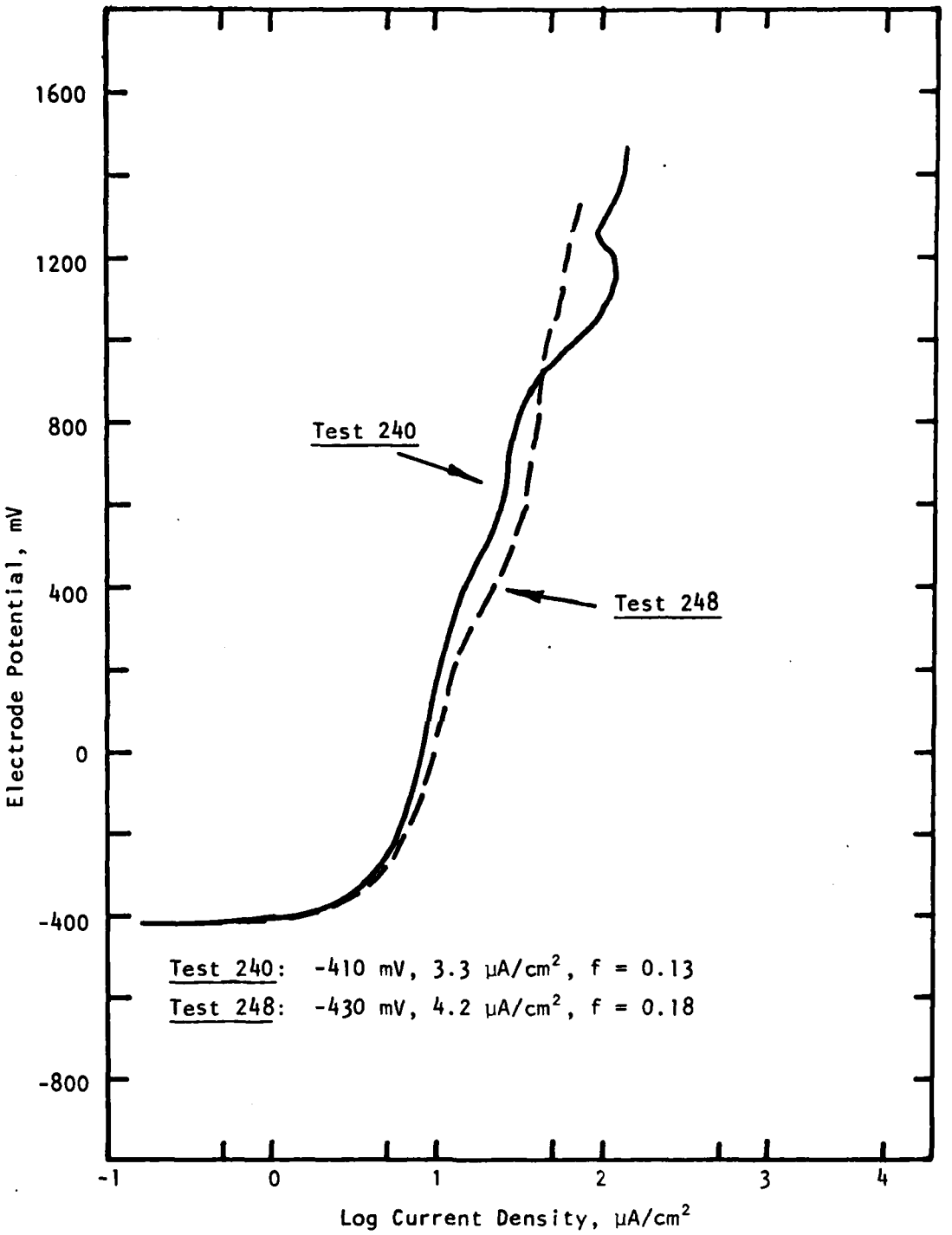

Figure 46. Polarization behavior of M50 steel tested in 100 ppm NaCl solution with 10% water-soluble oil under 16 lbf (71.2 N) at 10 cpm (170 mHz).

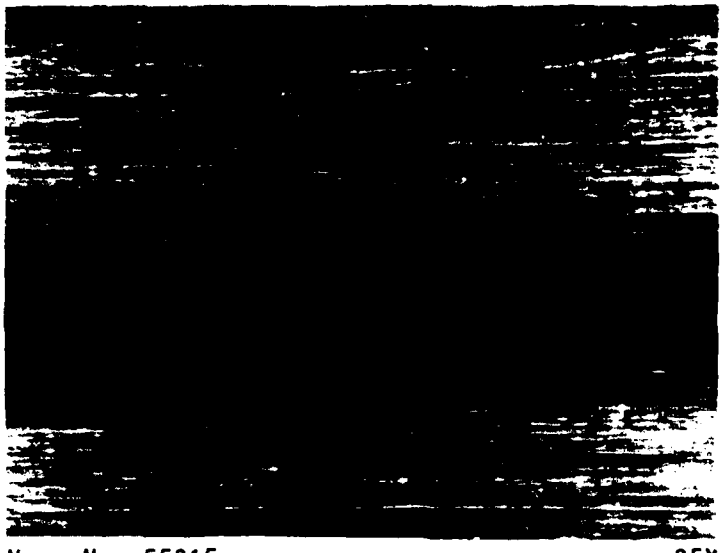

Neg. No. 55315 25X

Figure 47. Corrosion-wear surface morphology of M50 steel disk tested in 100 ppm NaCl solution with 10% water-soluble oil under 56 lbf (249 N) at 10 cpm (170 mHz) (test 244).

Neg. No. 55314 25X

Figure 48. Corrosion-wear surface morphology of M50 steel disk tested in 100 ppm NaCl solution with 10% water-soluble oil under 16 lbf (71.2 N) at 10 cpm (170 mHz) (test 240).

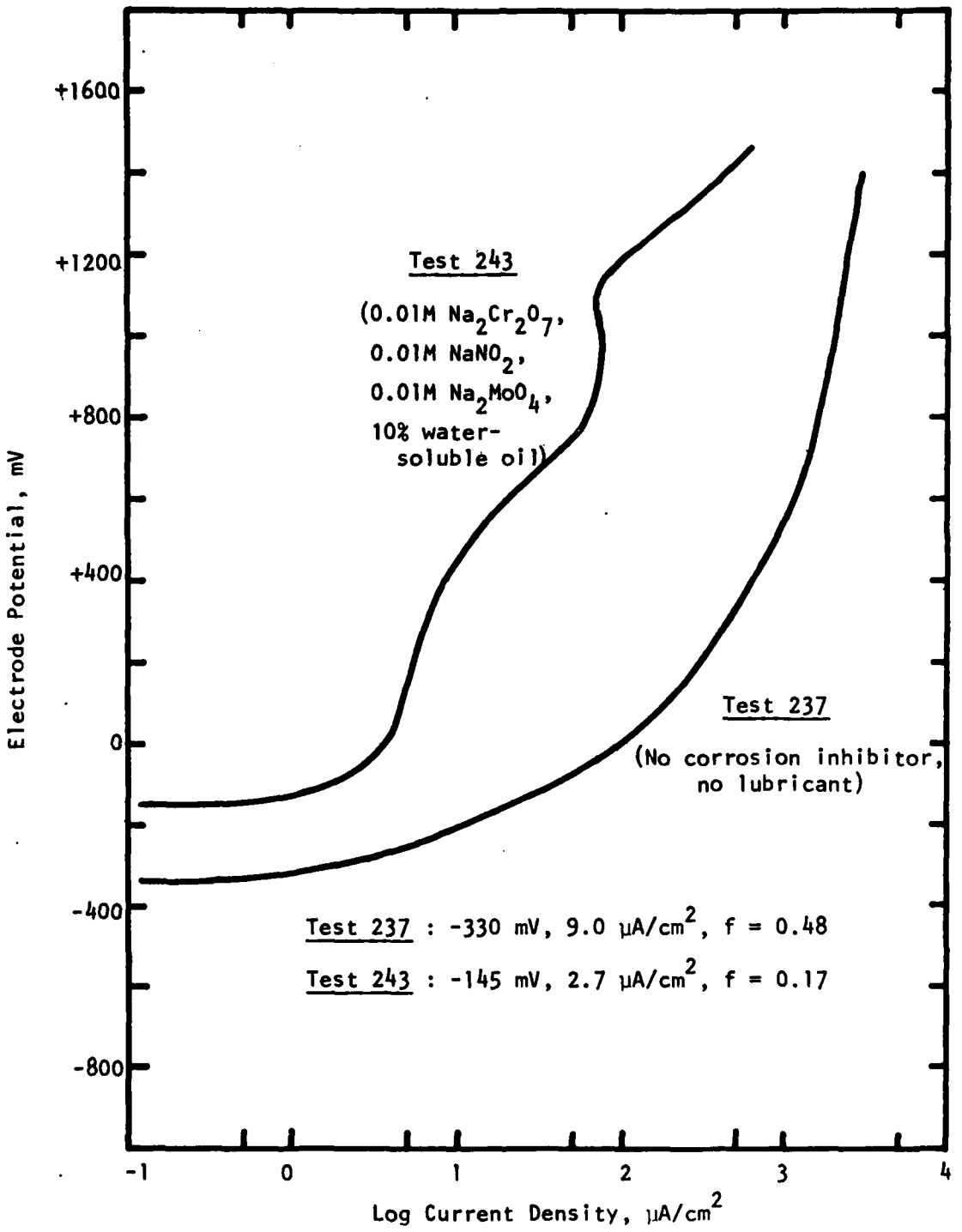

Figure 49. Combined effect of corrosion inhibitors and lubricant on the polarization behavior of M50 steel in 100 ppm NaCl solution under 16 lbf (71.2 N) at 1 cpm (17 mHz).

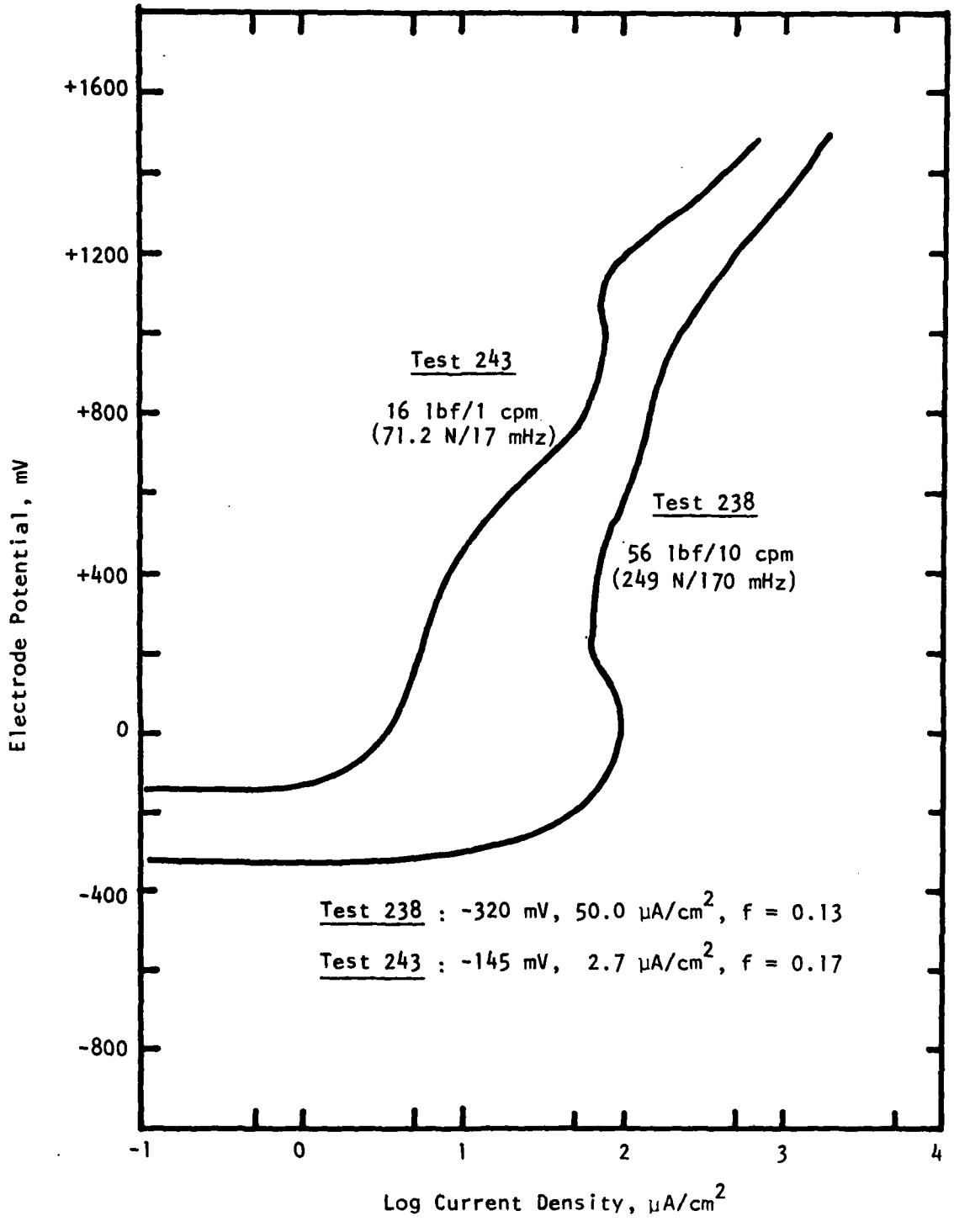

Figure 50. Combined effect of load and frequency on the polarization behavior of M50 steel in 100 ppm NaCl solution with 0.01M $NaNO_2$, 0.01M Na_2MoO_4, and 10% water-soluble oil.

corrosion current density by one and a half orders of magnitude. The effect of load and frequency on the anodic cell current was clearly observed in the entire anodic potential range. The change in friction coefficient due to an increase in load and frequency was marginal. It seems that friction behavior was more strongly and favorably influenced by the presence of water-soluble oil over the combined effect of load and frequency.

Test 250 was a replicate test of test 238, and the polarization behaviors of these two tests are compared in Fig. 51. Reproducibility in polarization measurement and friction coefficient values was not satisfactory. With the use of water-soluble oil, introduction of air in the cell tended to develop a separation of oil and aqueous electrolyte, and created difficulties in corrosion-wear potential-current measurements. Adaptation of an external stirring system effectively solved this problem and made it possible to measure the electrode polarization reaction under wear. However, this replicate test 250 showed that, with air saturation in the presence of the type of oil used and corrosion inhibitors, satisfactory reproducibility may be difficult to achieve and different oils should be sought. Nonetheless, a comparison of polarization behaviors between tests 243 (Fig. 50) and 250 (Fig. 51) clearly demonstrated the combined effect of load and frequency in the presence of oil in the electrolyte.

Figure 52 shows corrosion-wear surface morphology of the disk electrode from test 238. Deep wear tracks were observed; however, no wear-assisted corrosion was indicated. Free surfaces were effectively passivated. A similar surface morphology was observed on the disk electrode of test 250.

(g) Effect of Load and Sodium Dichromate (Tests 234 vs. 235)

Figure 53 compares the effect of load and sodium dichromate on the polarization behavior of M50 steel in 100 ppm NaCl solution with 0.01M $NaNO_2$ and 0.01M Na_2MoO_4. An addition of 0.01M $Na_2Cr_2O_7$ under 16 lbf (71.2 N) at 10 cpm (170 mHz) shifted the open-circuit potential in the anodic direction significantly and reduced the corrosion current density. The shift in the open-circuit potential may be attributed to the presence of $Na_2Cr_2O_7$ since a change in load at constant frequency usually resulted in no change in the open-circuit potential (see Figs. 23 and 40). The effect of load and $Na_2Cr_2O_7$ on the cell current density can be clearly observed over the entire anodic

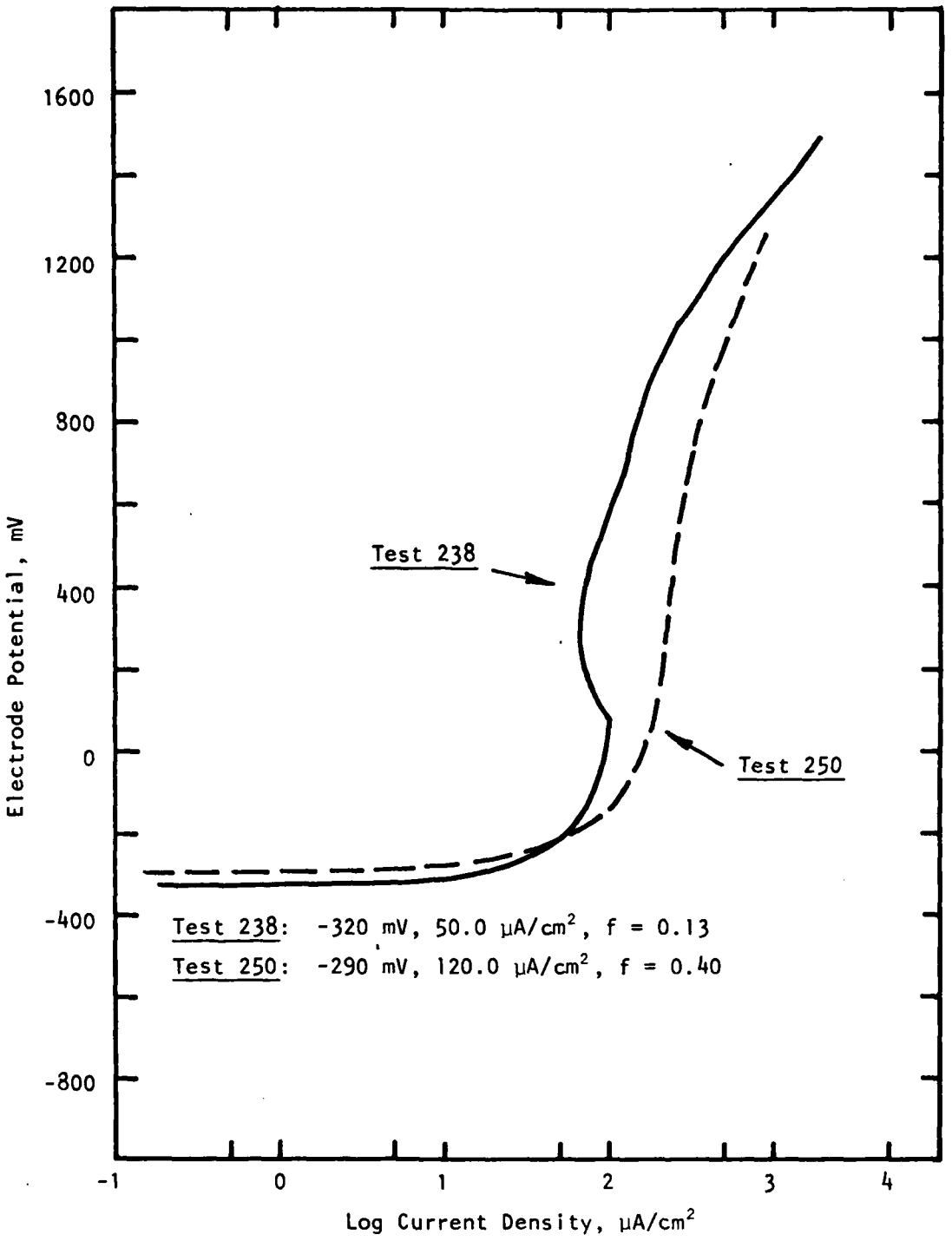

Figure 51. Polarization behavior of M50 steel tested in 100 ppm NaCl solution with 0.01M $Na_2Cr_2O_7$, 0.01M $NaNO_2$, 0.01M Na_2MoO_4, and 10% water-soluble oil under 56 lbf (249 N) at 10 cpm (170 mHz).

Neg. No. 55312 25X

Figure 52. Corrosion-wear surface morphology of M50 steel disk tested in 100 ppm NaCl solution with 0.01M $Na_2Cr_2O_7$, 0.01M $NaNO_2$, 0.01M Na_2MoO_4, and 10% water-soluble oil under 56 lbf (249 N) at 10 cpm (170 mHz) (test 238).

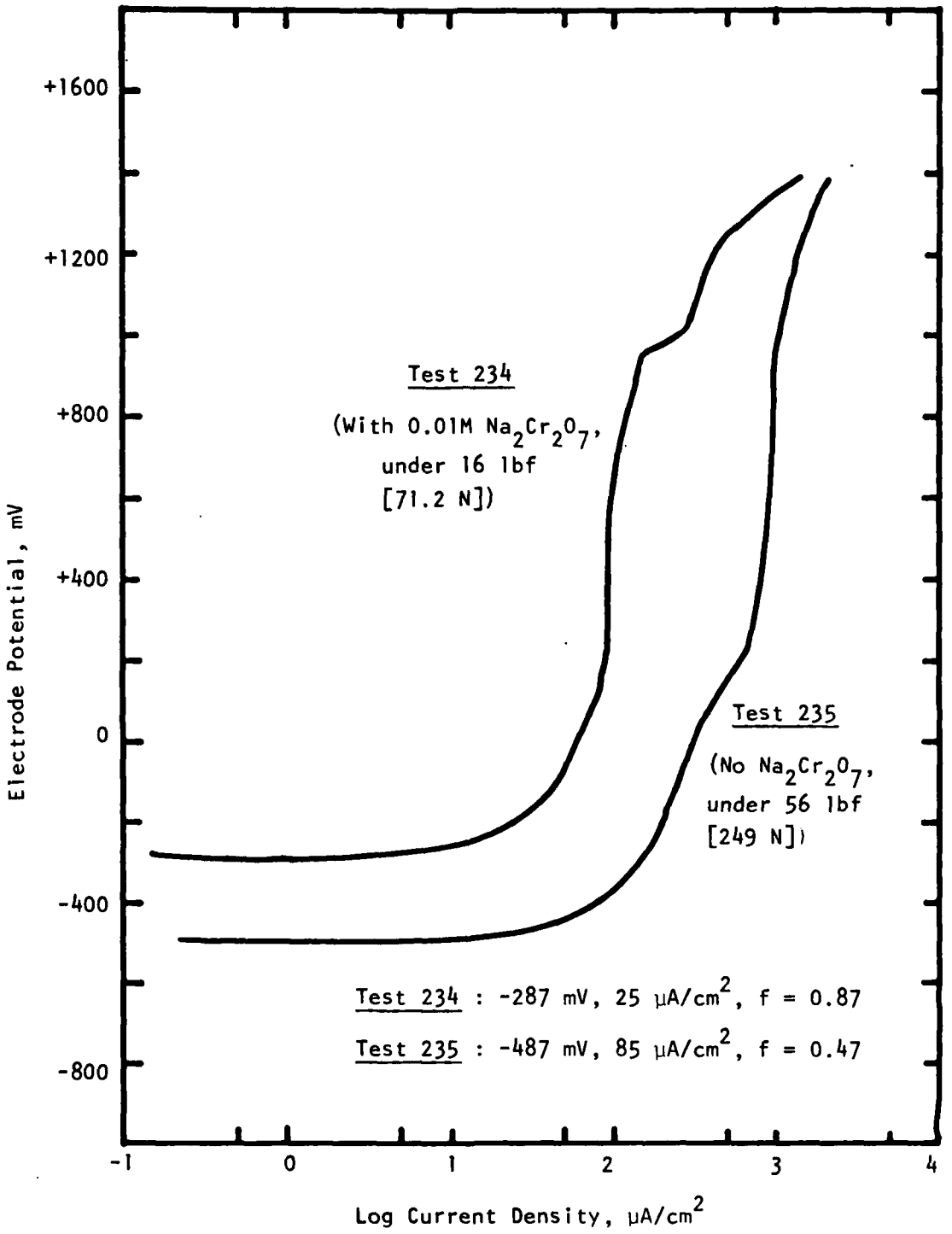

Figure 53. Effect of load and of sodium dichromate on the polarization behavior of M50 steel in 100 ppm NaCl solution with 0.01M $NaNO_2$ and 0.01M Na_2MoO_4 at 10 cpm (170 mHz).

potential range. The friction coefficient for test 234 was significantly higher than that of test 235. In test 234, the presence of chromic oxide at the interface would have a tendency to increase the friction coefficient while, in test 235, the effect of the higher load and absence of chromic oxide combined might have contributed favorably in decreasing the net shearing force of the oxide and metal asperity junctions--hence, a reduction in the friction coefficient.

(h) Effect of Sodium Dichromate (Tests 241 and 249 vs. 243)

Figure 54 compares the effect of sodium dichromate on the polarization behavior of M50 steel in 100 ppm NaCl solution with 0.01M $NaNO_2$, 0.01M Na_2MoO_4, and 10% water-soluble oil under 16 lbf (71.2 N) at 1 cpm (17 mHz) (tests 241 vs. 243). The presence of $Na_2Cr_2O_7$ with other corrosion inhibitors and lubricant shifted the open-circuit potential in the anodic direction; however, no particular difference in the cell current density was observed. Friction coefficient remained unaffected by the addition of $Na_2Cr_2O_7$ since the presence of water-soluble oil dominated the friction reaction.

Test 249 is a replicate test of test 241, and results are presented in Fig. 55. Reproducibility in both polarization measurement and friction coefficient values was unsatisfactory due to oil foaming and separation problems mentioned earlier for tests 238 and 250. A comparison between tests 243 and 241, however, had indicated that the presence of $Na_2Cr_2O_7$ with other corrosion inhibitors and lubricant may not be harmful although not particularly beneficial either, and caused no sudden increase in cell current density due to pit formation as was usually observed when $Na_2Cr_2O_7$ alone was used.

Figure 56 shows corrosion-wear surface morphology of the disk electrode in test 249. Light wear tracks without any wear-assisted corrosion were observed. Free surfaces were effectively passivated. A similar corrosion-wear surface morphology was observed on the disk electrode of test 241.

(i) Effect of Corrosion Inhibitors (Tests 238 and 239)

Figure 57 compares the effect of corrosion inhibitors on the polarization behavior of M50 steel in 100 ppm NaCl solution with 10% water-soluble oil under 56 lbf (249 N) at 10 cpm (170 mHz). The presence of corrosion inhibitors shifted the open-circuit potential in the anodic direction and increased

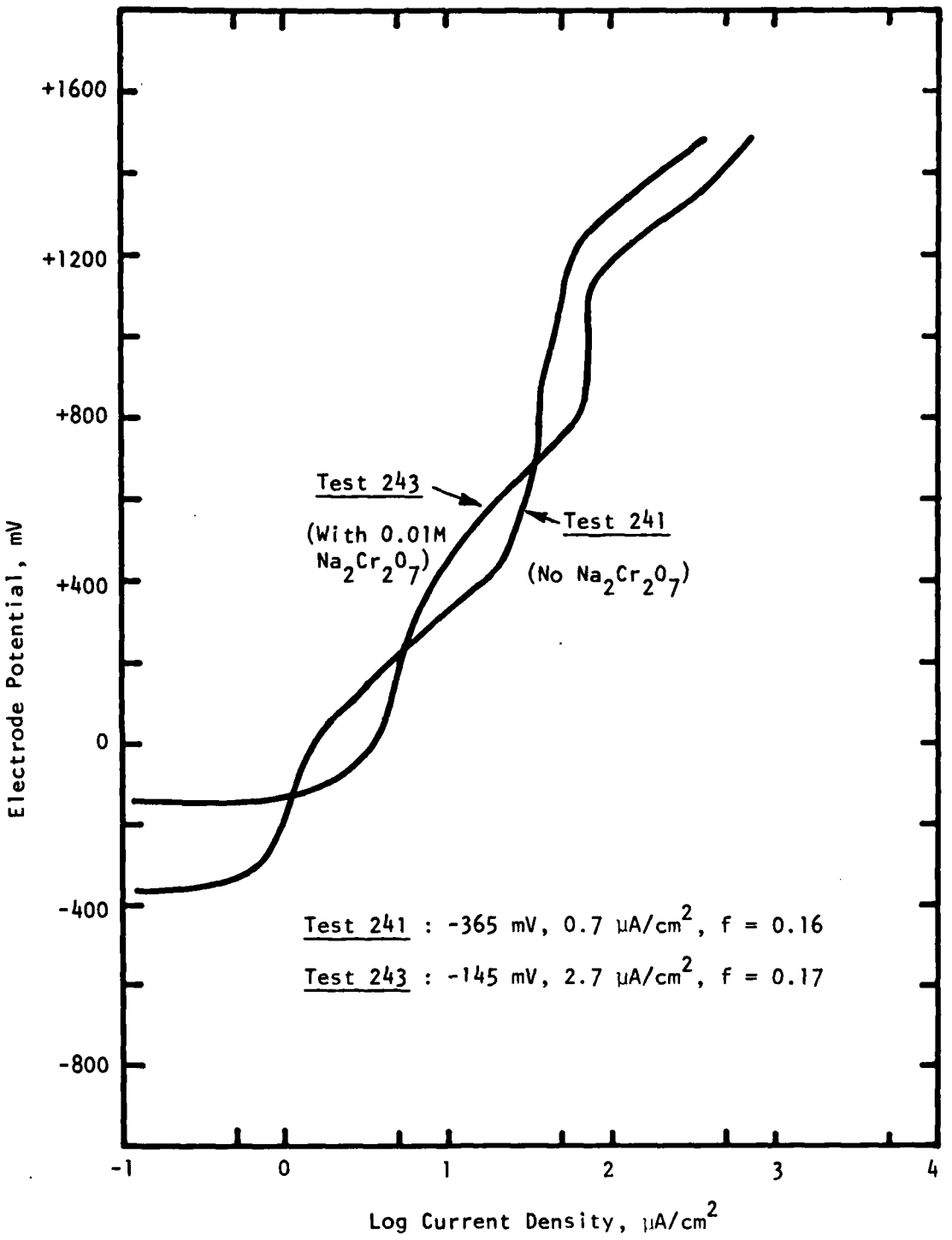

Figure 54. Effect of sodium dichromate on the polarization behavior of M50 steel in 100 ppm NaCl solution with 0.01M $NaNO_2$, 0.01M Na_2MoO_4, and 10% water-soluble oil under 16 lbf (71.2 N) at 1 cpm (17 mHz).

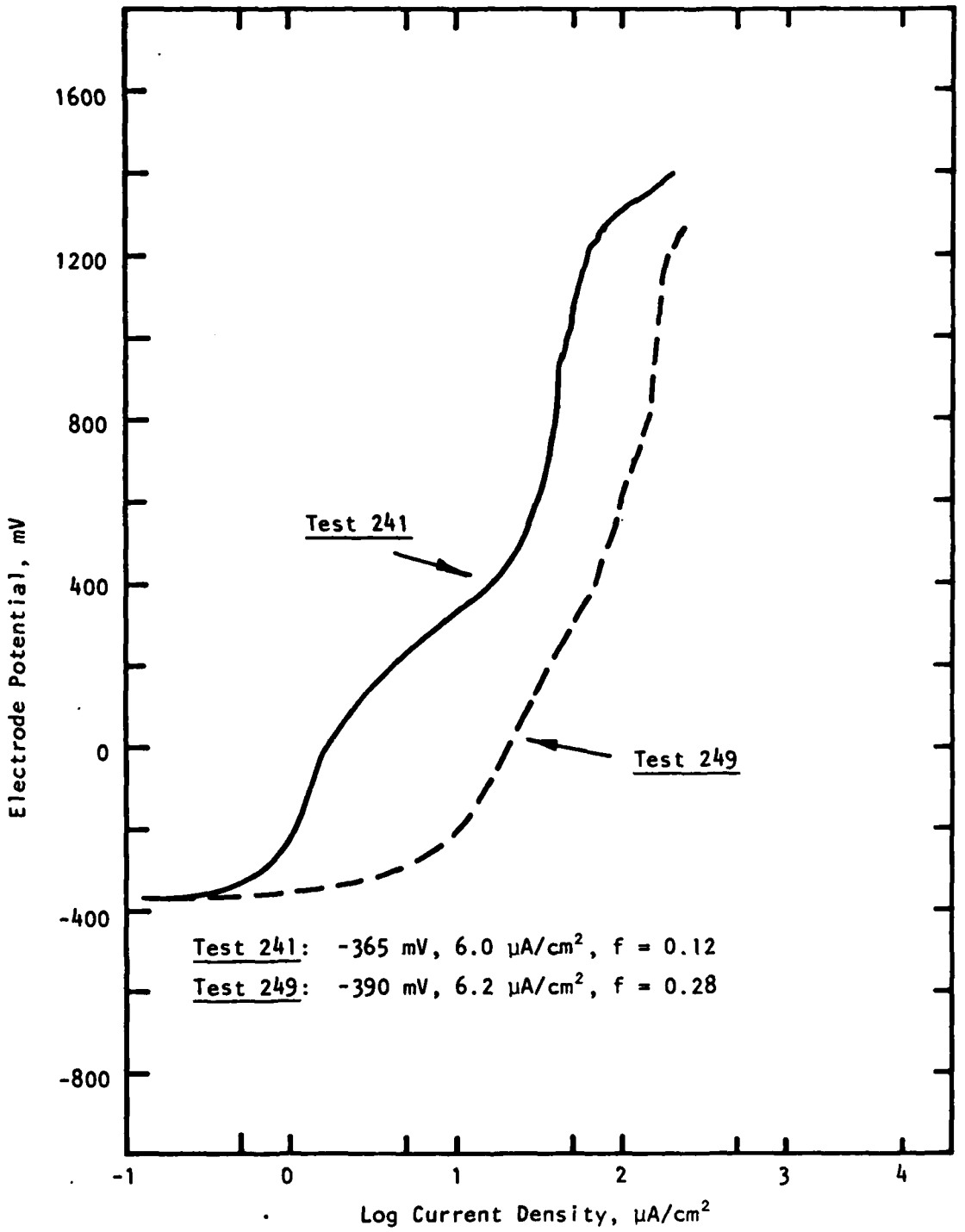

Figure 55. Polarization behavior of M50 steel tested in 100 ppm NaCl solution with 0.01M $NaNO_2$, 0.01M Na_2MoO_4, and 10% water-soluble oil under 16 lbf (71.2 N) at 1 cpm (17 mHz).

Neg. No. 55327 25X

Figure 56. Corrosion-wear surface morphology of M50 steel disk tested in 100 ppm NaCl solution with 0.01M $NaNO_2$, 0.01M Na_2MoO_4, and 10% water-soluble oil under 16 lbf (71.2 N) at 1 cpm (17 mHz) (test 249).

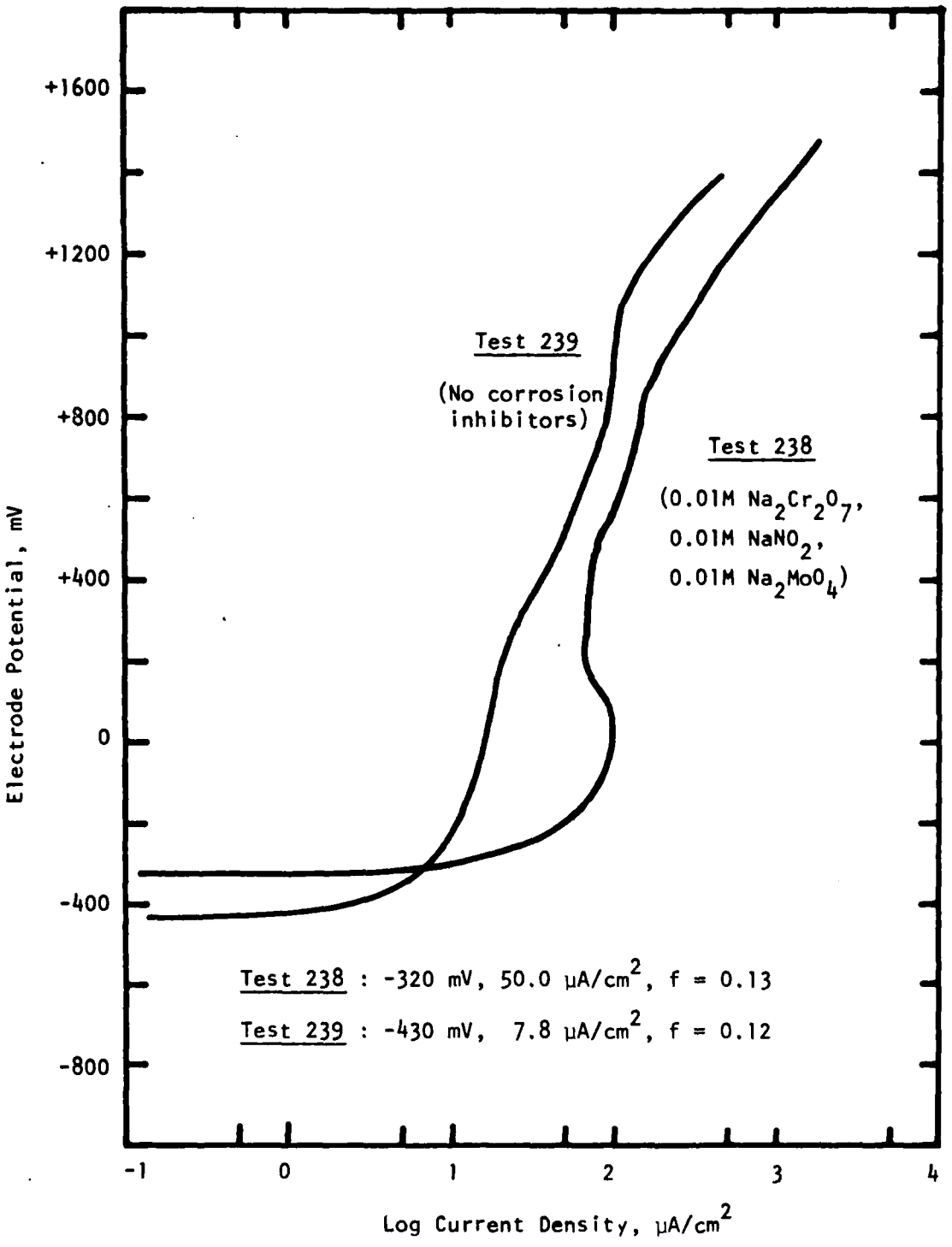

Figure 57. Effect of corrosion inhibitors on the polarization behavior of M50 steel in 100 ppm NaCl solution with 10% water-soluble oil under 56 lbf (249 N) at 10 cpm (170 mHz).

the corrosion current density significantly. No beneficial effect of corrosion inhibitors on polarization behavior was observed when lubricant was also present. No change in friction coefficient was observed between the two tests. It seems that the water-soluble oil dominated the friction reaction although the presence of corrosion inhibitors might have modified it to a certain extent.

5.6.2 Statistical Analysis

A statistical analysis was made to determine the significance of the effectiveness of test variables on observed corrosion-wear parameters. The test matrix used in this program is given in Table 11 following a standard Plackett-Burman design. A set of five variables was assigned to control independently corrosion-wear processes in each experiment, whereas the remaining six unassigned variables were used to estimate the experimental error. The computation procedure of the factor effect for a 12-run Plackett-Burman test is described in the literature.[4]

Table 12 summarizes all 19 corrosion-wear test data for statistical analysis of (1) open-circuit potential, (2) corrosion current density, and (3) friction coefficient. For this analysis, the 7 replicate test data were combined with their corresponding initial 7-test data and the average values were used in the analysis along with the initial 5 non-replicated test data. Results of test 246 alone were used instead of the average values of test 232 and 246 data because test 232 had a 19 h run-in instead of the 2 h run-in common to all the other tests.

The significance ratios for a Plackett-Burman type statistical analysis with 5 assigned variables were 1.440, 1.943, and 2.447 at 80%, 90%, and 95% confidence levels, respectively. Tables 13, 14, and 15 summarize the results of statistical analyses of the open-circuit potential, corrosion current density, and friction coefficient, respectively.

(a) Open-Circuit Potential

Table 13 summarizes the results of statistical analysis of the open-circuit potential. Using the unassigned variables, the significant factor effect (S_{FE}) was calculated to be 27.3. The minimum factor effect was 39.3, 53.0, and 66.8 at confidence levels of 80%, 90%, and 95%, respectively. At

TABLE 12. SUMMARY OF CORROSION-WEAR TEST RESULTS

Trial No.	Test No.	Wear Cond. Load, lbf[a]	Wear Cond. Freq, cpm[b]	Corrosion Inhibitors[c] and Lubricant $Na_2Cr_2O_7$	$NaNO_2$	$NaMoO_4$	Lubricant[d]	$E_{o.c.}$, mV	$I_{corr.}$, $\mu A/cm^2$	(mpy)	Fric. Coeff. (f)
1	238	56	10	X	X	X	X	-320±15	50.0	(23.0)	0.13
	250							-290±20	120.0	(55.0)	0.40
2	243	16	1	X	X	X	X	-145±15	2.7	(1.2)	0.17
3	240	16	10				X	-410±5	3.3	(1.5)	0.13
	248							-430±5	4.2	(1.9)	0.18
4	232	16	10	X				-260±10	54.0	(24.7)	0.78
	246							-245±10	17.0	(7.8)	0.58
5	233	56	1	X				-267±12	12.0	(5.5)	0.41
	245							-237±13	10	(4.6)	0.44
6	234	16	10	X	X	X		-282±17	25.0	(11.4)	0.87
7	239	56	10				X	-430±20	7.8	(3.5)	0.12
	244							-450±10	9.0	(4.1)	0.11
8	235	56	10		X	X		-487±12	85.0	(38.9)	0.47
9	241	16	1		X	X	X	-365±15	6.0	(2.7)	0.12
	249							-390±30	6.2	(2.8)	0.28
10	242	56	1	X			X	-297±17	6.0	(2.7)	0.12
11	236	56	1	X			X	-315±15	12.0	(5.5)	0.44
	247							-310±15	9.8	(4.5)	0.47
12	237	16	1		X	X		-330±25	9.0	(4.1)	0.48

[a] 1 lbf = 4.45 Newtons.

[b] 1 cpm = 17 mHz.

[c] In 100 ppm NaCl solution.

[d] 10% water-soluble oil.

TABLE 13. RESULTS OF STATISTICAL ANALYSIS OF OPEN-CIRCUIT POTENTIAL

Trial	Mean	X1	X2	X3	X4	X5	X6	X7	X8	X9	X10	X11	$\bar{Y}$, $E_{o.c.}$ (mV)
1	+	+	+	-	+	+	+	-	-	-	+	-	-305
2	+	+	-	+	+	+	-	-	-	+	-	+	-145
3	+	-	+	+	+	-	-	-	+	-	+	+	-420
4	+	+	+	+	-	-	-	+	-	+	+	-	-245
5	+	+	+	-	-	-	+	-	+	+	-	+	-252
6	+	+	-	-	-	+	-	+	+	-	+	+	-282
7	+	-	-	-	+	-	+	+	-	+	+	+	-440
8	+	-	-	+	-	+	+	-	+	+	+	-	-487
9	+	-	+	-	+	+	-	+	+	+	-	-	-378
10	+	+	-	+	+	-	+	+	+	-	-	-	-297
11	+	-	+	+	-	+	+	+	-	-	-	+	-313
12	+	-	-	-	-	-	-	-	-	-	-	-	-330
Sum +	-3894	-1526	-1913	-1907	-1985	-1910	-2094	-1955	-2116	-1947	-2179	-1852	
Sum -	0	-2368	-1981	-1987	-1909	-1984	-1800	-1939	-1778	-1947	-1715	-2042	
Overall Sum	-3894	-3894	-3894	-3894	-3894	-3894	-3894	-3894	-3894	-3894	-3894	-3894	
Diff.	-3894	842	68	80	-76	74	-294	16	-338	0	-464	190	
Effect	-324.5	140.3	11.3	13.3	-12.6	12.3	-49.0	-2.7	-56.3	0	-77.3	31.6	

S_{FE} = 27.3

[MIN] 1.440 x 27.3 = 39.3 (80% confidence level) — Significant Factors: X1, X10, X6

1.943 x 27.3 = 53.0 (90% confidence level) — Significant Factors: X1, X10

2.447 x 27.3 = 66.8 (95% confidence level) — Significant Factors: X1, X10

each confidence level, any assigned variable with an absolute factor effect value greater than the minimum factor effect would be considered to be statistically significant on the open-circuit potential. This analysis indicated that the presence of $Na_2Cr_2O_7$ (X1), oscillatory frequency (X10), and load (X6) were the variables affecting the open-circuit potential significantly at 80% confidence level. At higher levels of confidence, 90% and 95%, the load was not a significant factor. When compared to the analysis made from the initial 12-test data, the load variable was also not statistically significant at the highest confidence level of 95%.

If the numerical values of "effect" of each variable are compared, it may be noted that the effect of $Na_2Cr_2O_7$ on the open-circuit potential is predominant over all the other factors. The open-circuit potential is, in general, more cathodic without $Na_2Cr_2O_7$. An increase in the open-circuit potential in the anodic direction due to presence of $Na_2Cr_2O_7$ is attributed to the fast oxygen-reduction reaction because of a constant and large supply of air. Without additional tests conducted in the total absence or limited presence of air, the $Na_2Cr_2O_7$ role on open-circuit potential cannot be fully clarified.

The effect of frequency and load on the open-circuit potential was related to surface deformation. With increasing severity of surface deformation, the open-circuit potential became more electronegative.

(b) Corrosion Current Density

Table 14 summarizes the results of statistical analysis of the corrosion current density. The corrosion current density was determined by the Tafel extrapolation method. The reported values of corrosion current density had an error range of approximately ±10% since no clear linear Tafel region can be obtained from several of the polarization measurements in corrosion-wear systems. The statistical analysis showed the significant factor effect (S_{FE}) to be 13.3. The minimum factor effect was 19.2, 25.8, and 32.5 at 80%, 90%, and 95% confidence levels, respectively. At 80% confidence level, the frequency (X10), the presence of $NaNO_2$ and Na_2MoO_4 (X5), and the load (X6) showed statistically significant effects on corrosion current density. At 90% confidence level, however, the load effect was not significant. At the highest confidence level of 95%, none of the factors appear to have statistical significance in affecting the corrosion current density.

TABLE 14. RESULTS OF STATISTICAL ANALYSIS OF CORROSION CURRENT DENSITY

Trial	Mean	X1	X2	X3	X4	X5	X6	X7	X8	X9	X10	X11	$\bar{Y}$, $I_{corr.}$ $\mu A/cm^2$
1	+	+	+	-	+	+	+	-	-	-	+	-	85.0
2	+	+	-	+	+	+	-	-	-	+	-	+	2.7
3	+	-	+	+	+	-	-	-	+	-	+	+	3.8
4	+	+	+	+	-	-	-	+	-	+	+	-	17.0
5	+	+	+	-	-	-	+	-	+	+	-	+	11.0
6	+	+	-	-	-	+	-	+	+	-	+	+	25.0
7	+	-	-	-	+	-	+	+	-	+	+	+	5.9
8	+	-	-	+	-	+	+	-	+	+	+	-	85.0
9	+	-	+	-	+	+	-	+	+	+	-	-	3.5
10	+	+	-	+	+	-	+	+	+	-	-	-	6.0
11	+	-	+	+	-	+	+	+	-	-	-	+	10.9
12	+	-	-	-	-	-	-	-	-	-	-	-	9.0

Sum +	264.8	146.7	131.2	125.4	106.9	212.1	203.8	68.3	134.3	125.1	221.7	59.3
Sum -	0	118.1	133.6	139.4	157.9	52.7	61.0	196.5	130.5	139.7	43.1	205.5
Overall Sum	264.8	264.8	264.8	264.8	264.8	264.8	264.8	264.8	264.8	264.8	264.8	264.8
Diff.	264.8	28.6	-2.4	-14.0	-51.0	159.4	142.8	-128.2	3.8	-14.6	178.0	-146.2
Effect	22.06	4.76	-0.40	-2.33	-8.50	26.56	23.80	-21.36	0.63	-2.43	29.66	-24.36

S_{FE} = 13.3

		Significant Factors
[MIN]	1.440 x 13.3 = 19.2 (80% confidence level)	X10, X5, X6
	1.943 x 13.3 = 25.8 (90% confidence level)	X10, X5
	2.447 x 13.3 = 32.5 (95% confidence level)	

Frequency is significant at 90% confidence level in this set as well as in the analysis made from the initial 12-test data. In other respects, the results from this analysis are somewhat different from those observed in the analysis of the initial 12 tests where, in addition to frequency, lubricant was also a significant variable at 80% confidence level. One reason for this difference would be the difficulties in polarization measurements encountered in the presence of the type of lubricant used. Lubricant affects the resistance of the electrolyte. A proper mixing of the lubricant and water is essential to obtaining reproducible $I_{corr.}$ as well as friction coefficient. From a tribological viewpoint, the oscillatory frequency should be an important factor affecting the wear-corrosion kinetics. As the frequency increases under load, wear-corrosion rate increases, which means highly active surface is regenerated and corroded at a faster rate and, consequently, the corrosion rate increases. The presence of $NaNO_2$ and Na_2MoO_4 should have reduced the corrosion rate by forming protective films although those films were not stable under 100% sliding wear condition. However, under rolling/sliding condition, which is the typical motion of rolling element bearings, it is expected that the protective inhibitor films will offer greater protection and reduce wear. Whether such a situation is reliable can only be ascertained through tests (as recommended) under rolling/sliding conditions. Morphological examination of the corrosion-wear surfaces showed that no pits developed in the wear track zone when $NaNO_2$ plus Na_2MoO_4 was used.

(c) Friction Coefficient

Table 15 summarizes the results of statistical analysis of the friction coefficient. The analysis showed the significant factor effect (S_{FE}) to be 0.049. The minimum factor effects were 0.071, 0.095, and 0.120 at 80%, 90%, and 95% confidence levels, respectively. At 80% confidence level, all the assigned factors were statistically significant in affecting the friction coefficient with the lubricant variable showing the greatest and the presence of $Na_2Cr_2O_7$ showing the least effect. At the 90% confidence level, the presence of $Na_2Cr_2O_7$ became insignificant, while the lubricant was the only significant variable at 95% confidence level. The results from this analysis are similar to those obtained from the initial 12-test data, with the significant variables differing in degrees at different confidence levels.

TABLE 15. RESULTS OF STATISTICAL ANALYSIS OF FRICTION COEFFICIENT

Trial	Mean	X1	X2	X3	X4	X5	X6	X7	X8	X9	X10	X11	$\bar{Y}$, f
1	+	+	+	-	+	+	+	-	-	-	+	-	0.27
2	+	+	-	+	+	+	-	-	-	+	-	+	0.17
3	+	-	+	+	+	-	-	-	+	-	+	+	0.15
4	+	+	+	+	-	-	-	+	-	+	+	-	0.58
5	+	+	+	-	-	-	+	-	+	+	-	+	0.43
6	+	+	-	-	-	+	-	+	+	-	+	+	0.87
7	+	-	-	-	+	-	+	+	-	+	+	+	0.11
8	+	-	-	+	-	+	+	-	+	+	+	-	0.47
9	+	-	+	-	+	+	-	+	+	+	-	-	0.22
10	+	+	-	+	+	-	+	+	+	-	-	-	0.12
11	+	-	+	+	-	+	+	+	-	-	-	+	0.45
12	+	-	-	-	-	-	-	-	-	-	-	-	0.48
Sum +	4.32	2.44	2.10	1.94	1.04	2.45	1.85	2.35	2.26	1.98	2.45	2.18	
Sum -	0	1.88	2.22	2.38	3.28	1.87	2.47	1.97	2.06	2.34	1.87	2.14	
Overall Sum	4.32	4.32	4.32	4.32	4.32	4.32	4.32	4.32	4.32	4.32	4.32	4.32	
Diff.	4.32	0.56	-0.12	-0.44	-2.24	0.58	-0.62	0.38	0.20	-0.36	0.58	0.04	
Effect	0.360	0.093	-0.020	-0.073	-0.373	0.096	-0.103	0.063	0.033	0.060	0.096	0.006	

S_{FE} = 0.049

		Significant Factors
[MIN] 1.440 x 0.049 = 0.071	(80% confidence level)	X4, X6, X10, X5, X1
1.943 x 0.049 = 0.095	(90% confidence level)	X4, X6, X10, X5
2.447 x 0.049 = 0.120	(95% confidence level)	X4

This analysis indicated that friction coefficient can be affected significantly by diverse experimental parameters in corrosion-wear systems. As expected, the friction coefficient showed a strong correlation with the lubricant. The indicated dependence of friction on load is most likely due to the nature of the evaluated experimental motion, i.e., 100% sliding-reciprocating, which is quite unlike the rolling-sliding motion of rolling element bearing components. This load dependence would be unlikely to occur till extremely large Hertzian contact stresses were reached. It is generally known that friction coefficient is a complex function of tribochemical parameters. However, the present observations under tribochemical operating conditions indicate that the fundamentals of tribological parameters, though modified, remained effective. Building on this basic understanding, a realistic interface motion study will advance the application and service life of load-bearing components under corrosion-wear conditions.

5.6.3 Discussion of Statistical Data

Selecting the 90% confidence level as the discriminator, the statistical analysis revealed the following:

Factors Significant at the 90% Confidence Level	Corrosion-Wear Parameters Influenced
Oscillation frequency (X10)	Friction coefficient Open-circuit potential Corrosion current
$NaNO_2$ + Na_2MoO_4 (X5)	Corrosion current Friction coefficient
$Na_2Cr_2O_7$ (X1)	Open-circuit potential
Lubricant (X4)	Friction coefficient
Load (X6)	Friction coefficient

It is significant to note that both oscillation frequency and $NaNO_2$ + Na_2MoO_4 greatly affected both corrosion current and friction coefficient, the two interrelated aspects of the corrosion-wear problem under investigation. It is suspected that their interaction effect (X10)(X5) will also be strong, but this simple analysis does not permit determining the relative degrees of these effects. In other words, it is only possible with additional

statistical tests with frequency (X10) and inhibitors (X5) at different levels, and with the other factors fixed, to obtain a relationship as indicated below:

$$Y = b_0 + b_1(X10) + b_2(X5) + b_3X(10)(X5) + b_4(X10)^2 + b_5(X5)^2 + e$$

where
- Y = observed values of $I_{corr.}$, f, and $E_{o.c.}$
- b_0 = a constant
- b_i = coefficients
- X10 = oscillation frequency
- X5 = $NaNO_2$ + Na_2MoO_4 (inhibitor)
- (X10)(X5) = interaction term
- $(X10)^2, (X5)^2$ = quadratic terms of (X10) and (X5)
- e = error term.

The statistical tests conducted in this study only pointed to the direction and significance of individual factor effects and did not in any way determine their relative importance in affecting any of the measured parameters, namely $I_{corr.}$, f, and $E_{o.c.}$ In order to do that, it will be necessary to conduct a fractional factorial statistical study, which is recommended.

A discrimination of the wear factor (primarily due to sliding/oscillation) and the corrosion factor (primarily controlled by the inhibitor package) is essential to further advance the objective of this program. This can be achieved through the use of

- Rolling-sliding motion simulating ball bearing condition. In such a motion (as opposed to 100% sliding now employed), the inhibitor effect will have a chance to offer a protective film.
- New and developing inhibitors
- Much longer periods of testing at relatively higher speeds under rolling conditions
- More realistic simulation of the environment.

These suggestions are further elaborated on in Section 7.

6. CONCLUSIONS

The critical and extensive tests performed in this program have advanced our understanding of the corrosion-wear phenomena occurring in load-bearing components in sea environment. It was demonstrated again with oscillatory motion that the IITRI-designed "Dynamic Corrosion-Wear Cell" is a versatile tool capable of monitoring simultaneous occurrence of corrosion and wear in any electrolyte system using polarization techniques.

The effect of wear on the corrosion process was very significant on alloys which were able to form a passive film. Disruption of the passive film was the principal factor leading to an increase in corrosion rate and wear loss, while surface deformation by increasing load and motion within the range evaluated, appeared to be secondary. An increase in load at a constant frequency did not affect the polarization reaction processes as much as an increase in frequency at a constant load.

It was clearly demonstrated that wear controls the anodic polarization process significantly, but not the cathodic polarization process. This understanding of the corrosion-wear mechanism indicated that the stability and repairability of the passive film with critically selected corrosion inhibitors will be of paramount importance in these tribological systems.

In the unlubricated system, friction coefficient was observed to be a complex function of tribochemical parameters so that the effect of load, motion, and electrolyte composition on friction coefficient depended on the relative effectiveness of each of the competing parameters. However, it was noted that friction coefficient of tool steels (52100 and M50) in NaCl solutions tended to increase with the addition of corrosion inhibitors, most significantly by sodium dichromate. Addition of a small quantity of water-soluble oil, however, had an overwhelming influence in decreasing the friction coefficient significantly.

All corrosion inhibitors used in this program effectively passivated 52100 and M50 steels under no-wear condition. Under wear conditions, corrosion inhibitors decreased corrosion activities, but they were not always

equally beneficial to wear processes. The wear rate of M50 steel was constant without corrosion inhibitors, and tended to increase with inhibitors.

Analytical scanning electron microscopy and surface roughness measurements were essential in the understanding of corrosion-wear surface morphology and the degree of damage in the tribochemical experiments. Examination of surface morphology revealed that pits nucleated exclusively inside the wear track zone, and microcracks developing from interfacial motion under load were the precursors of these pits.

A set of statistical corrosion-wear tests based on Plackett-Burman design was performed to demonstrate the effectiveness and relative significance of tribochemical parameters on the corrosion-wear process. The variables having statistically significant effect on each corrosion-wear parameter at 90% confidence level were as follows:

Parameter	Variables
Open-circuit potential	Sodium dichromate, frequency
Corrosion current density	Frequency, sodium nitrite, and sodium molybdate
Friction coefficient	Lubricant, load, frequency, sodium nitrite, and sodium molybdate

The study demonstrated clearly the basic mechanisms governing tribochemical effects on tool steel materials. While a greater emphasis was placed in these tests on chemical and electrochemical parametric controls, we recommend that additional tests be conducted with more realistic and directly correlatable tribological parametric controls.

7. RECOMMENDATIONS

The Phase I results (NADC-79137-60) combined with the Phase II analysis presented in this report have accomplished the following:

- A basic understanding of the mechanisms of tribochemical (wear-corrosion) phenomena of bearing steels in aggressive environments and the role of inhibitors in mitigating wear-corrosion damage
- The development of dynamic equipment applying electrochemical techniques to obtain a thorough understanding of the wear-corrosion phenomena
- A clear definition of further direction and attainable goals of a program to advance the solution of the current naval aircraft bearing problems in marine environment.

Failure of critical components and load-bearing structures in naval aircraft with concomitant loss in reliability may be directly attributed to wear-corrosion under mechanical action and stress. The interrelated wear-corrosion phenomena can only be directly evaluated electrochemically in a dynamic wear-corrosion cell similar to the existing apparatus. However, the motion of interest to load-bearing structures such as bearings is not pure sliding, either unidirectional or oscillatory, but a combination of rolling-sliding motion. We recommend the following:

- Modify existing apparatus to simulate a combination rolling-sliding motion.
- Evaluate, modify, and combine inhibitors for best protection under rolling-sliding conditions.
- Increase the proportion of lubricant in electrolyte and correct for resistance-polarization problems. Search for better conducting lubricant, and evaluate likely candidates.
- Apply the conclusions and recommendations for potential use of data base to develop better techniques and methods to protect materials in service and improve their reliability in operation.

REFERENCES

1. K. Y. Kim and S. Bhattacharyya, "Wear and Corrosion of Components Under Stress and Subjected to Motion," Interim Report, NADC-79137-60, Naval Air Development Center, Warminster, PA, February (1982).

2. K. Y. Kim , S. Bhattacharyya, and V. S. Agarwala, in Wear of Materials, p. 772, Proc. 3rd Int. Conf. on Wear of Materials, ASME, San Francisco, CA (1981).

3. V. S. Agarwala, K. Y. Kim, and S. Bhattacharyya, in Materials Evaluation Under Fretting Conditions, S. R. Brown (ed.), p. 106, ATM STP 780 (1982).

4. K. Y. Kim and S. Bhattacharyya, "Electrochemical Evaluation of Corrosion-Wear Phenomenon of Bearing Materials in Aggressive Environments," ECS Fall Meeting Abstract No. 319, Detroit, MI (1982).

5. A. D. Sarkar, Wear of Metals, Pergamon Press, New York (1976).

6. K. Y. Kim, S. Bhattacharyya, and V.S. Agarwala, "Electrochemical Evaluation of Corrosion Inhibitors in Corrosion-Wear Systems," International Conference on Corrosion Inhibition, Paper No. 9, Dallas, TX (1983).

7. J. W. Dini and H. R. Johnson, "Use of Strategy of Experimentation in Gold Plating Studies," Plating and Surface Finishing, Vol. 68 (2), p. 52 (1981).

8. Electrochemical Corrosion Testing, F. Mansfield and U. Bertocci (eds.), ASTM STP No. 727 (1981).

APPENDIX A

OSCILLATORY MOTION AND TORQUE MEASUREMENT

In oscillatory motion experiments both frequency and amplitude can be varied as follows:

Frequency: 0.9-44 cpm (15-230 mHz)

Amplitude: 0° to 90° (0 to $\pi/2$ rad)

As shown in Fig. A-1, it is necessary to uniquely identify the position of a rotating electrode so that the resulting torque can be correlated under different test loads and environments. If, for example, the amplitude and frequency are 60° ($\pi/3$ rad) and 1 cpm (17 mHz), then the disk electrode will oscillate 30° in either direction every 30 seconds. The different positions in this motion are identified in this way:

1) When the connecting rod (F in Fig. 1) is in the extreme backward position, the wear track caused by the pin electrode ends at the front part of disk electrode. This is called "+30°" position.

2) When the connecting rod moves to the extreme forward position, the wear track ends at the rear part of the disk electrode. This is called "-30° position." With counterclockwise motion of the shaft (looking from the crankshaft end), the two intermediate positions are identified according to items 3 and 4.

3) A position at the track center called "+0°" occurs when oscillation proceeds from +30° to -30° position.

4) The same track center position is identified as "-0°" when oscillation proceeds from -30° to +30° position.

At the two central positions, a disk electrode is moving evenly under the pin while at the two end positions, the disk electrode stops momentarily and reverses direction. Thus, the 0° positions appear to be better for making measurements.

Using this position identification system, the torque induced by oscillation under no load was evaluated to obtain the background bearing friction. These data are given in Table A-1. The trace of corresponding frictional

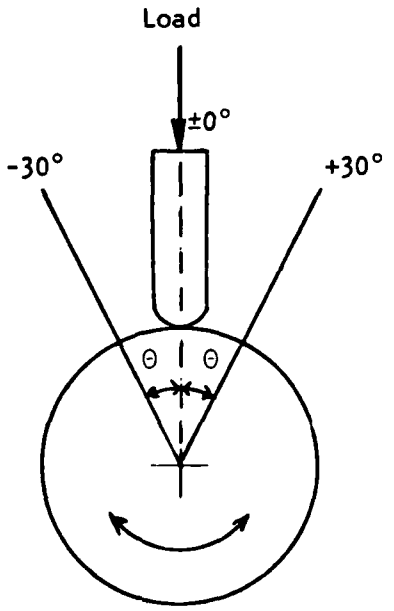

Figure A-1. Position identification in oscillatory motion.

TABLE A-1. TORQUE CELL STRAIN WITH OSCILLATION UNDER NO LOAD AND FORWARD REVOLUTION[a]

Strain Measured at Given Position, μin/in.			
+30°	+0°	-30°	-0°
-24[b]	+10	+23	-23
-24	+19	+23	-24
-24	+19	+24	-25

[a]Counterclockwise shaft motion, looking from crankshaft end.

[b]Only three values of the several hundred similar and steady values are indicated.

torque strain is graphically presented in Fig. A-2. It is observed from both Table A-1 and Fig. A-2 that the frictional torque strain induced under no-load oscillation has both tensile and compressive components. This may arise from three sources: (1) bearing friction--these bearings are normally designed for unidirectional motion; (2) out of roundness of the shafts; and (3) bending moments, because of minor misalignment. Under perfect conditions, the trace of strain might show a slightly wavy line. The strain readings given in Table A-1 were directly taken from the digital strain indicator, while the strain readings given in Fig. A-2 were obtained from conversion of mV values to μin/in values.

The identity between the values in Table A-1 and Fig. A-2 may be noted from the following:

Position	Strain Reading, μin/in.	
	Table A-1	Fig. A-2
+0°	+19	350
-0°	-23	392
Difference	42	42

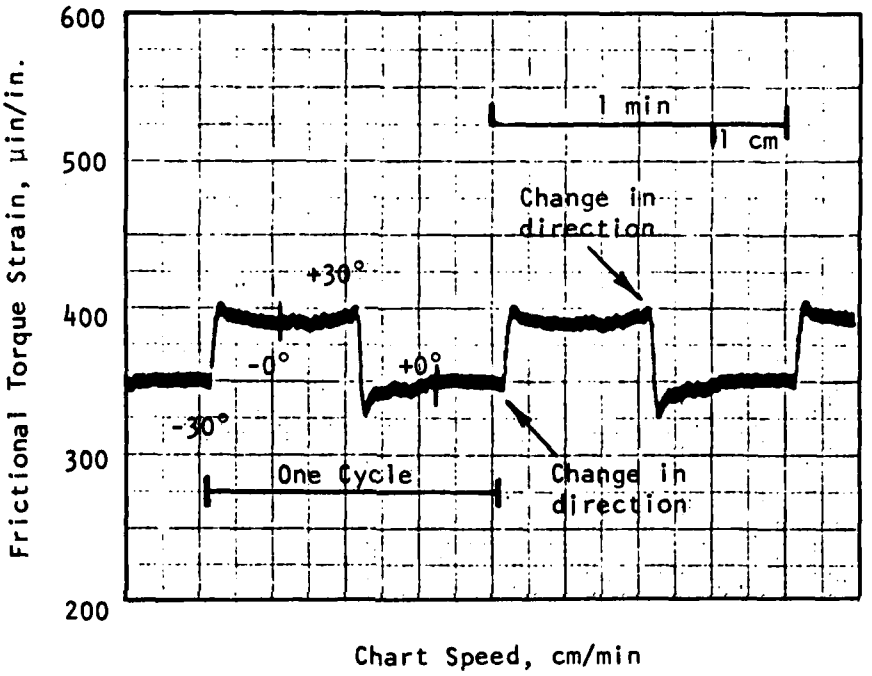

Figure A-2. Trace of frictional torque strain due to oscillation under no load during forward revolution of the crankshaft (counterclockwise looking from crankshaft end).

APPENDIX B

EVALUATION OF FRICTION COEFFICIENT

Friction coefficient between moving surfaces depends on the real areas of contact between the two loaded surfaces. It is customary to measure the observed strain or equivalent torque experienced by a moving component for a specific applied torque and to express the ratio between the two torques as a decimal fraction, called "f," the coefficient of friction. The f value of steel under non-lubricated conditions can vary between 0.6 and 1.0; under lubricated conditions, it may be as low as 0.03, depending on the lubricant and the nature of motion.

The friction coefficient f between the pin and disk electrodes was obtained by monitoring the strain (and equivalent torque) of the disk electrode and expressing it as a fraction of the torque applied to the disk electrode through the pin electrode. Thus

$$f = T_{obs}/T_{app}$$

where T_{obs} was obtained either from the digital strain indicator or the strip chart recorder and the calibration curve (Fig. 3). T_{app} was equal to r x P, where r is the radius of the disk electrode [0.75 in. (19 mm)] and P the load in lbf (N) including the weights of all components.

The strain induced by the applied load includes, in addition, the strain due to the bearing friction, which was observed to remain constant. The difference, when converted, gives the actual applied torque due to load alone.

In Appendix A, it is shown that 0° positions are suitable for making observations because of uniform motion in these locations. This concept was further developed from evaluation of strain traces shown schematically in Fig. B-1. From Fig. B-1, one obtains the following:

Method 1: $\Delta\varepsilon_1 = \frac{\overline{\Delta 1} - \overline{\Delta 2}}{2}$, using average values of at least ten $\Delta 1$ and $\Delta 2$ readings

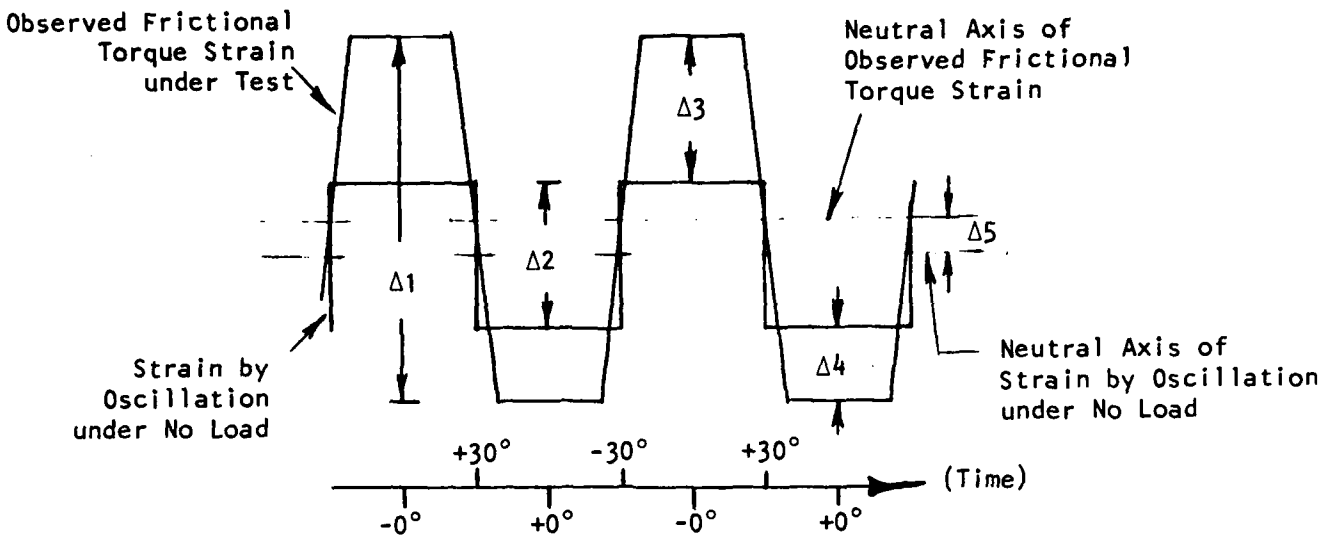

Δ1: Observed frictional torque strain under test obtained from difference between the strain components of tension and compression.

Δ2: Strain by oscillation under no load obtained from difference between the strain components of tension and compression.

Δ3: Strain difference between the observed frictional torque strain under test and the strain by oscillation under no load in tensional component (or at -0° position).

Δ4: Strain difference between the observed frictional torque strain under test and the strain by oscillation under no load in compressional component (or at +0° position).

Δ5: Deviation of neutral axis.

Figure B-1. Schematic illustration of strain observed with oscillatory motion. (Oscillating amplitude of 60° is considered.)

Method 2: $\Delta\varepsilon_2 = \frac{\Delta 1 - \Delta 2}{2}$, using individual values at +0° and -0° positions

Method 3: $\Delta\varepsilon_3 = \Delta 3$, using strain readings at -0° position only

Method 4: $\Delta\varepsilon_4 = \Delta 4$, using strain readings at +0° position only.

For Method 1, the average value of strain readings can be easily obtained from strip chart recordings of strain traces. On the other hand, strain readings directly taken from the digital strain indicator can be used for Methods 2, 3, and 4. A typical set of data is given in Table B-1 and shown in Fig. B-2.

The $\Delta\varepsilon$ values of test 203 determined by the four different methods from data given in Table B-1 are presented in Table B-2, together with the values of corresponding torque and friction coefficients. Examination of the values in Table B-2 indicates that Methods 1 and 2 give very similar values. However, Methods 3 and 4 result in significant deviations from the values determined by Methods 1 and 2. This is due to the deviation of the neutral axis of strain which is illustrated in Fig. B-1. Therefore, Methods 3 and 4 are more complicated to apply and are not recommended, though the average of the values obtained by these two methods results in approximately the same value obtained by Methods 1 and 2. Method 1 is recommended over Method 2 because the average strain readings will have more uniformity even under high load conditions. The average strain readings can be reasonably well determined from the strip chart recordings of strain trace, and the friction coefficient was determined by Method 1 throughout this program.

Depending on test conditions, friction between surfaces under load tends to change initially and then stabilize to a constant value provided the conditions remain unchanged. This is usually called run-in in tribology under lubricated condition. The period of run-in can vary from a few minutes to many hours. As shown in Table B-1, in air a higher torque was obtained after 2 h, after which it was noted to remain constant. In water the change was smaller, and a more constant value was obtained earlier; but a 2-h period is considered sufficient and was used in this program to determine the coefficient of friction.

TABLE B-1. OBSERVED FRICTIONAL TORQUE STRAIN DUE TO OSCILLATORY MOTION (TEST 203)

Time, h	Strain Measured at Given Position, μin/in. +30°	+0°	-30°	-0°
Case I: Under No Load				
	In Ambient Air			
	-5	+34	+35	+3
	-5	+34	+34	+3
	-4	+34	+34	+3
Case II: Under 16 lb load				
	In Ambient Air			
1/4	-102	+118	+126	-95
	-99	+119	+129	-94
	-100	+119	+128	-91
2	-188	+132	+135	-215
	-185	+131	+133	-215
	-188	+133	+133	-215
	In Distilled Water			
0[a]	-115	+104	+119	-102
	-114	+104	+119	-102
	-116	+105	+118	-103
2	-120	+99	+120	-97
	-115	+99	+119	-96
	-117	+99	+120	-97

Test conditions: Amplitude 60° (π/3 rad)
Frequency 1 cpm (17 mHz).

[a]Immediately after immersion; water added after 2 h test in air.

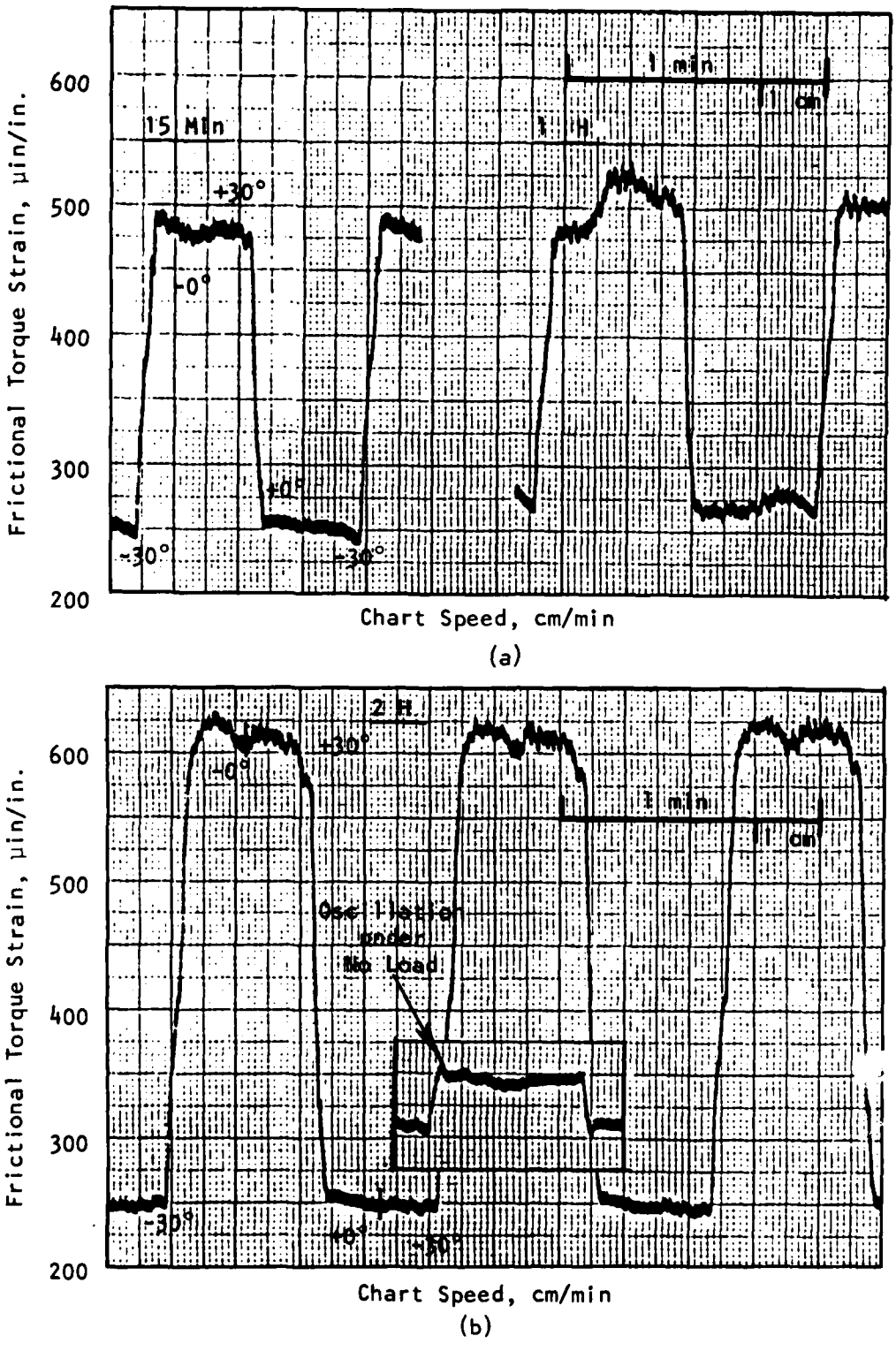

Figure B-2. Traces of frictional torque strain observed during various time periods for 52100 steel under 16 lbf (71.2 N) load in ambient air (test 203). Amplitude: 60° (π/3 rad), frequency: 1 cpm (17 mHz). (a) After 15 min and 1 h; (b) after 2 h.

TABLE B-2. VALUES OF FRICTIONAL TORQUE STRAIN, OBSERVED TORQUE, AND FRICTION COEFFICIENT

Method	$\Delta\varepsilon$, μin/in.	T_{obs}, in-lb[a]	Friction Coefficient (f)
	Ambient Air/2 h		
1	161.5	11.2	0.93
2	158.0	11.0	0.92
3	218.0	15.2	1.27
4	98.0	6.8	0.57
	Distilled Water/2 h		
1	84.0	5.8	0.48
2	82.5	5.7	0.47
3	100.0	7.0	0.58
4	65.0	4.5	0.37

Test conditions: Load 16 lbf (71.2 N)
Amplitude 60° (π/3 rad)
Frequency 1 cpm (17 mHz)

[a]1 in-lb = 1.15 cm-kg.

APPENDIX C

POTENTIAL SCANNING METHODS FOR POLARIZATION MEASUREMENTS

Three different potential scanning methods were used for polarization measurements as described below.

Method I (used for tests 206 through 213). The sequence of potential scanning was as follows:

Step 1 Upon reaching a steady open-circuit potential, scan downward from the open-circuit potential to the cathodic potential.

Step 2 After cathodic polarization, remove the externally applied cathodic overpotential and allow a steady potential to be attained close to the open-circuit potential which was observed before cathodic polarization.

Step 3 Then, scan upward from this potential to the anodic potential.

Method II (used for tests 214 through 228). During step 2 of Method I after cathodic polarization, the electrode potential rarely reattained the open-circuit potential which was observed before cathodic polarization even with sufficiently long time since the electrochemical property of the electrode surface had changed due to cathodic polarization. This created uncertainty in the polarization behavior of the anodic reaction at the lower anodic potentials. Mismatch of the open-circuit potential after cathodic polarization was more pronounced as the wear condition became severe. To eliminate this experimental artifact, a continuous scanning upward from cathodic potential to anodic potential was adopted and used, and was also noted in the literature.[5] However, for test 227, only scanning upward from the open-circuit potential to anodic potential was done.

---

[5] Electrochemical Corrosion Testing, F. Mansfeld and U. Bertocci (eds.), ASTM STP No. 727, 1981.

Method III (used for tests 232 through 250). Since corrosion-wear test results from test 206 to 228 showed that wear did not significantly affect the cathodic polarization process, only anodic polarization measurements were conducted for these tests. The disk electrode was immersed in the electrolyte through which air bubbles were introduced overnight for saturation. The disk electrode was held at 400 mV below the open-circuit potential (observed during air saturation) for 10 min. Upon reaching a steady-state potential, anodic polarization was performed at a scanning rate of 12 mV/min.

APPENDIX D

A COMPLETE SUMMARY OF CORROSION-WEAR ELECTROCHEMICAL TEST DATA

TABLE D-1. CORROSION-WEAR TEST CONDITIONS AND FRICTION COEFFICIENT OF 52100 AND M50 STEELS

Test No.	Electrolyte[a]		Wear Condition[b]		Friction Coeff. (f)
	NaCl, ppm	Inhibitor	Load, lbf[c]	Frequency, cpm[d]	
		52100 Steel			
202a[e]	-	None	8	1	0.83
202b	0	None	8	1	0.51
203a	-	None	16	1	0.93
203b	0	None	16	1	0.48
204a	-	None	56	1	0.71
204b	0	None	56	1	0.55
206	10	None	16	1	0.59
207	10	500 ppm $Na_2Cr_2O_7$ + 500 ppm Na_2MoO_4	16	1	0.92
208[f]	10	500 ppm $Na_2Cr_2O_7$ + 500 ppm Na_2MoO_4	16	1	0.23
209[f]	0	None	16	1	0.23
210[f]	10	None	16	1	0.23
211a	10	500 ppm $Na_2Cr_2O_7$ + 500 ppm Na_2MoO_4	16	1	1.03
211b	10	500 ppm $Na_2Cr_2O_7$ + 500 ppm Na_2MoO_4	16	1	0.72
211c	0	None	16	1	0.52
213	10	None	16	1	0.52
		M50 Steel			
214	10	500 ppm $Na_2Cr_2O_7$ + 500 ppm Na_2MoO_4	16	1	0.71
215	10	None	16	1	0.54
216	10	500 ppm $Na_2Cr_2O_7$ + 500 ppm Na_2MoO_4	56	1	0.47
217	100	None	16	1	0.52
218	100	500 ppm Na_2CrO_4	16	1	0.69
219	100	500 ppm Na_2MoO_4	16	1	0.61
220	100	500 ppm $NaNO_2$	16	1	0.52
221[f]	100	500 ppm $NaNO_2$	16	1	0.23
222	100	690 ppm $NaNO_2$ + 2060 ppm Na_2MoO_4	16	1	0.59
223	100	690 ppm $NaNO_2$ + 2060 ppm Na_2MoO_4	16	1	-
224	100	690 ppm $NaNO_2$ + 2060 ppm Na_2MoO_4	16	10	0.50
225	100	690 ppm $NaNO_2$ + 2060 ppm Na_2MoO_4	56	1	0.35

TABLE D-1 (cont.)

Test No.	Electrolyte[a] NaCl, ppm	Electrolyte[a] Inhibitor	Wear Condition[b] Load, lbf[c]	Wear Condition[b] Frequency, cpm[d]	Friction Coeff. (f)
226	100	690 ppm $NaNO_2$ + 2060 ppm Na_2MoO_4	56	10	0.53
227	100	690 ppm $NaNO_2$ + 2060 ppm Na_2MoO_4	--	1	-
229	100	690 ppm $NaNO_2$ + 2060 ppm Na_2MoO_4	16	1	0.59
230	100	None	16	1	0.48
231	100	690 ppm $NaNO_2$ + 1620 ppm Na_2CrO_4	16	1	0.59
232	100	2620 ppm $Na_2Cr_2O_7$	16	10	0.78
233	100	2620 ppm $Na_2Cr_2O_7$	56	1	0.41
234	100	2620 ppm $Na_2Cr_2O_7$ + 690 ppm $NaNO_2$ + 2060 ppm Na_2MoO_4	16	10	0.87
235	100	690 ppm $NaNO_2$ + 2060 ppm Na_2MoO_4	56	10	0.47
236	100	690 ppm $NaNO_2$ + 2060 ppm Na_2MoO_4	56	1	0.44
237	100	None	16	1	0.48
238[f]	100	2620 ppm $Na_2Cr_2O_7$ + 690 ppm $NaNO_2$ + 2060 ppm Na_2MoO_4	56	10	0.13
239[f]	100	None	56	10	0.12
240[f]	100	None	16	10	0.13
241[f]	100	690 ppm $NaNO_2$ + 2060 ppm Na_2MoO_4	16	1	0.16
242[f]	100	2620 ppm $Na_2Cr_2O_7$	56	1	0.12
243[f]	100	2620 ppm $Na_2Cr_2O_7$ + 690 ppm $NaNO_2$ + 2060 ppm Na_2MoO_4	16	1	0.17
244[f]	100	None	56	10	0.11
245	100	2620 ppm $Na_2Cr_2O_7$	56	1	0.44
246	100	2620 ppm $Na_2Cr_2O_7$	16	10	0.58
247[f]	100	2620 ppm $Na_2Cr_2O_7$	56	1	0.47
248[f]	100	None	16	10	0.18
249[f]	100	690 ppm $NaNO_2$ + 2060 ppm Na_2MoO_4	16	1	0.28
250	100	2620 ppm $Na_2Cr_2O_7$ + 690 ppm $NaNO_2$ + 2060 ppm Na_2MoO_4	56	10	0.40

[a]Distilled water was the medium.
[b]The oscillatory amplitude in all tests was 60° (π/3 rad).
[c]1 lbf = 4.45 Newtons.
[d]1 cpm = 17 mHz.
[e]Tested in air.
[f]10% water-soluble oil was added.

TABLE D-2. SUMMARY OF CORROSION CURRENT DENSITY AND OPEN-CIRCUIT POTENTIAL[a]

Test No.	Corrosion Current Density, $\mu A/cm^2$ (mpy)				Open-Circuit Potential, mV	
	No Wear		Wear		No Wear	Wear
206	-	-	0.80	(0.36)	-230	-240
207	-	-	0.35	(0.16)	-110	-190
208	-	-	0.15	(0.07)	-70	-220
209	-	-	0.03	(0.01)	-230	-380
210	-	-	0.16	(0.07)	-220	-410
211b	-	-	0.66	(0.30)	-110	-200
213	-	-	5.60	(2.56)	-365	-380
214	-	-	1.0	(0.46)	-110	-330
215	-	-	1.0	(0.46)	-300	-320
216	0.42	(0.19)	0.90	(0.41)	-75	-440
217	10.0	(4.58)	-	-	-360	-
218	0.6	(0.27)	-	-	-600	-
219	0.4	(0,18	-	-	-200	-
220	0.5	(0.23)	-	-	-180	-
221	0.3	(0.14)	-	-	-300	-
222	1.2	(0.55)	-	-	-220	-
223	0.9	(0.41)	12	(5.50)	-220	-320
224	-	-	60	(27.5)	-	-500
225	-	-	12	(5.50)	-	-320
226	-	-	100	(45.8)	-	-480
227	0.6	(0.27)	-	-	-220	-
232	-	-	54.0	(24.7)	-	-260
233	-	-	12.0	(5.5)	-	-267
234	-	-	25.0	(11.4)	-	-292
235	-	-	85.0	(38.9)	-	-487
236	-	-	12.0	(5.5)	-	-315
237	-	-	9.0	(4.1)	-	-330
238	-	-	50.0	(23.0)	-	-320
239	-	-	7.8	(3.6)	-	-430
240	-	-	3.3	(1.5)	-	-410

TABLE D-2 (cont.)

Test No.	Corrosion Current Density, $\mu A/cm^2$ (mpy)				Open-Circuit Potential, mV	
	No Wear		Wear		No Wear	Wear
241	-	-	6.0	(2.7)	-	-365
242	-	-	6.0	(2.7)	-	-297
243	-	-	2.7	(1.2)	-	-145
244	-	-	9.0	(4.1)	-	-450
245	-	-	10.0	(4.6)	-	-237
246	-	-	17.0	(7.8)	-	-245
247	-	-	9.8	(4.5)	-	-310
248	-	-	4.2	(1.9)	-	-430
249	-	-	6.2	(2.8)	-	-390
250	-	-	120.0	(55.0)	-	-290

[a]Refer to Table D-1 for details of test condition.

TABLE D-3. WEIGHT LOSS DATA FOR PIN ELECTRODES OF 52100 AND M50 STEELS UNDER VARIOUS WEAR CONDITIONS[a]

Test No.	Material	Wear Condition		Wear Scar Area, $cm^2 \times 10^{-3}$	Weight Loss, µg
		Load, lbf[b]	Time, h		
202[c]	52100 steel	8	-	9.1	167
203	52100 steel	16	-	14.1	398
207	52100 steel	16	-	13.2	352
209[d]	52100 steel	16	-	8.8	155
210[d]	52100 steel	16	55.3	16.2	532
211a	52100 steel	16	3	10.9	238
211b	52100 steel	16	23.5	16.7	562
211c	52100 steel	16	2	4.5	41
213	52100 steel	16	21	6.3	80
214	M50 steel	16	20.7	5.0	50
215	M50 steel	16	20	11.6	272
216	M50 steel	56	2.7	7.5	113
217	M50 steel	16	48	14.6	428
218	M50 steel	16	48	16.6	554
219	M50 steel	16	24	16.8	569
220	M50 steel	16	48	16.9	577
221[d]	M50 steel	16	48	13.8	385
222	M50 steel	16	48	17.4	609
223	M50 steel	16	3.8	1.74	609
224	M50 steel	16	24	31.4	2011
225	M50 steel	56	24	12.5	315
226	M50 steel	56	24	35.7	2625

[a]See Table D-1 for details.

[b]1 lbf = 4.45 N.

[c]Pin hardness was HRC 20-25 in tests 202-211a, and HRC 60-63 in tests 211b to 226. Disk hardness was HRC 60-63 in all tests.

[d]Lubricant was used.

DISTRIBUTION LIST (Continued)

REPORT NO. NADC-79137-60

	No. of Copies
National Bureau of Standards Attn: Dr. A. W. Ruff Materials Building, Rm. B266 Washington, DC 20234	1
U.S. Army Arament R&D Command DRDAR-SCM, Bldg. 355 Attn: Dr. W. T. Ebihara Dover, NJ 07801	1
Prof. H. Leidheiser, Jr., Director Center for Coatings and Surface Research Lehigh University Bethlehem, PA 18015	1
Dr. S. Bhattacharyya I.I.T. Research Institute 10 West 35th Street Chicago, IL 60616	2
NAVAIRDEVCEN (3 for Code 8131) (50 for Code 6062)	53

DISTRIBUTION LIST (Continued)

REPORT NO. NADC-79137-60

	No. of Copies
Wright-Patterson Air Force Base (AFWAL/MLSA), Attn: Bernie Cohen Dayton, OH 45433	1
Bolling Air Force Base AFOSR Attn: Dr. A. Rosenstein Washington, DC 20332	1
Army Research Office Attn: Dr. R. Reeber P.O. Box 12211 Research Triangle Park, NC 27709	1
U. S. Army Materials & Mechanics Research Center Attn: Dr. M. Levy Watertown, MA 02172	1
Chief, Material and Processes Grumman Aerospace Bethpage, LI, NY 11714	1
Chief, Material and Processes Vought Corporation P.O. Box 5907 Dallas, TX 75222	1
Chief, Materials and Processes Rockwell International 4300 East Fifth Avenue Columbus, OH 43216	1
Chief, Materials and Processes Boeing Aerospace P.O. Box 3707 Seattle, WA 98124	1
Chief, Materials and Processes Lockheed Aircraft Corporation 2555 North Hollywood Way Burbank, CA 91503	1
Defense Technical Information Center Cameron Station, Bldg. 5 Washington, DC 20361	12

DISTRIBUTION LIST

REPORT NO. NADC-79137-60

	No. of Copies
Naval Air Systems Command Department of the Navy Washington, DC 20361 (1 for Code AIR-31A) (2 for Code AIR-5304) (1 for Code AIR-5304C1) (2 for Code AIR-004D4)	6
Naval Air Propulsion Center Attn: Mr. A. J. Dorazio, Code PE-72 Trenton, NJ 08628	1
Office of Naval Research Attn: Keith Ellingsworth, Mechanics Division 800 N. Quincy Street Washington, DC 20362	1
Commander, Naval Air Force U.S. Atlantic Fleet (Code 528) Naval Air Station Norfolk, VA 23511	1
Commander, Naval Air Force U.S. Pacific Fleet (Code 7412) Naval Air Station North Island, San Diego, CA 92135	1
Naval Sea Systems Command Attn: Code 05R25 Washington, DC 20362	1
COMDTNSRDC Attn: Code 2813 Annapolis, MD	1
Naval Research Lab Attn: Mr. R. J. Goode, Code 6301 Washington, DC 20375	1
Office of Naval Research Attn: Dr. C. T. Lynch, Code 43 Washington, DC 20362	1
Office of Naval Research Attn: Mr. J. J. Kelly, Code MAT-0725 Washington, DC 20375	1

END

FILMED

10-84

DTIC